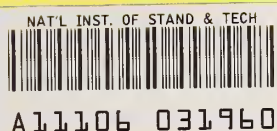


Reference

NBS  
PUBLICATIONS



NBSIR 84-3017

# MICROWAVE DETECTION OF LOST WELLS AND UNKNOWN WATER-FILLED VOIDS IN COAL MINES

---

National Bureau of Standards  
U.S. Department of Commerce  
Boulder, Colorado 80303

September 1984

QC  
100  
.U56  
84-3017  
1984



NBSIR 84-3017

# MICROWAVE DETECTION OF LOST WELLS AND UNKNOWN WATER-FILLED VOIDS IN COAL MINES

---

D. R. Belsher  
R. H. McLaughlin  
A. G. Repjar  
H. E. Bussey

Electromagnetic Fields Division  
National Engineering Laboratory  
National Bureau of Standards  
U.S. Department of Commerce  
Boulder, Colorado 80303

September 1984

Prepared for  
Bureau of Mines  
United States Department of the Interior



---

U.S. DEPARTMENT OF COMMERCE, Malcolm Baldrige, Secretary

NATIONAL BUREAU OF STANDARDS, Ernest Ambler, Director



REPORT DOCUMENTATION PAGE	1. REPORT NO.	2.	3. Recipient's Accession No.
4. Title and Subtitle Microwave Detection of Lost Wells and Unknown Water-Filled Voids in Coal Mines			5. Report Date September 1984
7. Author(s) D.R. Belsher, R.H. McLaughlin, A.G. Repjar, H.E. Bussey			6.
9. Performing Organization Name and Address Electromagnetic Fields Division National Bureau of Standards U.S. Department of Commerce Boulder, Colorado 80303			8. Performing Organization Rept. No. NBSIR 84-3017
12. Sponsoring Organization Name and Address United States Department of the Interior U.S. Bureau of Mines, Denver Mining Research Center Denver Federal Center, Denver, Colorado 80225			10. Project/Task/Work Unit No. 7233410
15. Supplementary Notes			11. Contract(C) or Grant(G) No. (C) H0272007 (G)
16. Abstract (Limit: 200 words)  Work on contract H0272007 is summarized for the period of January 1979 through March 1984. The development of improved antennas useable with both a pulse system or an FM-CW system is described. The development of a field prototype pulse sampling system is described. Initial theoretical work on the problem of dielectric loading of antennas as well as a study of potential system range is included.			13. Type of Report & Period Covered Final - Phase II Jan. 1979 to March 1984
17. Document Analysis a. Descriptors  Detection of mining hazards Detection of coal mining hazards			14.
b. Identifiers/Open-Ended Terms			
c. COSATI Field/Group			
18. Availability Statement  Available from NTIS	19. Security Class (This Report) Unclassified	21. No. of Pages	
	20. Security Class (This Page) Unclassified	22. Price	

## FOREWORD

This report was prepared by the National Bureau of Standards (NBS), Electromagnetic Fields Division, Boulder, Colorado, under USBM Contract number H0272007. The contract was initiated under the Minerals Health and Safety Program. It was administered under the technical direction of the Premining Hazards Division, Denver Research Center, with Mr. Richard L. Myers acting as Technical Project Officer. Mr. Dennis Maez was the contract administrator for the Bureau of Mines. This report is a summary of the work recently completed as a part of this contract during the period 23 January 1979 to 1 March 1984. This report was submitted by the authors on 1 May 1984 and published in September 1984.

The NBS thanks other staff members not named as authors who contributed indirectly to this work: Doyle A. Ellerbruch for helpful discussions on techniques, Douglas T. Tamura for assistance in the field, and James R. Andrews for helpful discussions on pulse theory.

The authors also wish to acknowledge the considerable help provided by the staff of the Kaiser Coal Mine at Raton, NM, especially that of Mr. Ed Moore, Mr. Richard E. Hood, Mr. Rod Lawrence, Mr. Terry Jordan, Mr. Ron Chavez, and Mr. Harry H. Elkin.

The assistance provided by personnel of the Bureau of Mines, Denver Research Center, is greatly appreciated, most notably that of project monitor Mr. Richard L. Myers and also Mr. R. J. Leckenby.

The authors regret the unavoidable delay in concluding this project. Progress was stopped for more than two years while manufacturers of critical sub-assemblies worked to meet the specifications.

# CONTENTS

	<u>Page</u>
FOREWORD.....	4
1. INTRODUCTION.....	11
2. ANTENNA CHARACTERISTICS.....	12
2.1 Antenna Construction.....	12
2.2 Antenna Response.....	13
2.3 Antenna Pattern.....	13
2.4 Isolation in the Bistatic Configuration.....	13
2.5 Operation Close to Surfaces.....	14
3. POTENTIAL FOR DIELECTRIC LOADING OF ANTENNAS.....	14
3.1 Infinite Bow-Tie Antenna.....	14
3.2 Finite Bow-Tie Antenna.....	15
3.3 Dielectrically Loaded Antennas.....	16
3.4 Directional Bow-Tie Antenna.....	17
3.5 Conclusions and Recommendations.....	17
4. SUBSURFACE RADAR RANGE LIMIT STUDY.....	18
4.1 Introduction.....	18
4.2 The Radar Equation.....	18
4.3 Interface Transformation Factors, $I C_d$ .....	20
4.4 Attenuation in the Medium.....	24
4.5 Radar Range Calculation from S/N.....	25
4.6 Radar Cross Section.....	25
4.7 Electromagnetic Theory of Scattering Cross Sections of Extended Targets.....	26
4.8 Cross Section of a Planar Interface.....	27
4.9 Half-period (Fresnel) Zones.....	27
4.10 The Strip Approximation of a Tunnel.....	29
4.11 Cross Section of a Dielectric Tunnel at Broadside Incidence....	30
4.12 Cross Sections of Circular Cylinders (Boreholes).....	31
4.13 Computer Routine for S/N Versus Range.....	33
4.14 Conclusions.....	33
5. PULSE RESPONSE SIMULATIONS.....	34
5.1 Waveform Comparisons.....	35
5.2 Borehole Detection Estimates.....	36
6. PULSE SYSTEM EQUIPMENT.....	37
6.1 High Voltage Impulse Generator.....	37
6.2 Receiver Preamplifier.....	37
6.3 High-frequency Sampler.....	38
6.4 Fiber-optic Transmission System.....	39
6.5 Digital Acquisition System.....	40

7.	FIELD TESTING.....	40
7.1	NBS Test Range.....	40
7.2	Coal Mine Results.....	41
8.	ADAPTATION OF SEISMIC DATA METHODS.....	41
9.	FUTURE DIRECTIONS FOR RADAR DETECTION OF UNDERGROUND ANOMALIES.....	42
9.1	Mining Needs.....	42
9.2	Antennas.....	42
9.3	Future System Types.....	43
9.4	Accessibility to Mine Test Areas.....	43
10.	REFERENCES.....	43
APPENDIX A.	COMPUTER PROGRAM FOR SIGNAL-TO-NOISE RATIO, AS A FUNCTION OF DISTANCE (RANGE) TO A SUBSURFACE TARGET.....	82



## LIST OF FIGURES

		<u>Page</u>
Figure 1.	Reflections due to the NBS-TQ antenna without the resistive material (1) and the same antenna with the resistive material (2).....	47
Figure 2.	Transmitted waveform from the TG antenna (curve 1) and the TQ antenna (curve 2).....	48
Figure 3.	Relative transmission in dB for the TG antenna (plain line) forward direction, the TQ antenna (squares) forward direction, and the TQ antenna (triangles) reverse direction at a range of 3/4 m.....	49
Figure 4.	Baffle arrangement for isolating TQ antennas when operated bistatically.....	50
Figure 5.	Response (1) of the system with the TQ antenna pair pointed at the sky and (2) to a 1.2 meter square metal plate 5 cm in front of the baffle.....	51
Figure 6.	Pulse system antenna return from an air-filled box target buried at 0.6 meter (1) and the same return corrected by subtraction of the sky return (2).....	52
Figure 7.	Non-coplanar fin antenna schematic.....	53
Figure 8.	Characteristic impedance of the non-coplanar fin antenna with equal fin angles (plotted from data presented by Carrel [9]).....	54
Figure 9.	Input impedance of biconical antennas with 5.4° cone angle and 0.054° cone angle as a function of the length, $\ell$ , of the cone in wavelengths, $\lambda$ (plotted from data presented by Kraus [12]).....	55
Figure 10.	Input impedance of single cones with ground plane as a function of cone length, $\ell$ , in wavelengths, $\lambda$ . Cone angles are 10°, 20°, 40°, and 60° (plotted from data presented by Kraus [12]).....	56
Figure 11.	Input impedance of single cone with ground plane versus $k\ell$ . $K$ is the wave number, $\ell$ is the cone length, and the cone angle, $\theta_0$ , is 60° (plotted from data presented by Papas and King [13]).....	57
Figure 12.	Characteristic impedance of a biconical antenna with equal cone angles, $\Psi_0$ (plotted from data presented by Carrel [9]).....	58

Figure 13a.	Sketch of the rays from source to field point (target). Rays are refracted into the second medium and partially reflected, $n_0 < n_1$ .....	59
Figure 13b.	Geometry for calculating Sommerfeld interface transmission. In this example, the source is in denser medium with refractive index $n_0 > n_1$ .....	59
Figure 14.	Signal-to-noise ratio for a CW radar system with the following parameters: 500 MHz source; horn antennas 50.8 cm x 76.2 cm; frequency = 0.5 GHz; complex permittivity = 9-j0 for low loss curves, 4-j0.16 for medium loss curves, 9-j0.9 for high loss curves. The upper curve of each group is for a flat mine tunnel wall 1.5 m high of infinite length with water in the tunnel. The lower solid curve of each group is for a 30 cm diameter cased borehole. The dashed curve is for a water-filled borehole without casing having a 30 cm diameter. The system noise is assumed to be 8 dB greater than Johnson noise in a 1 MHz bandwidth and clutter is ignored.....	60
Figure 15.	Simulated impulse waveforms having widths of 5, 2, 1, and 1/2 ns at the 50% point.....	61
Figure 16.	Resulting spectral energy distribution of the impulses shown in figure 15 in dB relative to $10^{-9}$ volt-seconds.....	62
Figure 17.	The signals resulting from transmission of the impulses shown in figure 15 over a 1.5 meter path with the TQ antennas.....	63
Figure 18.	Simulated sinusoidal pulse waveforms having 8, 4, 2, and 1 cycles.....	64
Figure 19.	Resultant spectral amplitude of the sinusoidal pulses shown in figure 18. 8-cycle pulse, dotted curve; 4-cycle pulse, triangles; 2-cycle pulse, squares; 1-cycle pulse, solid line with no marker.....	65
Figure 20.	The signals resulting from the transmission of the sinusoidal pulse waveforms shown in figure 18 over a 1.5 meter path using TQ antennas.....	66
Figure 21.	Simulated linear chirp pulse waveforms. 250-500 MHz in 10 nanoseconds, plain curve. 250-1000 MHz in 10 nanoseconds, square markers. 250-1000 MHz in 20 nanoseconds, triangle markers.....	67
Figure 22.	Resulting spectral amplitudes of the linear chirp pulse waveforms shown in figure 21. The curve markers correspond to figure 21.....	68

Figure 23.	Resulting signals after transmission of the linear chirp pulses over a 1.5 meter path using TQ antennas. The curve markers correspond to figure 21.....	69
Figure 24.	The result of transmitting a 300-600 MHz linear chirp pulse over a 1.5 meter path using the TQ antennas .....	70
Figure 25.	The result of autocorrelation of the waveform of figure 24 .....	71
Figure 26.	Autocorrelation of the transmitted waveform of the 4 cycle 250 MHz sinusoidal pulse.....	72
Figure 27.	Simulated response in relatively damp coal for a 15 cm radius hole at 1 meter range. (1) cased hole, (2) air-filled hole, (3) water-filled hole.....	73
Figure 28.	Simulated response in relatively damp coal for a 15-cm radius hole at a range of 1 meter (1), 2 meters (2), and 5 meters (3). The amplitude of the response at 5 meters has been amplified 50 times.....	74
Figure 29.	Simulated radar response in relatively damp coal for a 1.0 volt, 1 nanosecond input pulse reflected from a borehole. The given dimension is the borehole radius.....	75
Figure 30.	Simulated radar response in relatively dry coal for a 1.0 volt, 1 nanosecond input pulse reflected from a borehole. The given dimension is the borehole radius .....	76
Figure 31.	Preprototype pulse system block diagram.....	77
Figure 32.	Output waveform of the high-voltage impulse generator.....	78
Figure 33.	NSB range for subsurface anomaly measurements.....	79
Figure 34.	Pulse system response averaged over a sequence of 26 measurements (1). Single response from over the 0.6 meter deep air-filled target (2). The resulting response showing the target signal enhancement (arrow) obtained by subtracting sequence average from the response at one position (3).....	80
Figure 35.	A stacked series of modified responses obtained by subtracting the average response of the series from each measured response. Target signal at arrow.....	81



## MICROWAVE DETECTION OF LOST OIL WELLS AND UNKNOWN WATER-FILLED VOIDS IN COAL MINES

D. R. Belsher (retired), R. H. McLaughlin,  
A. G. Repjar, H. E. Bussy (retired)

Interference Characterization Group  
Electromagnetic Fields Division  
National Bureau of Standards  
Boulder, CO 80303

### 1. INTRODUCTION

This is the final report for work (Phase II) carried out by the National Bureau of Standards (NBS) under contract H0272007 with the Bureau of Mines.

Many thousands of oil wells pass through the coal beds of the United States. Of these, a very large number are in active underground coal mining areas. The casings of these wells are found, when possible, on the surface, and their underground positions are determined from drilling data or costly well-logging techniques. Many of these wells were drilled and abandoned years ago and are often impossible to locate at the surface. The drilling logs for those that can be located at the surface often do not exist. These "lost" wells are believed to have caused some major coal mine explosions. Some coal mine explosions have resulted in the loss of over a hundred lives in a single catastrophic event. The hazard is produced when the cutter teeth of a mining machine contact and penetrate a steel well casing. The resulting sparks can easily ignite the casing gas and the coal gas and dust present at the mining face. Where the location of a well casing is known, the law requires a coal pillar to be left surrounding the underground position. Even wells whose positions are known both on the surface and underground may be penetrated when new or inexperienced personnel misjudge their underground positions. The underground position of a cased well is often different from the surface position since many wells are not drilled vertically. As a result, mine managers must constantly check for any one of the many thousands of lost or undocumented cased and uncased wells.

Flooding is another coal mine hazard. Experience has shown that flooding generally occurs when coal is mined within approximately 3 m (10 ft) of a flooded area in a previously worked mine. Severe flooding can also occur by cutting into a water-filled well. This happens even when 6.10 m (20 foot) horizontal drilling guidelines are followed and mining is restricted to more than 15.3 m (50 feet) from old workings. Testing for old workings by drilling is often a cause of dangerous flooding since the drill hole can easily be enlarged by water flow. Also, old workings can be missed when mining personnel test by drilling.

A microwave technique appears to offer an excellent chance for success in detecting voids and well casings to ranges of 15 m (50 feet) or more. All of the prominent microwave techniques have potential advantages over other techniques in that:

- (1) The antenna need not physically contact the working face;
- (2) the antenna can be mounted on room and pillar mining machinery, or on longwall mining machinery, or it can be hand carried;
- (3) measurements can be made quickly with minimum interference to production; and
- (4) data can be analyzed and made available for immediate use by production personnel.

It was felt that the maximum benefit, for the available time and money provided in Phase I of this work, would be achieved by improvements in the antennas which would be useful for any microwave system. Accordingly, in Phase II of this work, the goals were to provide additional antenna improvements and to assemble a pre-prototype impulse radar system for delivery to the Bureau of Mines. Additional effort has been expended on studies of potential range (see section 4) and a study of dielectric loading of antennas (see section 3). A short comparison study of possible pulse types useable in underground radar has been included (see section 5). The general layout of the prototype impulse system is described.

## 2. ANTENNA CHARACTERISTICS

### 2.1 Antenna Construction

During Phase I of this contract, a broadband, TEM-type antenna was developed. Designated the NBS-TG, it consisted of two tapered leaves and had an impedance which varied exponentially from 50 ohms at the feed to 377 ohms at the aperture. The antenna has been improved by encasing it in a shielded enclosure and is now known as the NBS-TQ. This shielding improves the front-to-back ratio as well as the isolation when the antennas are used bistatically. Shielding was added by placing the antenna in a metal box having an aperture at the open end of 50 cm by 80 cm. The box was 63 cm deep and was lined with a 3/4-inch thickness of a commercially available conductive foam to suppress surface currents in the box. Additionally, two sheets of resistive material (approximately 100 ohms per square) 8 cm wide by 15 cm long were riveted to the tips of the antenna halves. The resistive sheets were not terminated on the box but were spaced away from the metal. The resistive strips were added to provide lower reflections at the aperture. Figure 1 shows a comparison in the time domain of the reflections due to the NBS-TQ antenna without the resistive material, curve (1) and the same antenna with the resistive material added, curve (2). Notice that the right-hand peak, which is the aperture reflection, is much reduced. The incident signals were 1/2 ns duration impulses of equal amplitude.

The antenna feed is by way of a type N feedthrough connector at the box and a 0.6-m length of RG-58 coaxial cable connected to the antenna using an SMA connector. The remaining space in the shielding box is filled with low density styrofoam to completely fill the box and support the antenna firmly in position. The aperture was covered with sheet plastic and sealed with heavy-duty tape.

## 2.2 Antenna Response

The measured transmitted pulse response, using an electrically small resistive dipole as a standard receiving antenna, of both the NBS-TG and the NBS-TQ antennas is compared in figure 2. It is obvious that the isolating box does introduce some changes in the transmitted waveform, but the reduction in transmission to the sides and back should make the overall system performance much better.

Unless otherwise noted, all measurements shown were made with the equipment described in the Phase I Final Report for this contract. That system included a commercially available digital-processing oscilloscope and an NBS-constructed impulse generator having a 45-volt amplitude into 50 ohms and 1/2-ns width (FWHM--full width, half maximum, or 50% amplitude points).

## 2.3 Antenna Pattern

A comparison of the forward and reverse transmitting transfer function amplitudes with the probe at a 3/4 m distance from the nearest antenna surface of the NBS-TG and the encased version, the NBS-TQ, is shown in figure 3. The transmitting transfer function characterizes the electromagnetic fields which are generated at a given distance by a known signal applied at the feed and has the units of volts/meter/volt. This concept is discussed in reference [3]. The front-to-back ratio for the NBS-TG is approximately 1; so even with some reduction in forward signal, the improvement in front-to-back ratio for the NBS-TQ is quite worthwhile. The improvement in front-to-back ratio is very important for use in the close confines of a mine and especially where noisy and highly reflective mining machinery is present. Thus, this task was given high priority.

## 2.4 Isolation in the Bistatic Configuration

A pair of the NBS-TQ antennas were mounted with the E-field directions parallel. They were then tested with different spacings between the antennas, different baffle configurations between the antennas, and different standoff distances from material surfaces. The results of this work generally showed that an optimum spacing between antennas should be about 36 cm with a baffle centered between the antennas and extending about 68 cm to the front. The most effective baffle tested consisted of a thin dielectric material (1/4-inch plywood) with a sheet of absorber glued to both sides (see figure 4). A metal baffle gave more isolation between antennas, but interacted with the antennas and the ground to give other responses which were undesirable.

## 2.5 Operation Close to Surfaces

For operation near a coal face, for example, the antennas should change their characteristics as little as possible as the surface is approached. This means that the effect of variations in spacing from the coal surface encountered during use will not be a source of confusion. If the antenna performance is insensitive to distance from the coal face, it is possible, as a first step in processing the measurement data, to subtract a background signal which is common to the system. The background signal can be obtained by pointing the antenna pair at the sky in a position where it is not near reflecting objects. Figure 5 shows a comparison of the response of the TQ antenna pair with the baffle pointed at the sky with the response from a metal plate. Figure 6 shows how this same system sky response may be subtracted from a ground signal to yield an enhanced response from a buried target. It can be noted that even though the target response (see arrow) is down in absolute amplitude, its relative amplitude increase makes it visually more obvious in the corrected waveform.

## **3. POTENTIAL FOR DIELECTRIC LOADING OF ANTENNAS**

The infinite "bow-tie" antenna belongs to the frequency independent class of antennas because its shape is defined entirely by angles [1,2]. As a result, its impedance, polarization, pattern, etc., are independent of frequency and the antenna is said to be broadband. The characteristics of such broadband antennas are necessary for accurate impulsive electromagnetic field measurements [3] which can be used for the detection and analysis of prominent features in a geophysical environment [4].

The overall purpose of this section is to investigate the characteristics of a practical, i.e., finite, bow-tie antenna with the following specifications. The antenna should be broadband, matched to a 50-ohm source line, and have some directionality [5,6]. The frequency range of interest for this study is specified to be from 10 MHz to 1 GHz. To achieve these goals, considerations are given to dielectrically filling the antenna which also increases its electrical size [5]. Resistively loading the antenna to achieve broadbanding from 500 MHz to 1 GHz is currently being studied at NBS [7,8].

First, the characteristics of the infinite bow-tie antenna as a function of its shape [2,9] will be presented. Also, the effect of a dielectric medium on its electrical properties is shown. Next, the "finite" bow-tie antenna is considered, followed by a discussion on dielectrically loading antennas. By the use of non-symmetrical dielectric loading, a directional bow-tie antenna is then investigated. Finally, conclusions and recommendations are presented.

### 3.1 Infinite Bow-Tie Antenna

The problem of finding the characteristic impedance,  $Z_0$ , of an antenna consisting of two infinitely long conical conductors which have a common apex has been solved by Carrel [9]. The examples presented include the coaxial biconical antenna [10], the non-coaxial biconical antenna [11], the coplanar fin antenna, and the non-coplanar fin antenna. The infinite bow-tie antenna



can be simply treated as a special case of either of the latter two examples. See figure 7. Due to recent interest in TEM horns [7], it is appropriate to consider the infinite bow-tie antenna as a special case of the non-coplanar fin antenna (see figure 7). The solution for the characteristic impedance,  $Z_0$ , is given by

$$Z_0 = \eta K/K' \quad (1)$$

where  $\eta = \sqrt{\frac{\mu}{\epsilon}}$ , the intrinsic impedance of the medium between the conductors. Here, it is only necessary to mention that  $K$  and  $K'$  are the complete elliptic functions and inevitably depend only on the angles  $\psi_0$  and  $\theta_0$  defined in the figure.  $\mu$  and  $\epsilon$  are, of course, the permeability and dielectric constant of the medium, respectively.

In figure 8, the characteristic impedance of the non-coplanar fin antenna with equal fin angles is given as a function of  $\psi_0$  and  $\theta_0$ . For the infinite bow-tie antenna,  $\theta_0 = 180$  degrees. It should be noted that the values obtained from figure 8 are for an antenna in free space which has a dielectric constant,  $\epsilon_0$ .

In a dielectric medium with a relative dielectric constant,  $\epsilon_r$ , the characteristic impedance,  $Z_0(\epsilon_r)$ , is

$$Z_0(\epsilon_r) = \frac{Z_0(\epsilon_0)}{\sqrt{\epsilon_r}} \quad (2)$$

where  $Z_0(\epsilon_0)$  is the characteristic impedance in free space.

It is apparent that the characteristic impedance of an infinite bow-tie antenna thus depends on both the fin angle,  $\psi_0$ , and the dielectric constant,  $\epsilon_r$ . These factors should be considered when matching the antenna to a 50-ohm source line and/or a dielectric medium.

### 3.2 Finite Bow-Tie Antenna

The input impedance equals the characteristic impedance for the infinite bow-tie antenna and for the infinite biconical antenna [12]. However, the theoretical input impedance has only been obtained for the "finite" biconical antenna. For the finite biconical antenna whose half-angle,  $\psi_0$ , is less than about 3 degrees, the input impedance has been calculated [12]. For the wide-angle biconical antenna, the input impedance has been calculated [12, 13]. For these cases, it is significant that the wider biconical antenna has not only a lower characteristic impedance, but also an input impedance that is more constant as a function of cone length than the narrower antenna (see figure 9). From this result, it has generally been concluded that wider antennas are more suitable for broadband application. To further substantiate this trend, Kraus shows that, for cones with half angles of 5°, 10°, 20°, and 30°

[12] and characteristic impedances of 188, 146, 104, and 80 ohms, respectively, the input impedance variation reduces with increasing cone angles (see figure 10). It also appears evident that the input impedance varies about the characteristic impedance, as is further seen in figure 11. The existence of these factors should be determined by measurement for the finite bow-tie antenna so that matching to a 50-ohm source line may be accomplished. It should be noted that the results in [12] and [13] are for the cases where the lower cone is replaced by a ground plane. Hence, the impedance values are half of those which would be obtained for the biconical antenna. For reference, the characteristic impedance of the infinite biconical antenna with equal cone angles is given in figure 12.

### 3.3 Dielectrically Loaded Antennas

The basis for determining the characteristics of the bow-tie antenna in the presence of a dielectric has, in part, been discussed earlier in this section. To extend this basis, it is appropriate to study the cases where either a dipole [14] or biconical antenna [15] is imbedded in a spherical dielectric of radius  $a$ , since the case for the bow-tie antenna has not been solved. By letting  $a$  approach infinity, one could then study the effect of matching the dielectric filling to the dielectric medium [16].

For the above cases, consider the dielectric sphere to have a dielectric constant,  $\epsilon_1$ , and let the dielectric constant of the medium be  $\epsilon_2$ . For the dipole case and for  $k_1a$  and  $k_2a \ll 1$ , the radiation resistance decreases as  $\epsilon_1$  increases [14]. However, the radiation power factor, which denotes the available product of bandwidth and efficiency [14,17], increases only slightly for  $1 < \epsilon < 4$ , where  $\epsilon \equiv \epsilon_1/\epsilon_2$ , and decreases for larger values of  $\epsilon$ . Over the range  $1 < \epsilon < 4$  the radiation resistance decreases by a factor of 4. Hence, although the resistance can be varied to possibly match to a 50-ohm line, which is in itself desired, one might not expect a significant increase in bandwidth.

For the wide-angle biconical antenna and for  $k_1a$  and  $k_2a \ll 1$ , the radiation power factor decreases as the dielectric loading,  $\epsilon$ , increases [15]. Also the conductance is independent of  $\epsilon$ . It should be pointed out that the above results assume the electric field to be tangential to the dielectric boundary. However, these results, along with those for the dipole case, may be indicative of what to expect for the bow-tie antenna; that is, that the power factor may not significantly increase and the radiation resistance may decrease as  $\epsilon$  decreases. Dielectric loading may not offer a significant improvement in antenna performance unless the antenna can be placed in contact with the medium of interest--the coal seam in this case.

### 3.4 Directional Bow-Tie Antenna

Lytle [6] has shown that a miniaturized directional antenna can be obtained by placing sources offset in material with a high dielectric constant. In a similar manner, one could offset the bow-tie antenna in a dielectric sheet such that the radiation would be maximized in one-half plane and would be minimized in the other half plane. In principal, the wavelength in the dielectric material,  $\lambda_1$ , is

$$\lambda_1 = \frac{\lambda_2}{\sqrt{\epsilon}} \quad (3)$$

where  $\lambda_2$  is the wavelength in the medium and  $\epsilon = \epsilon_1/\epsilon_2$ , where  $\epsilon_1$  and  $\epsilon_2$  are the dielectric constants in the material and medium, respectively. Hence, by offsetting the antenna from one side of the dielectric sheet a distance  $d_1$ , such that  $d_1 = (2\ell + 1) \lambda_1/4$ ,  $\ell$  an integer, and requiring the width of the material to be such that the antenna is a distance,  $d_2$ , from the other side, where  $d_2 = n\lambda_1/2$ ,  $n$  an integer, one would maximize the radiation on the former side and minimize the radiation on the latter side. This design can only be optimized over a narrow bandwidth using frequency independent dielectrics. Further work is required in order to develop dielectrics or ferroelectrics which have dielectric constants inversely proportional to the square of frequency over the bandwidth of interest.

### 3.5 Conclusions and Recommendations

The input impedance of an infinite biconical or infinite non-coplanar fin antenna, which may be an infinite bow-tie as a limiting case or an infinite TEM horn, depends only on the angles defining the antenna and on the permeability and dielectric constant of the medium. When these antennas become finite, it appears that the input impedances of the wide-angle antennas are more constant as a function of frequency than are narrow-angle antennas and vary about the characteristic impedance. Such antennas, which include the wide-angle bow-ties, are considered to be broadband.

By enclosing the bow-tie antenna in a sheet of dielectric, one may increase the directionality of the antenna in a given band of frequencies, but the radiation resistance may decrease as the dielectric constant increases.

Based on the above, one can design either a wide-angle TEM horn or bow-tie antenna such that the input impedance is known within bounds for a given dielectric medium. Thus, one can optimize the antenna so that its input impedance can be matched to a 50-ohm source to maximize power transfer. Using dielectric media such as air and water, it is recommended that the theory be verified to determine its applicability. In particular, the input impedance for the antenna in both media should be measured over the frequency range from 10 MHz to 1 GHz. It would then be feasible to increase the directionality of

the antenna over a frequency range by enclosing the antenna in a dielectric sheet. The accuracy of the theory could be verified and the bandwidth of the antenna immersed in the dielectric sheet could be compared to those obtained for the infinite media.

The above recommendations could effectively be accomplished by using image theory and performing the experiments using a ground plane, thereby avoiding the use of a broadband balun, which can be a drawback for precise and accurate measurements.

#### 4. SUBSURFACE RADAR RANGE LIMIT STUDY

##### 4.1 Introduction

This section gives theoretical estimates of the radar range limit of buried targets. Cook, in 1974 and 1975 [18,19], investigated the subject. The main parameters of the radar range equation are discussed, and the detection range is found with appropriate receiver noise assumed and no clutter.

The theory needs to be augmented by practical experience with "radar clutter," i.e., reflections from miscellaneous targets. This clutter is rather analogous to precipitation and atmospheric turbulence clutter during aircraft detection. The coal "atmosphere" has inhomogeneities that may act as false targets, giving clutter.

The desired targets considered are a borehole and a mine tunnel. The radar cross sections of these targets are obtained by suitable modifications of known theory for homogeneous dielectric and metallic cylinders and for a strip approximating an old workings tunnel. An outline of this section is as follows: The radar signal equation is given which contains the source power, the antenna gain and area, the dielectric loss, interface loss, and inverse distance loss of propagation in the medium, and the radar cross section of the target. Cross sections for the targets of interest are derived in some detail, including new results for cross sections that depend on range. Finally, with assumed system parameters, including the noise figure, the radar range equation is solved (Appendix A).

##### 4.2 The Radar Equation

The radar equation is developed in many radar books, e.g., Berkowitz [20]. In our application, the radar back scattered received signal power in a homogeneous lossy atmosphere (the coal) is calculated as

$$S = \frac{PG_1}{4\pi R^2} \frac{\sigma}{4\pi R^2} \frac{\lambda_0^2 G_2}{4\pi} I C_d D e^{-4\alpha R} \quad (4)$$

where

- $P$  = emitted power during the rf pulse, or the effective power level of the "continuous" wave of an FM-CW radar, watts,
- $G_1, G_2$  = gains of transmitting and receiving antennas (gains may differ from specifications if target is closer than  $\text{diam}^2/\text{wavelength}$ ),
- $\sigma$  = target radar cross section area,
- $\lambda_0$  = wavelength of EM wave in air,
- $\alpha$  = attenuation coefficient of the EM field due to the material dielectric, loss specifically,  $\alpha$  = the real part of  $(-\omega^2\mu\epsilon)^{1/2}$  where  $\omega$  is the radian frequency and  $\mu$  and  $\epsilon$  are the magnetic permeability and electric permittivity of the material,
- $\epsilon$  =  $\epsilon_0(\epsilon' - j\epsilon'')$ , where  $\epsilon_0$  is the permittivity of vacuum, and  $\epsilon'$ ,  $\epsilon''$  are the real and imaginary parts of the relative complex permittivity  $\epsilon^* = \epsilon' - j\epsilon''$  (with  $\exp(+j\omega t)$  time dependence), and  $n \cong \sqrt{\epsilon'}$ , a useful refractive index for finding  $\theta$  in Snell's law.
- $I$  = the reflection power loss at the air-to-material interface counting both the entrance and the exit of the radar beam,
- $D$  = a dispersion effect which arises only from the broadening and consequent decrease in height of the signal pulse due to dielectric dispersion in the medium. An extended target (noncompact) may broaden the pulse. The radar antennas and components may disperse the pulse. Both of these effects are included in the FFT synthetic pulse calculations in section 5 and are not included in  $D$ ,
- $R$  = range, distance from radar antenna to target,
- $R_1$  = the part of the range distance that is in the coal,
- $C_d$  = convergence-divergence product to give the change of the signal  $S$  due to refraction of the incident and the target returned signals through the interface.

In (4), the first fraction is the power density at the target and the second fraction is the returned power density at the radar, both in assumed free space. The third fraction is the receiving area of the radar. The terms  $I$ ,  $C_d$ ,  $D$ ,  $\exp(-4\alpha R_1)$  represent various losses due to the ponderous medium and interface.

In the remaining discussion, the case of  $R_1 \neq R$  will be recognized only for the factors  $D$ ,  $C_d$ , and  $\exp(-4\alpha R_1)$ .

Separation of the attenuation,  $\exp(-4\alpha R_1)$ , from the dispersion effect,  $D$ , is an approximation. In section 5, these factors are taken into account by convolving the impulse response of the dispersive medium with transmitted and reflected pulses.

### 4.3 Interface Transformation Factors, $I$ $C_d$

Factors of the interface problem are obtained by what is often called Sommerfeld's method for a dipole in a half space. Hufford, in 1969 [22], gave a rigorous derivation and practical results for the far field (obtained by geometrical optics) and for the ground wave, both in the air half space with a buried electric or magnetic dipole source. The treatise by Baños [34], is detailed; see especially his "Expansions valid over an entire hemisphere." Brekhovskikh's 1980 treatise [35] is useful because, with the source in either space, it gives specific equations for the geometrical optics term, the ground wave term, and a third term--the lateral wave. One of the authors of this report (HEB) has extended the geometrical optics solution to all ranges, from the interface to infinity in the refracted beam (as was necessary because the target was usually quite near the interface). Although our solution looks different, it agrees exactly with Brekhovskikh's first term.

Our solution will be briefly developed for an isotropic point source of power in a half space and assuming classical geometrical ray optics with energy conservation in the reflected and refracted ray-bundles (infinitesimal solid angles) of the problem--see figure 13. Finally, to get the radar factors  $I$  and  $C_d$  of equation (4), the results must be applied twice. The point source in air transmits to the target which then transmits back to the radar.

The geometry of the problem in a spherical coordinate system is completely specified by assigning  $z_0$ , the perpendicular distance from the source to the interface,  $n_0$  and  $n_1$  the refractive indices of the source space and the other half space, respectively, and the location of the receiving point (field point) at a distance,  $z_1$ , from the interface and  $\rho_1$  from the  $z$  axis. From Snell's law, the ray paths are found giving the angles  $\theta_0$  and  $\theta_1$ , and  $r_0$  and  $R_1$ , the distances from the source to the point of refraction and from there to the field point, respectively. The source power is denoted as  $W_0$  watts. The power density at distance  $r_0$  is  $s_0(r_0) = W_0 / (4 \pi r_0^2)$   $W/m^2$  in homogeneous space.

Now consider the power transport by the rays in an infinitesimal solid angle,  $d\Omega_0$ , at incidence angle,  $\theta_0$ , that will refract to the target. The incident rays from the source are homocentric. Therefore, the power flow in the solid angle is  $dW_0 = s_0(r_0) r_0^2 d\Omega_0$  at distance  $r_0$  as it intersects the interface. Note that the E-field rms magnitude may be obtained from  $s_0 = E_0^2 n_0 Y_0$  where  $Y_0$  is the wave admittance of the vacuum. The transmitted power of the refracted rays is the incident minus the reflected power. Thus,

Fresnel's interface reflection coefficient,  $\Gamma$ , gives the power transmission coefficient,  $(1 - |\Gamma|^2)$ . The power density,  $s_1$ , of the refracted beam based on energy conservation is expressed as

$$s_1(R_1) d\sigma_1(R_1) = s_0(r_0) d\sigma_0(r_0) (1 - |\Gamma|^2) , \quad (5)$$

where  $d\sigma$  is the area of a solid angle at the distance indicated.

It remains to find  $d\sigma_1$  of the refracted beam. The solid angle of an incident beam element at angle  $\theta_0$  may be written in spherical coordinates as

$$d\Omega_0 = \sin \theta_0 d\phi_0 d\theta_0 ,$$

where  $\phi$  = azimuthal angle and  $\theta$  = polar angle.

For the refracted rays by symmetry,  $d\phi_1 = d\phi_0$  and by Snell's law

$$d\theta_1 = (n_0/n_1) \cos \theta_0 d\theta_0 / \cos \theta_1 .$$

However, to find the area of the refracted beam, we must recognize the astigmatism of the refraction. At distance  $R_1$  in the solid angle  $d\Omega_1$ , the range distance back to the apparent source of the ray bundle in medium 0, as determined by tracing back two rays diverging by  $d\phi_1 \equiv d\phi_0$ , is  $R_1 + r_1$  where

$$r_1 = r_0 n_1 / n_0 .$$

(From this we find that the origin of the segment  $r_1$  is a point on the  $z$  axis.) Therefore, one dimension of the refracted solid angle,  $d\Omega_1$ , is

$$(R_1 + r_1) \sin \theta_1 d\phi_1 .$$

The range distance to an apparent source point as determined by tracing back two rays diverging by the angle  $d\theta_1$  is  $(R_1 + r_2)$  where

$$r_2 = r_1 (\cos \theta_1 / \cos \theta_0)^2 .$$

The cross-section area of the refracted rays is then obtained at any distance,  $R_1$

$$d\sigma_1(R_1) = (R_1 + r_1) (R_1 + r_2) \sin \theta_1 d\phi_1 d\theta_1 . \quad (6)$$

Finally, substituting into (5), including Fresnel's  $\Gamma$ , we find the transmitted power density,  $s_1$ ,

$$\frac{s_1(R_1)}{s_0(r_0)} = \frac{r_0^2}{(R_1 + r_1)(R_1 + r_2)} \frac{n_1^2 \cos \theta_1}{n_0^2 \cos \theta_0} \frac{4 n_0 n_1 \cos \theta_0 \cos \theta_1}{(n_0 \cos \theta_0 + n_1 \cos \theta_1)^2}_{\text{TE}} \quad (7)$$

where TE denotes the TE mode, i.e., when the E-field is parallel to the interface. For the TM mode, replace the TE quantity by

$$(n_0 \cos \theta_1 + n_1 \cos \theta_0)^2_{\text{TM}} .$$

Equation (7) may be evaluated at the interface  $R_1 = 0$ . It reduces to

$$|E_1(R_1 \rightarrow 0)/E_0(r_0)| = 2 n_0 \cos \theta_0 / (n_0 \cos \theta_0 + n_1 \cos \theta_1)_{\text{TE}}$$

and, similarly, for the TM mode, both agreeing exactly with Fresnel's interface transmission coefficients (Stratton, 1941) [36].

We will show next that (7) reduces to Hufford's far-field solution as  $R_1$  tends to  $\infty$ . First, we must renormalize (7) to Hufford's reference field,  $E_f$ . The field,  $E_f$ , is defined as the field that would exist at the receiver from the isotropic power source,  $W_0$ , if all space were homogeneously filled with the material having refractive index  $n_1$ ,

$$E_f^2(r) = W_0 / (4 \pi r^2 n_1 \gamma_0) , \quad (8a)$$

and  $r$  is the direct distance from the source to the receiving point. The incident  $E_0^2$  and  $s_0$  have already been defined in terms of  $W_0$  and  $r_0$ . After taking the square root of (7) with  $R_1 = \infty$ , which makes  $r = \infty$ , and replacing  $E_0(r_0)$  by  $E_f(r) (r/r_0) (n_1/n_0)^{1/2}$ , we have

$$\left| \frac{E_1(R_1)}{E_f(r)} \right| = \frac{2 n_1^{3/2} \cos \theta_1}{n_0^{1/2} (n_0 \cos \theta_0 + n_1 \cos \theta_1)_{\text{TE}}} . \quad (8b)$$



For the TM mode, use  $(n_0 \cos \theta_1 + n_1 \cos \theta_0)_{TM}$ . Equation (8b) agrees exactly with Hufford's far-field result for his interface transmissions  $|L C_e|$  and  $|L C_m|$  (TE and TM) when specialized to his case; namely,  $n_1 = 1$  in the air and  $n_0$  is of the dense material in which the source is buried. Also, Hufford obtained  $(\text{Re } n_0)^{1/2}$  instead of our  $n_0^{1/2}$  and he gave the phase of  $E_1/E_0$ . Having started with power densities, we lose the phase and must assume the dielectric loss tangents are less than 0.1 to yield square roots of  $n_0$  and  $n_1$  with less than 1% error.

The following tabulation gives computer results for  $|E_1(R_1)/E_f(r)|$  (found from equations (7) and (8a), valid at any value of  $R_1$  consistent with  $z_1 > \lambda_1$ , the wavelength in medium (1), of figure 13, and also gives results for Brekhovskikh's  $\Psi(R_1)$  multiplied by  $r$ --the distance defined in  $E_f$ , equation 8a. Reciprocal paths were calculated. The fields,  $\Psi_1$ , exhibit reciprocity as expected. The last column shows that  $|E_1/E_f/\Psi(R_1)| = (n_1/n_0)^{1/2}$ .

---

$n_0/n_1$	$\theta_0$	$r_0, R_1$	$ E_1/E_f $	$r\Psi(R_1)$	$E_1/(E_f r \Psi(R_1))$
2	20.7°	1, 1	0.546	0.7724	0.707
1/2	45°	1, 1	1.092	0.7724	1.414
2	20.7°	5, 1	0.788	1.115	0.707
1/2	45°	1, 5	1.577	1.115	1.414

---

The refraction contributes divergence when  $n_0/n_1 > 1$  and convergence when  $n_0/n_1 < 1$ . Hufford's normalization is especially appropriate for practical calculation because  $|E_1/E_f|^2$  is the power loss (or gain) of the interface.  $|E_1/E_f|$  correctly changes value accordingly as divergence or convergence, d or c, occurs. The separate factors I and  $C_d$  are given, respectively, by  $(1 - |\Gamma|^2)^2$  (which is the last fraction in (7) squared) and by the first two fractions in (7) evaluated in each direction and multiplied. The total interface radar power transfer is

$$I C_d = |E_1/E_f|_d^2 |E_1/E_f|_c^2, \quad (8c)$$

evaluating equation (7) first with subscript 0 denoting parameters in the denser medium and 1 denoting the rarer medium, convergent case, and then again with all parameters interchanged, divergent case. For the above example, where  $r_0$  and  $R_1$  are 1, 5 and then 5, 1 on return, the value of  $IC_d$  is ~ 1.545, using the table.

Summarizing, we have developed a convenient expression for Sommerfeld's geometrical optics term which is valid from the interface,  $R_1 \cong \lambda_1$  to  $R_1 = \infty$ . The ground and lateral wave terms have not been included, a valid approximation when  $\theta_0$  and  $\theta_1$  are small and  $z_0$  and  $z_1$  are greater than  $\lambda_0$  and  $\lambda_1$  in the two media. However, when the source is at or on the interface, Engheta, [37] and Lewis [38] have demonstrated large correction of the optical term.

Our expression for this area in the refracted beam seems to be new, but agrees with Brekhovskikh. His area term is somewhat reminiscent of an equation in optics for the caustic which gives the location of the origin of our segment,  $r_2$ , cf. Martin and Welford [39]. Their equation is  $ax^{2/3} + by^{2/3} = 1$  in a Cartesian system, where  $a$  and  $b$  are functions of  $n_0$ ,  $n_1$ , and  $z_0$ .

Our caustics may be described as follows: The origin of  $r_1$  is in medium 0 on the  $z$ -axis at a distance

$$z_1 = z_0 \tan \theta_0 / \tan \theta_1$$

from the interface. The origin of  $r_2$  is found by tracing the refracted ray at angle  $\theta_1$  backward into medium 0 a distance

$$r_2 = r_0 (n_1/n_0) (\cos \theta_1 / \cos \theta_0)^2 .$$

These equations hold no matter which medium contains the source.

#### 4.4 Attenuation in the Medium

The term  $\exp(-4\alpha R_1)$  gives the power loss in the medium during the round trip. The factor  $\alpha$  is the attenuation factor of the propagation constant in the medium,

$$\alpha + j\beta = (-\omega^2 \mu \epsilon)^{1/2} . \quad (9)$$

A good approximation for coal media at frequencies of interest is

$$\alpha \cong 0.5\beta \epsilon'^{1/2} \tan \delta \quad (10)$$

where  $\tan \delta = \epsilon''/\epsilon'$  for the medium, and  $\beta_0 = \omega (\mu_0 \epsilon_0)^{1/2}$ , the phase factor of free space. The error of the approximation, (10), is proportional to  $0.5 \tan^2 \delta$  if  $\tan \delta < 0.1$ .

Section 5 uses exact complex scattering coefficients of a homogeneous cylinder to obtain exact synthetic pulse computer predictions of signatures of the various cylinders. Synthetic pulse trials also allowed the factor D of eq (4) to be estimated by comparing the pulses in dispersive coal and fictitious nondispersive coal. From this we chose a very approximate value of  $D = 0.5$ , for a range sufficiently large to bring S/N down to approximately 2. (To a good approximation, D is proportional to  $d\epsilon'/d\omega$  in the radar frequency band, and to range  $R_1$ . Lynch [42] approximates  $d\epsilon'/d\omega$  as proportional to  $\tan\delta$ .)

#### 4.5 Radar Range Calculation from S/N

The ultimate radar range may be defined by setting the signal power, S, of equation (4) equal to the noise power, N, of the radar receiver

$$S/N = 1, \quad (11)$$

and solving for R.

The noise power must be suitable for the type of radar, detection method, search method, time duration of display, etc. However, we will use the noise power often given for common rf pulse radar,

$$N = kTB NF \quad (12)$$

where the Boltzman constant,  $k = 1.38 \times 10^{-23}$  watt/Hz Kelvin,  $T =$  temperature = 290K,  $B =$  receiving bandwidth in Hz, and  $NF$  is the multiplicative noise figure. We have used  $NF = 6.31$ , which is 8 dB. This figure is somewhat higher than that for well designed systems where 4 dB to 5 dB might be attained. The noise figure theory is discussed in Mumford and Scheibe [23]. For baseband pulse radar, the S/N may be obtained using the reflected pulse voltage, S, divided by the rms noise voltage, N, of the usual A-scope presentation. By signal processing, S/N can be enhanced by integration over many pulses with a sampling scope. The latter method may detect a signal smaller than noise, but may require a significant amount of time depending on the pulse repetition rate, pulse broadening by dispersion, and volume in the earth to be examined.

#### 4.6 Radar Cross Section

The factor  $\sigma$  is given by the equation (Bowman, Senior, and Uslenghi, equation I.30) [24],

$$\lim (R \rightarrow \infty) \sigma |E_i|^2 = 4\pi R^2 |E_s|^2, \quad (13)$$

where  $E_i$  is the field strength of the wave incident on the target and  $E_s$  is the field strength of the scattered field at the receiving antenna.  $R$  is the separation distance of the target and radar.  $E_s$  must be either calculated or measured. Approximate calculations for a borehole and dielectric strip are given in sections 4.7 through 4.14 and used in Appendix A. (Exact cylinder scattering was used in section 5.)

The use of  $\sigma$  in (4) is simply a way of stating the value of  $|E_s/E_i|^2$  of the target. The use of  $\sigma/4\pi R^2$  in (4) requires the  $\sigma$  defined in (13). The so-called cylinder cross section,  $\sigma^c$ , cannot be used directly, even for a cylinder, in solving equation (4).

Values of  $\sigma$  are often available based on the theory of a plane wave, the source at infinity. As will be discussed, we deduce correction factors of 0.5 and 0.25 to the theoretical  $\sigma$  of infinite cylinders and an infinite plane, respectively, when the source is at a finite distance as for practical radar.

#### 4.7 Electromagnetic Theory of Scattering Cross Sections of Extended Targets

The radar cross section in (4) and (13) may be essentially constant, i.e., independent of range,  $R$ , for compact targets. Then, e.g.,  $\sigma$  of a large metal sphere is  $\pi r^2$ ,  $r$  = sphere radius  $R \gg r > \lambda$ . For a general convex, large, compact metal body

$$\sigma = \pi r_1 r_2,$$

where  $r_1$  and  $r_2$  are the two radii of curvature at the reflection point.

For extended bodies, however, the cross section is usually a function of the range distance,  $R$ . For example,  $\sigma$  of an effectively infinite planar metallic interface is  $\pi R^2$ . With this cross section, the signal in (4) decays as  $R^{-2}$ , instead of  $R^{-4}$  as for compact targets. Cook [19] deduced  $R^{-3}$  dependence, qualifying it as being only for a rough surface.

The references on radar cross sections, (Berkowitz, p. 556) [20], (Kerr, sect. 6.2) [25], (Ruck) [26], and the basic EM scattering treatises, e.g., (Bowman, Senior and Uslenghi) [24], do not specifically give these range-dependent cross sections. The basic theory is the basis for the cross sections that we will give for cylinders representing boreholes, and for strips representing old workings tunnels. The purpose here will be to obtain theoretical values for such targets, including the necessary range dependence. Tarantolo and Unterberger [27] deduced a dependence on range, beamwidth, and pulse length. Our results differ from theirs. In particular, the beamwidth is not a necessary parameter for usual conditions.

#### 4.8 Cross Section of a Planar Interface

Consider, as a simple example, a small radar antenna interrogating an infinitely extended flat metallic interface. The field is  $E_0$  at 1 m from the source point. The incident field at the target at distance  $R$  is then

$$E_i = E_0/R.$$

By image theory, the radar receiving antenna may be at distance  $2R$  with the interface removed. Therefore, we deduce that the received (scattered) field is

$$E_s = E_i/2 \equiv E_0/2R.$$

These fields in eq (13) give

$$\sigma = \pi R^2 \quad (14)$$

dependent on range as was stated previously.

#### 4.9 Half-period (Fresnel) Zones

Radar aspects of scattering from a plane, a strip, and a cylinder may be obtained by Kirchhoff-Fresnel-Huygens' concepts of wave surfaces and scattering surfaces as intermediate sources. There are half-period (Fresnel) zone areas on the surfaces that contribute a range of phases from zero to  $\pi$ ,  $\pi$  to  $2\pi$ , and so on. Kerr [25], section 6.2, obtained radar cross sections of plane and curved surfaces by the vector Kirchhoff-Huygens method. He states, p. 417, that Fresnel zones may be defined on reflecting surfaces.

The scalar Kirchhoff-Huygens method will be used here to obtain an approximate solution for a strip, and to obtain a rather good estimate of the difference between theoretical plane wave incidence, and practical point-source, radar cross sections. First the planar surface will be reconsidered and (14) redeveloped from diffraction theory to illustrate the Kirchhoff method.

In a Cartesian coordinate system, consider a planar reflecting intermediate surface lying in the  $yz$ -plane at  $x = 0$  with a point receiver at  $x = R$  and a point source at  $x = R'$ , both on the  $x$ -axis. The radius of the circular first half-period zone on the intermediate surface is

$$r_1 = \sqrt{R' R \lambda / (R' + R)}, \quad (15a)$$

assuming  $R, R' \gg \lambda$ . In the case of monostatic radar  $R' = R$ ,

$$r_1 = \sqrt{R \lambda/2} . \quad (15b)$$

In the case of a fictitious plane wave incident radar,  $R' = \infty$ ,

$$r_1 = \sqrt{R \lambda} . \quad (15c)$$

There are successive annular half-period zones surrounding the first zone. For more discussion see, e.g., Jenkins and White [31], chapter 18, and Kerr [25], chapter 5.

The total reflected field from a smooth flat or curved intermediate surface is almost proportional to the area of the first zone. For a planar target, the areas and consequent relative scattered fields,  $E_s/E_i$ , for monostatic and for bistatic plane wave incident radar are proportional to the circle areas,  $\pi R \lambda/2$  and  $\pi R \lambda$ , respectively, from (15b, 15c). The scattered fields proportional to these areas are (by a calculation similar to Fresnel's integrals in equation (17))

$$E_{s,m} = E_i/2 , \quad (16a)$$

$$E_{s,pwi} = E_i ,$$

where  $m$  denotes monostatic, and  $pwi$  denotes plane wave incident radar.

The interesting conclusion may be drawn that the concept of half-period zones enables us to solve, approximately, the problem of how to obtain monostatic point-source radar cross sections from known canonical plane wave incident scattering solutions, as will be further demonstrated below.

For the radar interrogation of an infinite planar interface, equations (16a) in (13) give

$$\begin{aligned} \sigma_m &= \pi R^2 \\ \sigma_{pwi} &= 4 \pi R^2 . \end{aligned} \quad (16b)$$

$\sigma_m$  here correctly agrees with equation (14).

#### 4.10 The Strip Approximation of a Tunnel

Consider next an infinitely long dielectric strip representing one side wall of an old workings tunnel. The reflection of the farther side wall of the tunnel will be discussed qualitatively later. Assume that the width of the strip is 1.5 m (5 feet), which equals 1 to 5 wavelengths in air (more in coal), for radar whose main spectrum is in the band 0.2 GHz to 1.0 GHz. With these parameters, the reflection coefficient of the assumed strip may be represented by a physical optics approximation, which means that the discontinuities at the edges of the strip are disregarded.

It is useful to discuss a metallic strip initially instead of the dielectric interface strip. When the range,  $R$ , to the radar (which is located on a normal from the center of the strip) is of the order of the strip width,  $2w$  ( $\sim 1.5$  m), of the order of a few wavelengths or less, the cross section is approximately that of an infinite planar interface, i.e.,  $\sigma \sim \pi R^2$ , from (16b). The reflection will be relatively strong at such a close distance. It may be shown by means of Fresnel integrals that  $\sigma$  will vary by about  $\pm 2.5$  dB from  $\pi R^2$ , depending on  $w/r_1$  ( $w$  = half width of strip).

The important case of the strip far from the radar, presenting a small cross section, may be solved by application of the Kirchhoff-Huygens method. Assume the width,  $2w > \lambda$ , so that the discontinuities at the edges of the strip may be neglected, and the range,  $R \gg w$ , so that the waves are approximately at perpendicular incidence over the first Fresnel zone. The results for plane wave incident (pwi) radar and for monostatic radar look the same; E-scattered is

$$E_s = E_i \frac{(1 + j)}{\lambda R} r_1^2 [C(u) - j S(u)] \quad (17)$$

where  $E_i$  is incident field,  $C$  and  $S$  are Fresnel's cosine and sine integrals (tabulated functions) and  $u = \sqrt{2} w/r_1$ . (The total phase lag of  $R' + R$  is suppressed.) For pwi radar  $R' \rightarrow \infty$  and (15c) is used. For monostatic radar  $R' = R$  and (15b) is used. For the conditions assumed, especially  $R \gg w$  which gives  $r_1 \gg 2w$ , the approximations  $C(u) = \sqrt{2} w/r_1$  and  $S(u) = 0$  hold, giving

$$|E_s/E_i|_m = \sqrt{2} w/\sqrt{\lambda R} \text{ (monostatic) } , \quad (18a)$$

$$|E_s/E_i|_{pwi} = 2 w/\sqrt{\lambda R} \text{ (pwi) } . \quad (18b)$$

These field ratios in (13) give range-dependent cross sections,

$$\sigma_m = 8 \pi R w^2/\lambda \equiv 4 k_0 w^2 R , \quad (19a)$$

$$\sigma_{pwi} = 16 \pi R w^2/\lambda \equiv 8 k_0 w^2 R . \quad (19b)$$

It may be confirmed that these results are a good approximation by suitable comparison with eq 7.4 - 17 (Fig. 7-17) of Ruck [26], which gives

$$k_0 \sigma^C \sim 1 + (2 k_0 w)^2 \quad (20a)$$

where  $\sigma^C$  is the cylindrical cross section per unit length, not a function of range,  $R$ . The cylindrical cross section in (20a) is defined as  $\sigma^C = \lim_{R \rightarrow \infty} 2 \pi R |E_S/E_i|^2$ , in the limit as  $R \rightarrow \infty$ . (As was discussed, the correct  $\sigma$  radar is obtained by putting  $E_S/E_i$  in equation (13)). However, for the present comparison, we want  $\sigma^C$  (from (18b)) which is obtained as

$$\begin{aligned} \sigma^C &= 8 \pi w^2 / \lambda, \\ k_0 \sigma^C &= 16 \pi^2 w^2 / \lambda^2 \equiv (2 k_0 w)^2, \end{aligned} \quad (20b)$$

almost agreeing with Ruck, i.e., with (20a) but missing the 1 of (20a) because we have neglected edge effects, which is valid because  $w/\lambda > 1$ . It is concluded that our range-dependent cross sections (19a) and (19b) are correct approximations, neglecting edge effects.

#### 4.11 Cross Section of a Dielectric Tunnel at Broadside Incidence

The necessary next approximation is to assume that the cross section of a dielectric strip interface may be obtained from that of a metal strip by the relation

$$\sigma_{\text{diel}} = \sigma_{\text{metal}} |\Gamma|^2 \quad (21)$$

where  $\Gamma$  is the reflection coefficient at the tunnel interface. Using the notation refractive index,  $n = \epsilon^{*1/2}$ , the reflection coefficient in passing from medium 1 to medium 2 is

$$\Gamma = (n_1 - n_2) / (n_1 + n_2) .$$

For example,  $\Gamma$  from coal with  $\epsilon_1 = 5$  and a water-filled shaft,  $\epsilon_2 = 81$ , is

$$\Gamma_w = - 0.60$$



and from coal to a gas such as methane or air is

$$\Gamma_a = + 0.38 .$$

These values in (21) show that  $\sigma$  of a water-filled shaft is 2.5 times greater than for a gas, depending upon the assumed permittivity of the coal medium. The farther wall of a tunnel has a reflection coefficient of the same magnitude as the first wall. There are multiple reflections in the time domain. However, the EM power returned by the second wall is

$$(1 - |\Gamma|^2)^2 \quad (22)$$

weaker than from the first wall, due to the transmission loss in each direction at the first wall. (Equation (22) is the square of the factor in (5).) These multiple reflections will be seen as successively smaller reflections in the time domain, or as interfering varied amplitude returns with an FM-CW swept radar.

We note that, with gas in a shaft, the sign of the reflection coefficient at the first wall is positive. With water, the sign is negative. The opposite occurs at the second wall. In effect, this is also true for detecting a borehole when  $k_0 a n_2$  is large.

We conclude that, at least theoretically, the radar return signature may be used to identify the target, i.e., to solve the inverse problem. The magnitude and sign of the reflection coefficient, and/or the rate of decay of successive reflections (influenced by attenuation of water) may give the width of the shaft and distinguish between water and gas filling. Successive reflections are seen in the simulated pulse study in section 5.2. Thus, detailed data could contribute to solving the inverse problem. Wittmann [40] has demonstrated comparable synthetic pulses in a planar layered medium. Roe and Wittmann [41] gave a synthetic analysis of the phasor signals of the FM-CW radar scattering from a planar layered medium, to distinguish  $n_1 < \text{or} > n_2$ .

#### 4.12 Cross Sections of Circular Cylinders (Boreholes)

The radar scattering of circular cylinders involves concepts similar to those brought out in the scattering of a strip (tunnel). Just as for the strip, we will convert to the monostatic radar case by observing that the significant excited length along the cylinder is 0.707 of that for the canonical plane wave incidence case.

The scattering of a small cylinder is much greater with TM polarization than with TE polarization. Only the TM case will be discussed. In the mine, the antennas should be oriented to give a vertical E-field. However, it would be useful to rotate them by 90° in trying to solve the inverse problem of identifying a target, e.g., to distinguish a borehole from a tunnel and to identify clutter.

The scattering from a metallic cylinder with plane wave incidence and the receiving point at distance  $\rho \gg a$ ,  $a$  = cylinder radius, is

$$\lim(\rho \rightarrow \infty) E_s = E_i (2/\pi k\rho)^{1/2} \rho, \quad (23)$$

$$P = - \sum_{n=0}^{\infty} (-1)^n e_n J_n(ka) \cos n\phi / H_n^{(2)}(ka) \quad (24)$$

where  $e_n = 1$  for  $n = 0$  and  $e_n = 2$  otherwise, and

$$k = (\omega^2 \mu_0 \epsilon_0 \epsilon^*)^{1/2}. \quad (25)$$

The  $J_n$  are Bessel functions,  $\phi = 0$  for monostatic radar, and the  $H_n^{(2)}$  are Hankel functions for outgoing waves, section 2.2.1 [23], [26]. In (23) the phase factor,  $\exp(-jk\rho - j\pi/4)$ , has been omitted. The  $\epsilon^*$  is of the surrounding medium.

Using  $E_s/E_i$  of equation (23) in (13), which amounts to assuming that there is a bistatic radar with the source at infinity and the receiver at  $R = \rho$ , we get

$$\sigma_{pwi} = 8 R |P|^2 / k. \quad (26)$$

However, for practical monostatic radar the  $\sqrt{2}$  is removed from the numerator of (23) giving

$$\sigma_m = 4 R |P|^2 / k. \quad (27)$$

As in equation (16) for the strip,  $\sigma_m = 0.5 \sigma_{pwi}$ . The  $k$  is in the medium. It may be shown that in the geometrical optics approximation, i.e.,  $a > \lambda$ ,  $|P|^2 = k\pi a/4$ , which in (27) gives

$$\sigma_{m,G.O.} \sim R \pi a. \quad (28)$$

The dependence of cross section on range,  $R$ , was also demonstrated in the development of equations (14) and (19a,b). The change in cross section for the case of plane wave incident radar and monostatic radar, a factor of 4 in (17b) and factor of 2 in (19a, b), was deduced. The reasons for all of these results may be based on the concept of the first Fresnel zone area as a function of  $R$  and the consequence that  $\sigma_m = 0.5 \sigma_{pwi}$  for a long cylinder.

The method of obtaining the monostatic cross sections of strips and cylinders by multiplying  $\sigma_{pwi}$ , by 0.5 furnishes a very simple approximation which avoids difficult calculations for a full wave [28], point source radar solution in place of eq (23). Our approximate results are, however, believed to be reasonably accurate for  $R \gg a$ ,  $R \gg \lambda$ . (We recently found that Brysk [32] deduced the factor  $0.5 = \sigma_m / \sigma_{pwi}$  and a range dependent  $\sigma$ .)

#### 4.13 Computer Routine for S/N Versus Range

The appendix lists a computer program for calculating the signal/noise ratio, S/N, of an FM-CW radar. The program is in BASIC language and is suitable for a desk top computer. It solves for S of (4) divided by N of (12) as a function of range, R. The approximation of equations (21) and (22) are reasonable for large water-filled bore holes; but for air filling, the ranges are too optimistic--especially if the hole diameter is less than the wave length in the coal. (For the tunnel, (21) and (22) are good approximations.)

Figure 14 shows curves of S/N as a function of distance for detecting a 30-cm diameter well. Reasonable values for two coal "atmospheres" and three borehole contents: metal, water, and gas are assumed.

The exact solution (23) is used for metallic cylinders in the intermediate range,  $ka$ , of the order of 1. For small  $ka$ , an accurate Rayleigh-type approximation is used. For large  $ka$ , the geometrical optics value,  $\sigma^c = \pi a$ , as modified (28) for monostatic radar, is used. The cross sections with dielectric filling were assumed to be the above multiplied by  $|\Gamma|^2$ , equation (21).

#### 4.14 Conclusions

The radar signal equation was modified to take into account changes in the signal due to the coal "atmosphere". These effects include mainly the air-to-coal interface, the attenuation of the waves by the dielectric loss, and the spreading of the pulse by dielectric dispersion in the coal. The last effect had to be estimated; more research on dispersion could be useful.

Regarding the target locations, they were idealized as being straight ahead of the working antennas. A borehole off to the side would, theoretically, give a weaker signal because the radar antenna gives maximum gain straight ahead. Preliminary experiments to evaluate the degradation of the range capability for off-side boreholes would be useful.

The old tunnel may give a small cross section if it is higher or lower than the radar antennas and, also, when it is not perpendicular to the working tunnel surface. Regarding the relative heights, the inevitable roughness of the old tunnel wall will furnish some non-specular reflections, thus permitting some reflection, though weak compared to the specular reflection cross

section used in (19a). For non-perpendicular intersection of the old and new tunnels, the antenna gain pattern,  $G_0$ , of the radar antennas for the ray angle that arrives at perpendicular incidence on the old tunnel will determine the change in the cross section.

There is a real need for experience with clutter. The scattering of various clutter targets both attenuates the wave to and from the desired target and gives interfering signals that may, in effect, raise the noise figure, NF, of (13).

It may be noted that Ruck [26], devoted Chapter 9 to rough surface effects. Their work could be useful in extending the present work.

We have attempted to give a clear explanation of the cross sections of infinite planes, cylinders, and strips. Some of our results may be new. The modification of plane wave scattering theory for point-source radar scattering was investigated and solved. To find  $\sigma$  for eq (4) from  $\sigma^C$  use  $\sigma = 2R\sigma^C$ .

Finally, it seems necessary to caution that with the targets off-side, higher and lower, walls not perpendicular, rough targets, and also clutter, we cannot expect ranges to be as great as those calculated in the figures.

The antenna pattern in the material is limited to forward directions. For example, if the pattern in air covered the whole forward hemisphere, then the pattern in coal with  $\epsilon' = 9$  would cover only  $19.5^\circ$  from straight ahead of the significantly illuminated area of the interface.

## 5. Pulse Response Simulations

Impulsive signals have typically been used at NBS for geophysical probing because they are relatively easy to generate at high repetition rates, and they have a broad spectral content and a short duration which permits discrimination between closely-spaced returns. On the negative side, it's very difficult to construct efficient, portable antennas with sufficient bandwidth. In addition, the higher frequency components of the 1/2-ns NBS impulse generator are severely attenuated in lossy materials such as coal.

At the contract monitor's suggestion, a comparison of potentially useful pulse waveforms was done by simulating the transmission between the two TQ antennas in air. The received signals are examined for amplitude, width, distortion, and for the feasibility of using additional signal-processing techniques. The analysis is extended to include transmission through a lossy medium and reflection from a borehole as described in chapter 4. The result is an estimate of the likelihood of detecting a borehole at a given range with an actual measurement system.

## 5.1 Waveform Comparisons

The two TQ antennas, separated by 1.5 m, are treated as a two-port network. The simulated response of this network to any signal is the convolution of the input waveform with the measured network impulse response. Impulses of 1-volt amplitude and 1/2-, 1-, 2-, and 5-ns duration at the 50% point were approximated by the raised cosines shown in figure 15 with the spectral distributions of figure 16. Clearly, the 5-ns impulse has so little energy in the pass band of the antennas (see figure 3) that only a very small signal would be expected at the receiving antenna terminals. The results of the convolution operation (figure 17) confirm that impulses with a duration of much more than 2 ns will be too inefficiently transmitted to be useful with the TQ antennas.

Similar comparisons using 1 volt peak-to-peak sinusoids of 1, 2, 4, and 8 cycles are illustrated in figures 18 through 20. The carrier frequency was chosen as 250 MHz to approximate the transition duration of the impulse generator to be delivered to the Bureau of Mines as a part of this contract. The monocycle, with its reduced energy at lower frequencies, may be an improvement over the impulse. The received signal is no better for the other three 250 MHz examples, and the additional pulse width would make detection of adjacent geologic features more difficult.

Above-ground radar systems use pulse compression schemes to combine a narrow response with higher average power. This can be accomplished by transmitting a carrier frequency which is a linear function of time, a so-called chirp, and cross correlating the returns with a replica of the chirp. Hardware is becoming available which could potentially perform the same function quickly in a coal mine environment without extensive computer processing.

A set of linear chirp waveforms are shown in figure 21. These were chosen as an estimate of what might be usefully transmitted using the TQ antennas. The three waveforms are: 250-500 MHz in 10 ns, 250-1000 MHz in 10 ns, and 250-1000 MHz in 20 ns. The spectra of these pulses are shown in figure 22. The resulting received waveforms, after transmission over a 1.5 m path with a pair of TQ antennas, are shown in figure 23. Correlation techniques would be less effectively applied to the upper waveform which shows little evidence of the frequency change. The higher frequencies of the other two waveforms would be severely attenuated in the coal. That additional distortion could limit the system's effectiveness. A fourth chirp was numerically generated covering 300-600 MHz with a 20-ns duration. Figure 24 shows that the simulated received waveform retains the chirp characteristic. The autocorrelation of that waveform as depicted in figure 25 demonstrates the extent of the pulse compression possible. Compare this result to the autocorrelation of the 4-cycle, 250 MHz sine wave presented in figure 26. Both received waveforms are about 25 ns in duration, but the chirp has a much narrower autocorrelation function.

Multi-cycle sinusoids will be less effective sources than will simpler waveforms until rapid coding schemes can be perfected. Chirps, on the other hand, offer distinct advantages if the "clutter" signals can be suppressed. Some additional work is certainly warranted in this area. At present, it seems that 1- to 2-ns wide impulses or monocycles are optimal choices for the antennas and detection system.

## 5.2 Borehole Detection Estimates

It is helpful to have a method which predicts the response of a measurement system to a particular mining threat. One can combine an incident waveform with the antenna impulse response as was done in the previous section, correct for the attenuation in a lossy dielectric material, include the reflection characteristics of a given target, and thereby estimate the amplitude and form of the received signal. The analysis can predict the ability of a given system and data processing technique to discriminate between targets and background responses and can estimate the limiting range of the system.

A 1-volt amplitude, 1-ns duration impulse (figure 15) was chosen as the incident waveform and convolved with the TQ antenna impulse response. The antennas were assumed to be immersed in the dielectric medium, i.e., no corrections were made for the air/coal interface in the simulation. The antennas might well be placed directly against the work face when the system is to achieve maximum range. Typical surface roughness and contours add great uncertainties to any estimate of the reflection at that interface.

The coal seam was modeled as a frequency independent dielectric with infinite extent. Dry coal was assigned a relative dielectric constant of 3.65 and a loss tangent of 0.03; for damp coal, it was 6.5 and 0.05, respectively. These are reasonable approximations since our primary operating range lies above 200 MHz. When measured values of dry coal permittivity versus frequency were substituted for the frequency independent value, the results were not substantially changed. We are not aware of measurements on damp coal covering a broad enough spectrum for this analysis.

Vertical boreholes representing the uncharted, abandoned wells are the mining threats of greatest interest for this work. Based on Bowman [24], the complex reflection coefficient was computed at each of the component frequencies of the simulated pulse for several types of boreholes in dry and damp coal. The antennas are considered as point sources. The responses to a metal-cased 15-cm radius borehole, an empty hole, and one that is water-filled are given in figure 27 for a 1-m range. As expected, the response from the cased hole is larger and inverted when compared to the empty hole return. The water-filled, uncased pattern is much more complicated. The slightly saline solution delays the signal enough that each reflection across the diameter of the pipe is distinct and inverted from the previous one. Thus the sign, amplitude, and pattern of a response may well indicate the type of threat encountered. Figure 28 illustrates the rapid attenuation of the response to a cased 15-cm radius borehole in relatively damp coal as the target range is increased. The received signal drops by more than 30 dB as the range is increased from 2 m to 5 m.

A summary of these simulations is presented in figures 29 and 30. The predicted responses from five types of boreholes at ranges to 10 m in dry and damp coal are shown. Since the noise introduced by the sampling circuitry of a time domain receiver is on the order of 1 mV, high voltage pulses, pre-amplification, and signal averaging will be required if the system is to recognize boreholes at even a five meter range. Electromagnetic (EM) techniques have been used over large ranges in salt domes. The response of the

system to a 15-cm borehole in rock salt at various ranges is also shown on figure 29. A relative dielectric constant of 6.5 and a loss tangent of 0.001 was assumed for rock salt. Clearly, operation at much larger ranges is possible in a low loss material such as salt.

## 6. Pulse System Equipment

A prototype time domain measurement system has been assembled for delivery to the Bureau of Mines at the conclusion of Phase II. The design goals emphasized a portable system that could be readily interfaced to the existing equipment at both the Bureau of Mines and NBS and which offered flexibility and fast waveform acquisition. As shown in figure 31, the equipment includes the TQ antennas described in chapter 2, and an impulse generator and equivalent-time sampler located at the antennas. A two-channel fiber-optic link carries the analog signal and trigger to a remotely-located digital acquisition unit where the waveforms are analyzed and stored on floppy disks. In this arrangement, laboratory equipment has been integrated into a wide bandwidth system useful for a variety of subsurface measurements.

### 6.1 High-voltage Impulse Generator

A specially constructed pulser supplies 500-volt high,  $\sim 2$ -ns wide impulses to the 50-ohm transmitting antenna at a pulse repetition frequency (prf) of 10 kHz (see figure 32). The spectral content of the pulse overlaps the operating ranges of the TQ's and other Bureau of Mines' antennas. A stable pretrigger, adjustable from 50 ns to 300 ns, is furnished to the high-frequency sampler. The unit may be operated from either the power line or a 12-volt battery. Always set the 10-turn voltage control to 0 (full counter-clockwise) and the RATE switch to OFF before turning the power ON. Allow a two-minute warm up, set RATE to ON to enable the clock circuitry and pretrigger, and increase the 10-turn voltage control. Set that control to 0 again before turning the pulser OFF.

### 6.2 Receiver Preamplifier

An optional 29-dB amplifier between the receiving antenna and the high-frequency sampler provides two functions in the system. It boosts low-level signals of up to 30 mV. The amplifier has good fidelity and a bandwidth of 10 MHz to 2 GHz. In addition, it acts as a limiter for signals of up to 1/2 volt at its input, holding the output to about 1 volt maximum. The amplifier compresses the signals from the receiving antenna, enabling the sampler to recover returns which otherwise would be buried in the sampling noise while protecting the sampling diodes from damaging voltages. The unit has a quick recovery from saturation. The input to the amplifier must be limited to not more than 7 volts for 3 ns or the unit may be damaged. When using the high-voltage impulse generator, take care that the peak received signal (usually from the air/coal interface) does not exceed 1/2 volt. Add attenuators and/or remove the amplifier when large signals are likely.

### 6.3 High-frequency Sampler

The sampler is used to construct a discrete, equivalent-time replica of the repetitive signal from the receiving antenna/preamplifier. By sequentially acquiring one point per repetition at increasingly delayed times over 1024 signals, the system assembles a waveform which resembles the input signal but with a duration of about 100 ms instead of 200 ns. This longer waveform can easily be digitized in real time and transferred to a computer for further processing.

The high-frequency sampler is a modified version of a commercial oscilloscope plug-in and is compatible with the present equipment at both NBS and the Bureau of Mines. The unit uses replaceable sampling heads which offers several advantages. First, if a sampling diode bridge were damaged on a field measurement, the head alone could be exchanged; there would be no need to send the modified sampling plug-in for repair. Second, a higher performance sampling head could be substituted if wider bandwidth signals were to be measured. The sampling head furnished with this system covers dc to 1 GHz at - 3 dB, but models are available with responses to 12 GHz. Finally, the sampling head is quite small, and possibly a long extender cable could be integrated into the sampler in the future to allow the head to be lowered into a borehole. This potential was attractive to the Bureau of Mines. The normal input range of the sampler is up to 1 volt peak-to-peak with a tangential noise of 1 mV, indicating a dynamic range of 54 dB without signal averaging.

The high-frequency sampler could be set up as follows for a coal-seam measurement:

TIME-DISTANCE	:	0, X1
TIME/DIV	:	20 ns
PRESET	:	Out
HIGH RESOLUTION	:	Out
mV	:	In
ATTENUATOR	:	200 mV/div
STABILITY	:	ccw
LEVEL	:	cw
SLOPE	:	+

With that arrangement, a 200-ns time window would be acquired which represents a 10- to 15-m range. Since the time corresponding to the left edge of the window can be varied from 0 ns to 1000 ns, the total observable range is from 0 m to between 60 m and 90 m, depending on the permittivity of the coal. If shorter ranges are desired, set the time-distance dial to X.1, which permits a viewable range in damp coal of at least 10 m from the face.

The output of the sampling process is a discrete waveform resembling a staircase in which each step corresponds to a single sample. The frequency at which the samples are taken is constant regardless of the time window selected and is equal to the prf of the impulse generator. The SCAN control must be adjusted to set the width of the equivalent-time waveform so that enough samples are included to accurately characterize the sampler input signal. At



least 5 samples/nanosecond are required for the high-voltage impulse generator. The product of that number, the TIME/DIV setting, and 10 divisions yields the total number of samples in the equivalent-time waveform--in this case, 1000. The duration of that waveform is the number of samples divided by the impulse generator pulse repetition frequency, 10 kHz for this case. Thus, the impulse generator prf (or 30 kHz, whichever is less) dictates the rate at which samples are taken, the scan control determines the number of samples in the equivalent-time waveform, and the TIME/DIV setting maps the real time window into equivalent-time. At full clockwise, the SCAN control selects about 512 samples. That number increases as the knob is turned counterclockwise. Connect an oscilloscope to the SWEEP OUT jack, and adjust the SCAN control until the ramp is the correct duration.

The plug-in "blanking" signal provides the trigger marking the start of the equivalent-time waveform. The output waveform is derived from the plug-in "VERT SIG OUT" which is scaled to 1 volt peak-to-peak to be compatible with the fiber-optic system. The high-frequency sampler may be connected to the digital acquisition system through the fiber-optic link or through up to 20 m of coaxial cable by reconnecting two coaxial cables within the sampler. The plug-in may also be removed from the sampler and inserted directly in an oscilloscope for laboratory use.

#### 6.4 Fiber-optic Transmission System

A two-channel, fiber-optic transmission system provides low noise signal paths from the high-frequency sampler, which is located at the receiving antenna, to the digital acquisition system at a remote point. The system consists of two channels, one used to transmit the equivalent-time replica of the received signal and the second for a trigger marking the start of that waveform. Each path consists of a transmitter, approximately 125 m of fiber-optic cable, and a receiver. The system has a maximum signal, in or out, of 1 volt peak-to-peak and a frequency response of 15 Hz to 25 MHz. The dynamic range has been verified at greater than 50 dB.

Both commercial transmitters have been modified. The input impedances have been increased to 600 ohms to reduce the loading of the previous stages. In addition, an R-C differentiating circuit was added to the transmitter in the trigger path to condition the TTL "blanking" signal to the bandwidth and input voltage limits of the fiber-optic system. As a result, the transmitter units are not interchangeable and damage may result if the cables to the transmitters are reversed.

The receiver units require 50-ohm terminations. A feedthrough terminator must be used on the signal path. The trigger signal is terminated and transformed to > 2 volts to reliably trigger the digital acquisition system. No additional termination is required for that channel.

## 6.5 Digital Acquisition System

The digital acquisition system consists of a microprocessor-controlled waveform recorder, monitor, and 5 1/4-inch floppy disk drive. The waveform recorder can acquire up to 10,000 points at a 66 kHz rate with 12-bit A/D conversion. It can average repetitive waveforms to reduce the effects of random noise, correct for time and amplitude scaling, apply time-weighted-gain functions, and subtract previously acquired waveforms such as background or clutter waveforms. The measurements, setups, and procedures are stored on diskettes or transferred to a controller/computer via either RS-232 or GPIB interfaces.

The unit would normally be used in the averaging mode, external trigger at 10% level, with the sweep time equal to the duration of the high-frequency sampler's equivalent-time waveform, and with 1000 element arrays.

## 7. FIELD TESTING

### 7.1 NBS Test Range

An indoor test range has been installed at NBS (see figure 33). This test range holds both air-filled and water-filled voids for use in checking underground void measurement or imaging systems. The loss in the soil of the range goes from about 25 dB per meter at 300 MHz to about 50 dB per meter at 1 GHz. This loss is quite high for operation of any radar system at these frequencies and thus represents a rather stringent test of any detection system.

Several series of measurements were taken with the pulse and FM-CW systems using different antennas and antenna arrangements. Using the TQ antennas with a center baffle (as described in section 2.4), a sequence of 26 measurements was made starting at the end of the range having the air-filled targets. The transmitting and receiving antennas with the septum were moved along the range as an assembly. Responses were recorded at 5-cm intervals. Figure 34 shows a typical result using a possible data handling method. Curve 1 shows the average background response for the series. Each point on that curve is the mean of the 26 responses at that relative time. Curve 2 shows one of the response curves taken over the 0.6-m deep target. Curve 3 is obtained by subtracting an average background from a response taken over a target to show how the target signal may be enhanced. The target response is shown by the arrow in figure 34. A series of enhanced responses is shown stacked in figure 35. The hyperbolic contour of the target signal (arrow) can be relatively easily seen.

Other approaches to the deconvolution problem were tried, but at this time no significant results are available. A large number of measurements were made using the FM-CW system with very similar results to those of the pulse system.

## 7.2 Coal Mine Results

Measurements of borehole returns were made at the Kaiser mine near Raton, New Mexico. The useable boreholes were located in a bench of coal approximately 1.6-m thick which was left in an open pit area of the mine. The borehole diameter was 12 cm. All the measurements made at the mine site were done with the FM-CW system.

The most notable result is that there was much more consistency from point to point in a series of measurements with the hole refilled and tamped with coal than in a similar series run with the boreholes either empty or with a metal pipe inserted. Placing a pipe in the hole especially alters the response pattern over a wide frequency range and a wide spacial range much more than would be indicated by simple theory. Probably, more theoretical work is needed on the FM-CW system before proceeding much further with hardware implementation.

Some series were run using a variable-density recorder to display results. It appears that this approach may be useful to help visually interpret a large amount of data.

Long delays in delivery of equipment ordered for this project precluded additional tests that had been planned for that site and a location at the Pittsburgh seam.

## **8. ADAPTATION OF SEISMIC DATA METHODS**

A local commercial company, suggested by the Bureau of Mines, was approached to suggest methods for applying its proprietary seismic data analysis techniques to electromagnetic pulse-type responses. The results of the initial discussion seem promising; but thus far in the program, we have not been able to provide the multiple results in the pattern which their method demands.

It should be noted that the suggested approach utilizes a modification of the common depth point (CDP) method. This is not an ideal approach for an underground radar, since one must know approximate range or position of the target in advance and multiple sets of measurements must be made. This technique is not amenable to a near, real-time scan method at a coal face, but may have some value for other survey work.

## 9. FUTURE DIRECTIONS FOR RADAR DETECTION OF UNDERGROUND ANOMALIES

### 9.1 Mining Needs

This contract was initiated with the goal of developing a system to locate old mine workings and old wells penetrating coal seams near present coal mining activity. The next phase in this ongoing program is to be devoted to the construction and testing of a model system that will detect these hazards. It is believed that the goals should be expanded to cover clay veins and faults in coal seams in any future effort. The time allocated to the overall effort would have to be increased, but the expenditures of funding would be more effective if applied to these closely related problems in the same program.

The location of clay veins and faults in coal seams has become of much greater importance in the last few years, since these situations are severe impediments to production, especially when mining is done with longwall machinery. The location of clay veins is important, since the coal seam may have different heights on each side. This situation is difficult to mine effectively with longwall machinery because the longwall machine cannot be angled up or down enough to accommodate the sudden shift in coal height. The clay can be hard enough to damage the cutters on mining machines. The roof structure near faults or clay veins is usually unstable and requires extensive bolting. It would be helpful to know ahead that such a situation exists so as to start turning a longwall machine or to make the most economic choice on allocating manpower or machinery to the job of mining the clay vein. Since a clay vein may act as a partial barrier to methane drainage, the mining through a clay vein may suddenly release large quantities of gas. This gas can quickly become a safety problem which can be best solved when one is forewarned. As a consequence, one future goal should be to make any hazard detection system adaptable to use with longwall mining machines.

### 9.2 Antennas

The antennas developed for this work are useable with both the FM-CW system and pulse system. This development effort has been carried only as far as is consistent with progress in other areas of the work. The work done on them to this point indicates further improvements in performance can be made. The present indications are that improvements can best be brought about by careful use of dielectric loading to reduce the physical size, resistive loading to reduce unwanted reflections, and perhaps by investigating the general bow-tie antenna (see section 3) or a wideband microstrip approach [30].

### 9.3 Future System Types

This effort, in both the Phase I work as well as Phase II work, has been confined to exploiting the time domain or pulse-type system primarily and the Frequency-Modulated, Continuous-Wave (FM-CW) system to a lesser degree. Recent improvements to both systems continue to make them important candidates for an ultimate solution. Geophysical hazard detection is a very difficult problem. The solution requires many design compromises which subsequently limit the system applications and the analysis of the responses. At this writing, no technique is clearly superior to all others. It is important to this program that a number of methods are developed in parallel and that new designs are carefully evaluated.

NBS has done some introductory theory development work on the Planar Near Field Reconstruction (PNFR) technique and also, more recently, has made some beginning measurements to verify this theory [4]. The results have been good enough to suggest that this system should also be looked at very seriously in any underground radar mapping work.

### 9.4 Accessibility to Mine Test Areas

In any future effort, a test area meeting several requirements is crucial. It must have a well-described physical arrangement of rock and coal as well as the anomaly to be detected. The anomaly must be available at the proper ranges and be of the appropriate type. A very important feature of any test area is that access be available for a relatively long period of time. This should be done so that comparisons of test results can be made to detect small changes or improvements in system performance as the work progresses.

The test range constructed by NBS during this phase has been invaluable to this work, but it does not provide all the elements needed. It is felt that a dedicated test area in an actual mine environment is necessary for this type of work.

## 10. REFERENCES

- [1] Rumsey, V. H., Frequency Independent Antennas. Academic Press, New York (1966).
- [2] Carrel, R. L., The Characteristic Impedance of the Fin Antenna of Infinite Length. Antenna Laboratory Technical Report No. 16, Electrical Engineering Research Laboratory, Engineering Experiment Station, University of Illinois, Urbana, Illinois (1957).
- [3] Lawton, R. A. and Ondrejka, A. R., Antennas and the Associated Time Domain Range for the Measurement of Impulsive Fields. Nat. Bur. Stand. (U.S.) Tech. Note 1008; 1978 November.

- [4] Jesch, R. L., Johnson, R. B., Belsher, D. R., Yaghjian, A. D., Steppe, M. C., and Fleming, R. W., High Resolution Sensing Techniques for Slope Stability Studies. FHWA-RD-79-32 (January 1979).
- [5] Buettner, H. M., Antenna Design for Geophysical Application. URSI Digest, North American Radio Science Mtg., Laval University, Quebec, Canada (June 2-6, 1980).
- [6] Lytle, R. J. and Laine, E. F., Design of a Miniature Directional Antenna for Geophysical Probing from Boreholes. IEEE Trans. on Geoscience Electronics, Vol. GE-16, No. 4, (Oct. 1978).
- [7] Kanda, M., The Effects of Resistive Loading on TEM Horns. Nat. Bur. Stand. (U.S.) NBSIR 79-1601; 1979 August.
- [8] Kanda, M., The Characteristics of a Linear Antenna with Tapered Resistive and Capacitive Loading. Digest of IEEE/AP-S International Symposium, Laval University, Quebec, Canada (June 2-6, 1980).
- [9] Carrel, R. L., The Characteristic Impedance of an Infinite Biconical Antenna of Arbitrary Cross Section. Antenna Laboratory, Technical Report No. 25, Electrical Engineering Research Laboratory, Engineering Experiment Laboratory, Engineering Experiment Station, University of Illinois, Urbana, Illinois (1957).
- [10] Schelkunoff, S. A., Electromagnetic Waves. D. Van Nostrand Co. Inc., New York, (1943).
- [11] Schelkunoff, S. A., Advanced Antenna Theory. John Wiley and Sons, Inc., New York (1952).
- [12] Kraus, J. D., Antennas. McGraw-Hill Book Co, Inc., New York, (1950).
- [13] Papas, C. H. and King, R., Input Impedance of Wide-Angle Conical Antennas Fed by a Coaxial Line. Proc. of I.R.E., pp. 1269-1271, (Nov. 1949).
- [14] Galejs, J., Antennas in an Inhomogeneous Medium. Pergamon Press, New York, (1969).
- [15] Galejs, J., Dielectric Loading of Electric Dipole Antennas. Journal of Research of the Nat. Bur. Stand. (U.S.), Digest Radio Propagation, Vol. 66D, No. 5, (Sept.-Oct. 1962).
- [16] Balanis, C. A., Jeffrey, J. L., and Yoon, Y. K., Electrical Properties of Eastern Bituminous Coal as a Function of Frequency Polarization and Direction of the Electromagnetic Wave and Temperature of the Sample. IEEE Trans. on Geoscience Electronics, Vol. GE-16, No. 4 (Oct. 1978).
- [17] Wheeler, H. A., Fundamental Limitations of Small Antennas. Proc. IRE(12), 1479-84, (1947).

- [18] Cook, J. C., Status of Ground-Probing Radar and Some Recent Experiments. Reprinted by Am. Soc. of Civil Engrs., from Proc. of Engineering Foundation Conference on "Subsurface Exploration for Underground Excavation and Heavy Construction", Henniker, N.H., Aug. 1974.
- [19] Cook, J. C., Radar Transparencies of Mine Tunnel Rocks. Geophysics, vol. 40, pp. 865-885, 1975.
- [20] Berkowitz, R. S., Modern Radar (Analysis, Evaluation, System Design). John Wiley & Sons, New York, 1965.
- [21] Bussey, H. E.; Larsen, E. B., Buried Antenna Performance; Development of Small Resonant Antennas. Rome Air Development Center, Griffiss AFB, New York, RADC-TR-74-169, June, 1974 (Defense Documentation Center No. AD 783-274).
- [22] Hufford, G. A., UHF Propagation from Buried Antennas. ESSA Research Laboratories, ITS, Tech. Memorandum ERLTM-ITS191, 68 pp, July, 1969.
- [23] Mumford, W. W., Scheibe, E. H., Noise Performance Factors in Communication Systems. Horizon House-Microwave, Inc., 1968.
- [24] Bowman, J. J., Senior T. B. A., and Uslenghi, P. L. E., Electromagnetic and Acoustic Scattering by Simple Shapes. North Holland Pub. Co., Amsterdam, 1969.
- [25] Kerr, D. E., Propagation of Short Radio Waves. McGraw Hill Book Co., New York, 1951
- [26] Ruck, G. T., Barrick, D. E., Stuart, W. D., and Krichbaum, C. K., Radar Cross Section Handbook. Plenum Press, New York, 1970.
- [27] Tarantolo, P. J. and Unterberger, R. R., Radar Detection of Boreholes in Advance of Mining. Geophysical Prospecting, vol. 26, pp. 359-382, 1978.
- [28] Wait, J. R., Electromagnetic Radiation from Cylindrical Structures. Pergamon Press, New York, 1959.
- [29] Jesch, R. L., Void Detection. Final report to Navy, National Bureau of Standards, Boulder, CO (August, 1980).
- [30] I-Ping, Yu, Multiband Microstrip Antenna. NASA Tech Briefs, vol. 5, no. 1, Spring 1980.
- [31] Jenkins, F. A.; White, H. E., Fundamentals of Physical Optics. McGraw-Hill, 1937.
- [32] Brysk, H., The radar cross section of a semi-infinite body. Can. Jour. Physics, vol. 38, pp. 48-56, 1960.

- [33] Bussey, H. E.; Richmond, J. H., Scattering by a lossy dielectric circular cylindrical multilayer, numerical values. IEEE Trans. on Ant. & Propa., vol. AP-23, pp. 723-725; September 1975.
- [34] Baños, A., Jr., Dipole radiation in the presence of a conducting half-space. Pergamon Press, New York, 1966.
- [35] Brekhovskikh, L. M., Waves in layered media. Academic Press, New York, Second Edition, 1980.
- [36] Stratton, J. A., Electromagnetic theory. McGraw-Hill, New York, 1941.
- [37] Engheta, N.; Papas, C. H.; Elachi, C., Radiation patterns of interfacial dipole antennas. Radio Science, vol. 17, No. 6; November-December 1982.
- [38] Lewis, R. L., Far-field computation inside a dielectric media for an antenna above a planar interface. National Radio Science Meeting, U.S. Nat. Committee/URSI, 24-28 May 1982, Univ. of New Mexico, Albuquerque.
- [39] Martin, L. C.; Welford, W. T., Technical optics, vol. I. Pitman Pub. Corp., New York, 1966 (second edition).
- [40] Wittmann, R. C., Simulated pulse techniques for measuring coal layer thickness. Ch. 6, pp. 287-297 in J. R. Wait, Ed., Analytical bases for electromagnetic sensing of coal properties, final technical report to U.S. Dept. of Energy ET-75-G-01-8972, July 1978.
- [41] Roe, K. C.; Wittmann, R. C., Improved coal interface detector, report to U.S. Dept. of Energy. Nat. Bur. Stand. (U.S.) NBSIR-82-1663, 1982 May.
- [42] Lynch, A. C., Relationship between permittivity and loss tangent. Proc. IEEE (London), vol. 188, pp. 244-246, 1971.



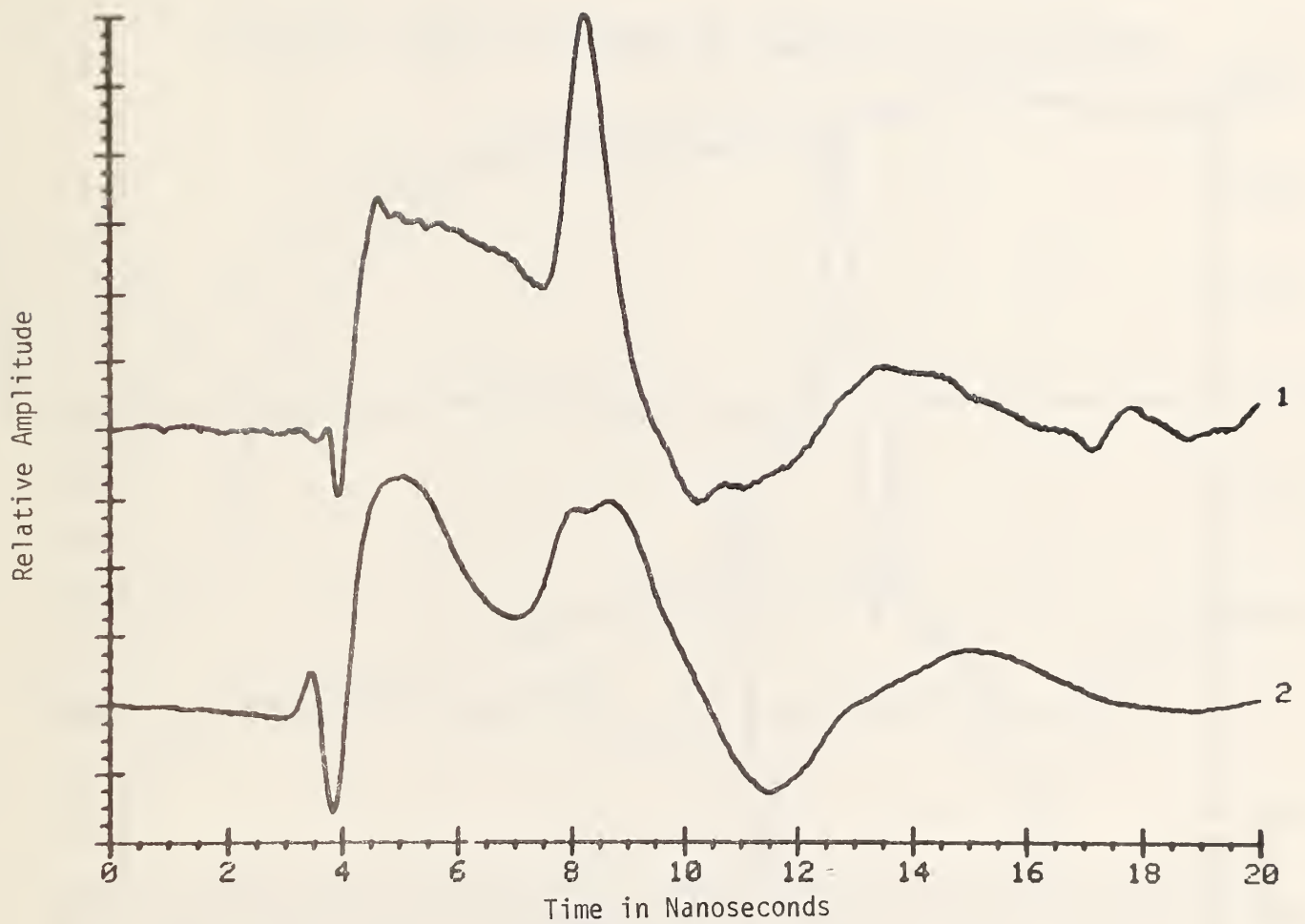


Figure 1. Reflections due to the NBS-TQ antenna without the resistive material (1) and the same antenna with the resistive material (2).

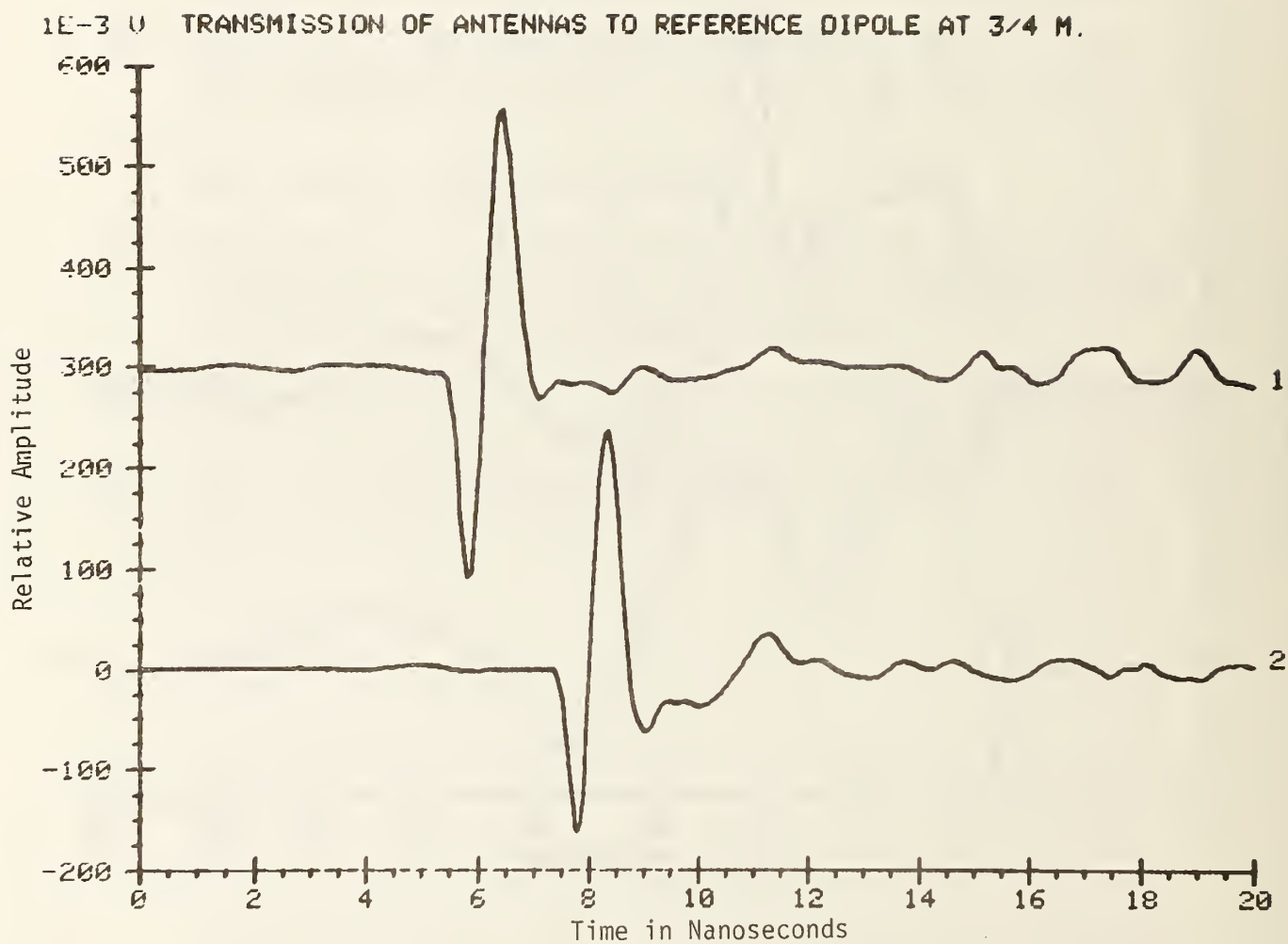


Figure 2. Transmitted waveform from the TG antenna (curve 1) and the TQ antenna (curve 2).

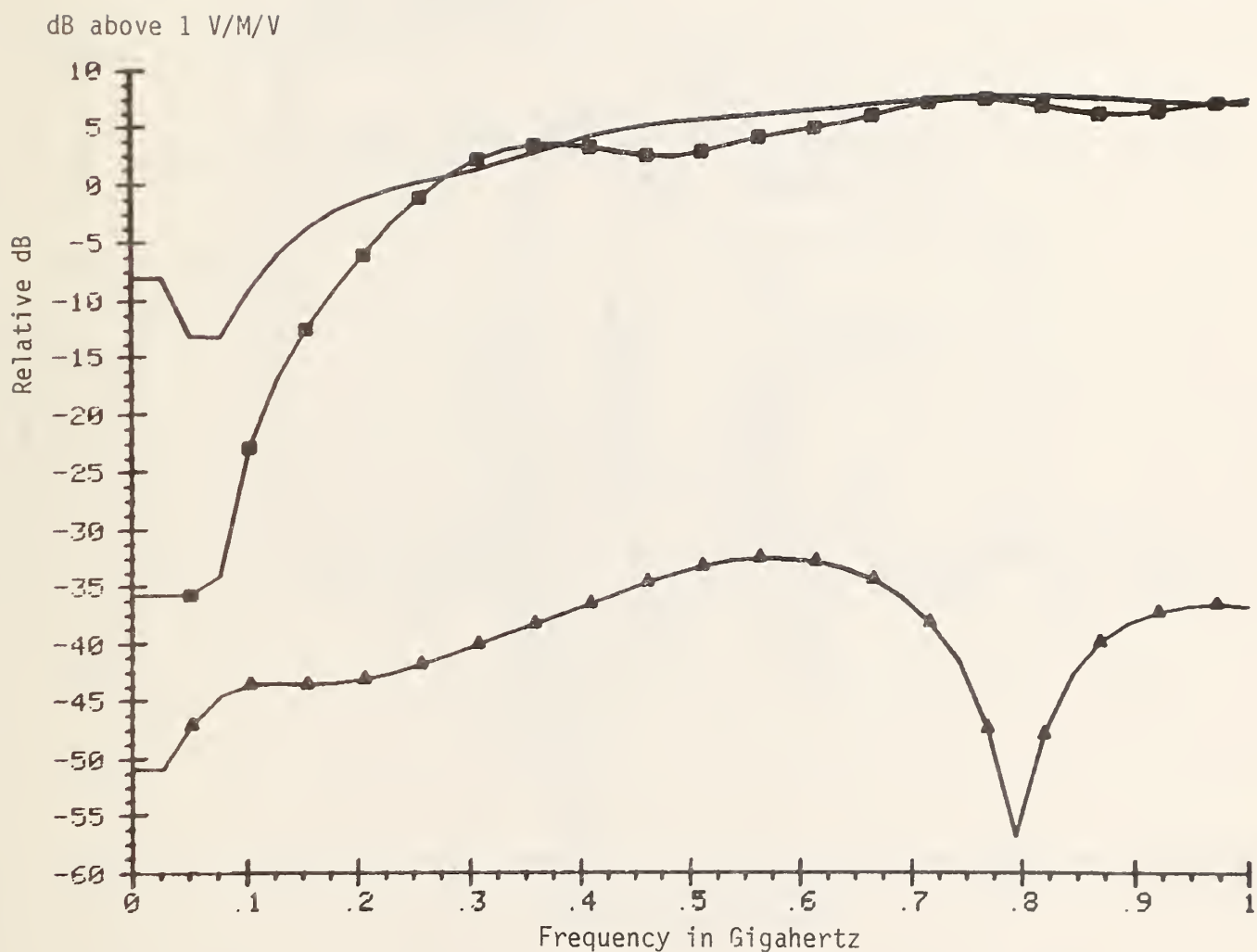


Figure 3. Relative transmission in dB for the TG antenna (plain line) forward direction, the TQ antenna (squares) forward direction and the TQ antenna (triangles) reverse direction at a range of 3/4 m.

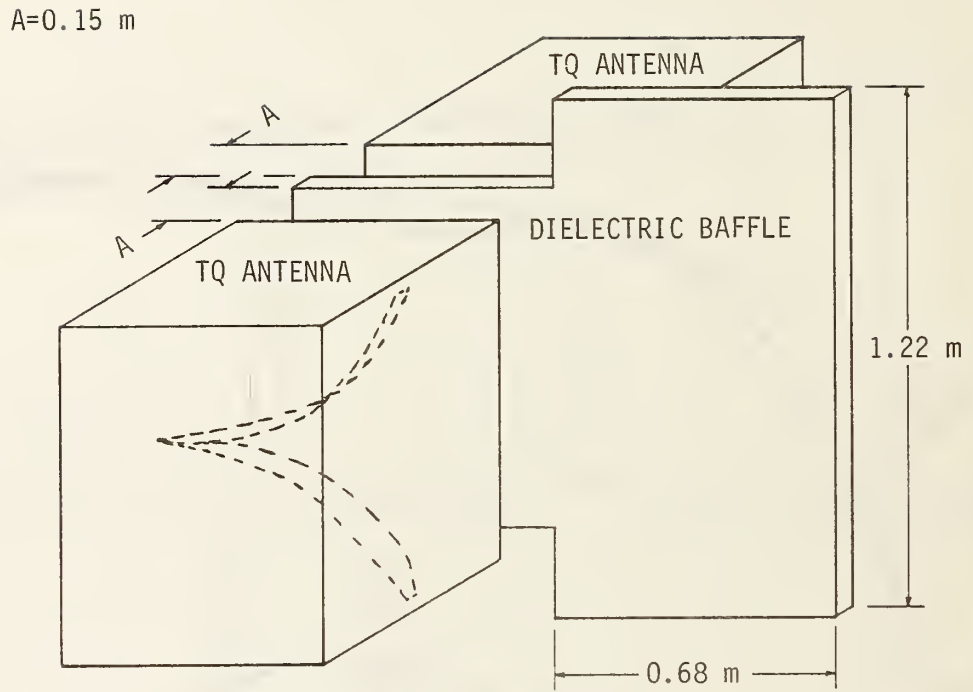


Figure 4. Baffle arrangement for isolating TQ antennas when operated bistatically.

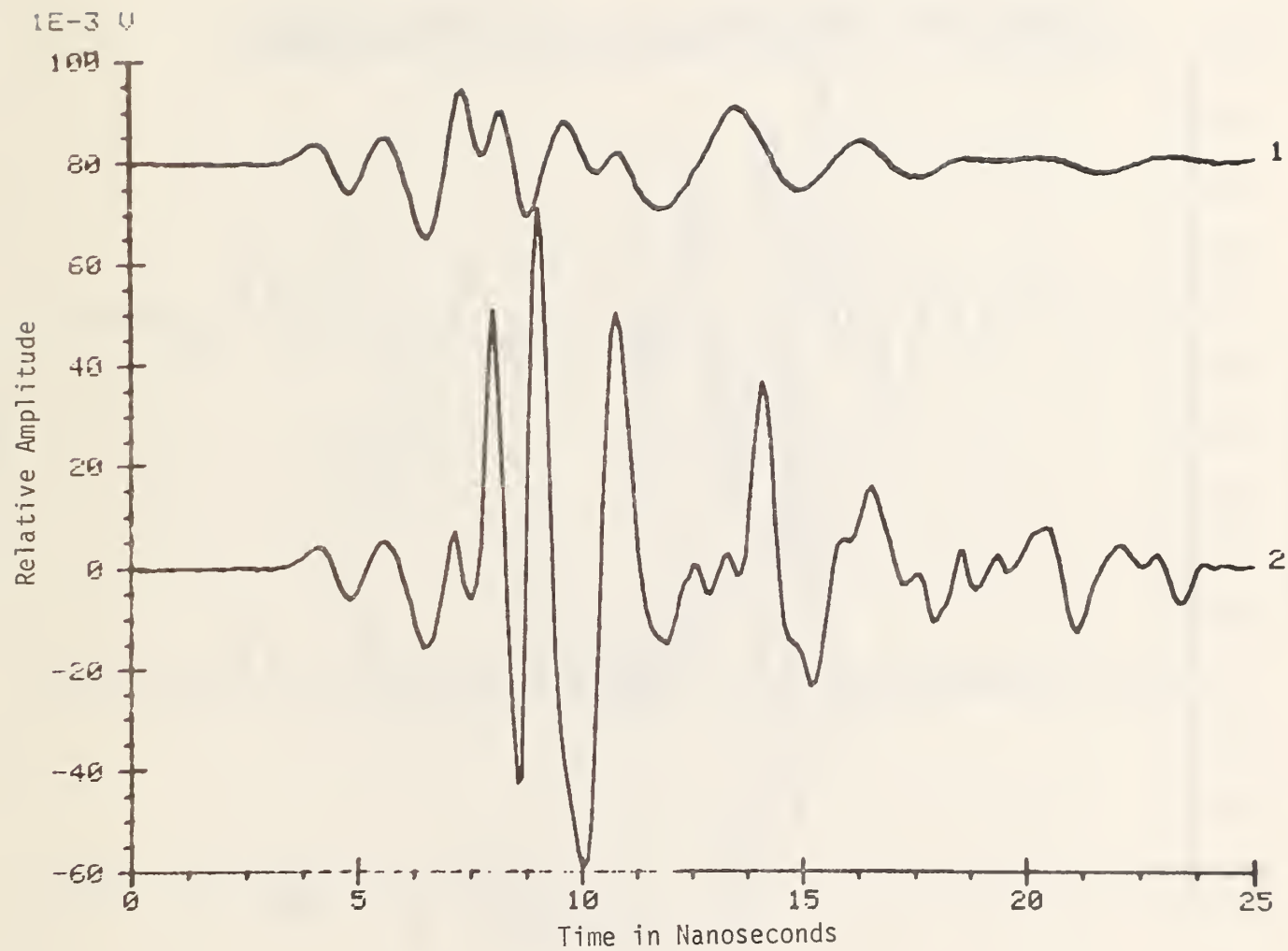


Figure 5. Response (1) of the system with the TQ antenna pair pointed at the sky and (2) at a 1.2 meter square metal plate 5 cm in front of the baffle.

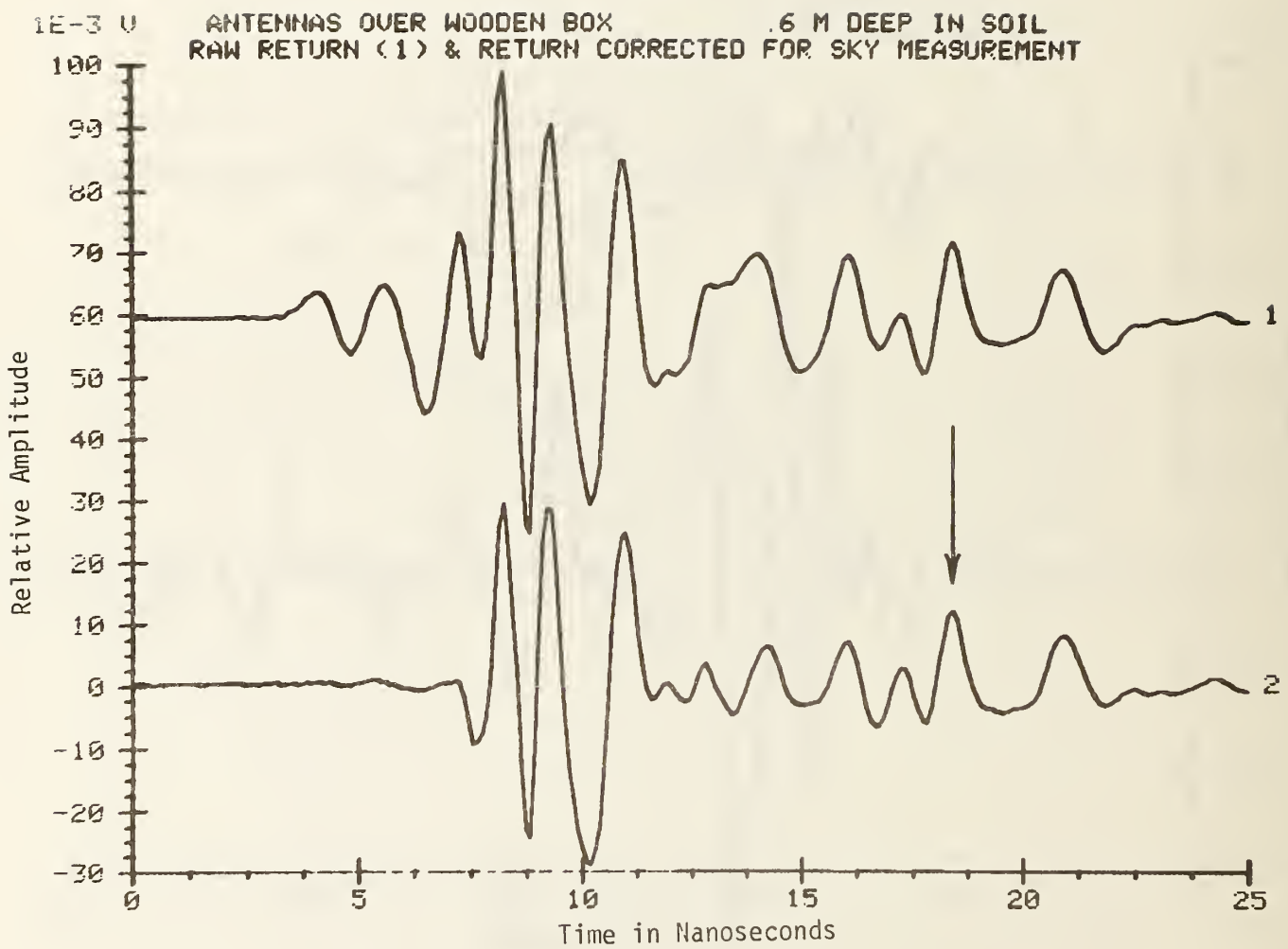


Figure 6. Pulse system antenna return from an air filled box target buried at 0.6 meter (1) and the same return corrected by subtraction of the sky return (2).

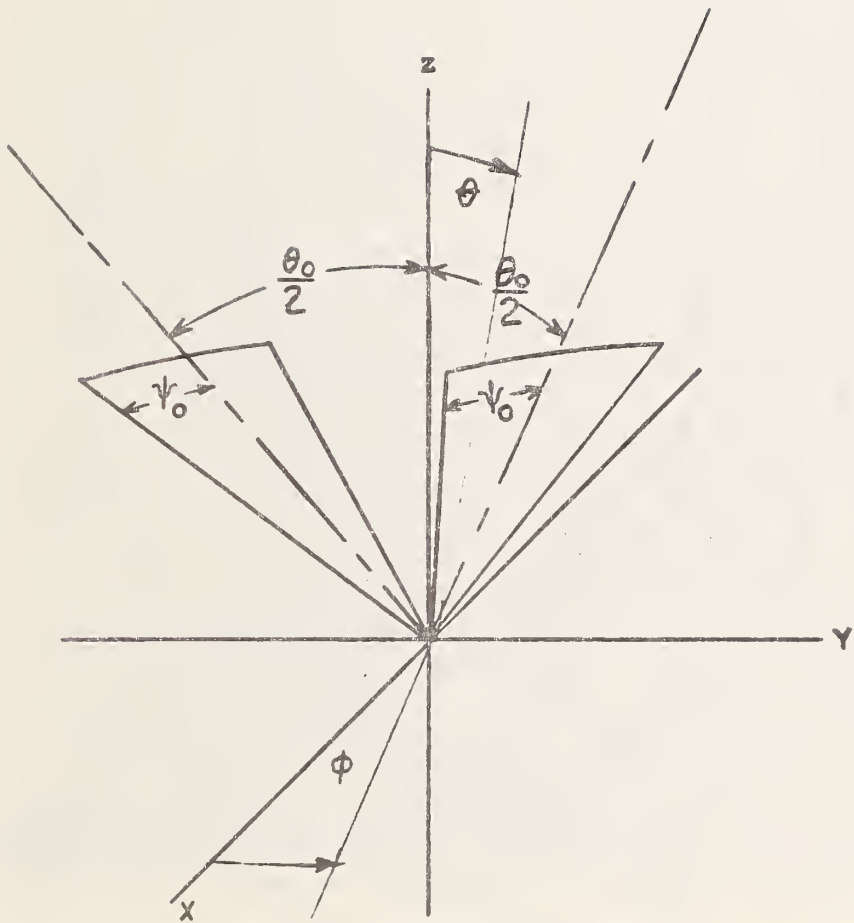


Figure 7. Noncoplanar fin antenna schematic.

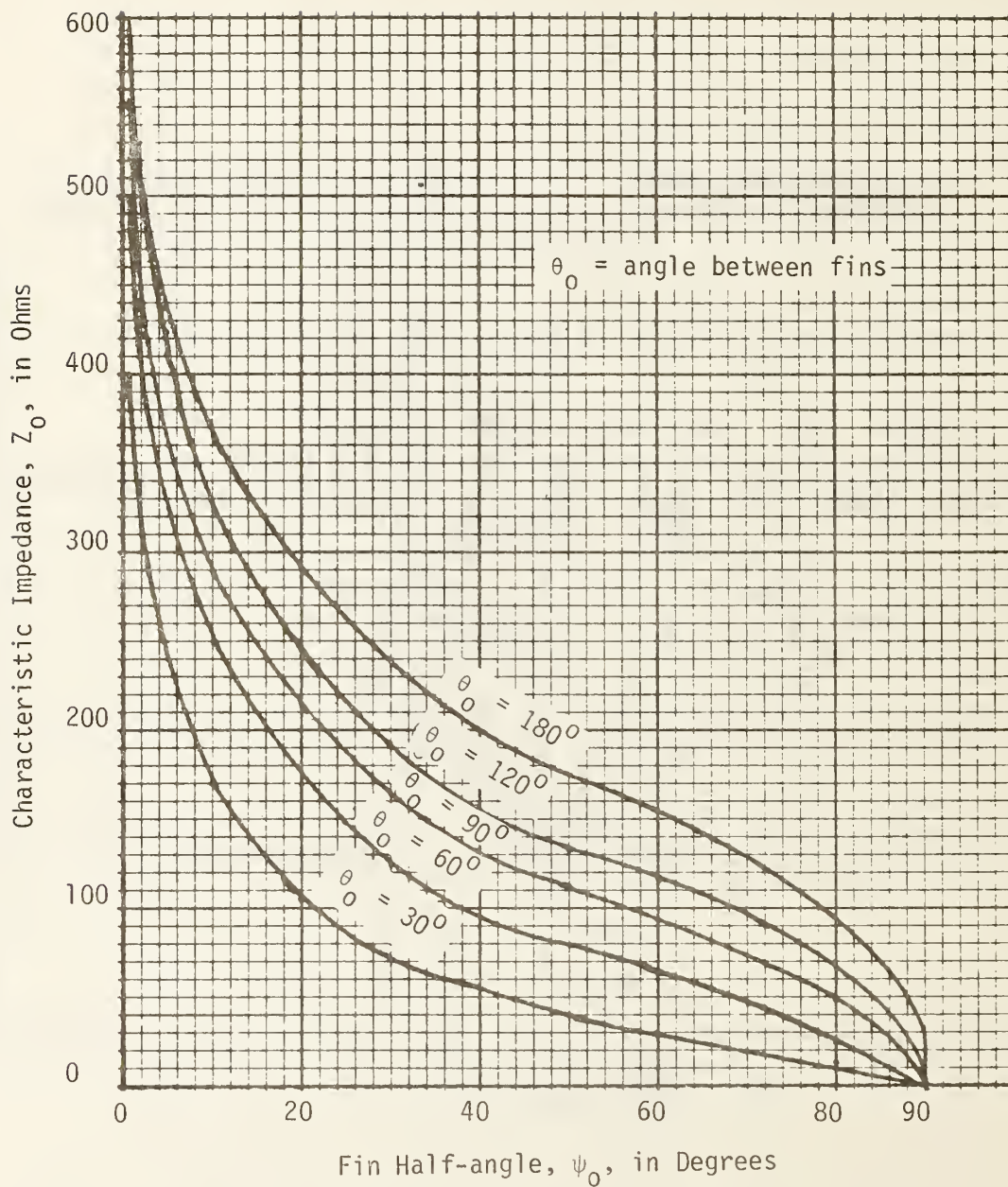


Figure 8. Characteristic impedance of the non-coplanar fin antenna with equal fin angles (plotted from data presented by Carrel [9]).



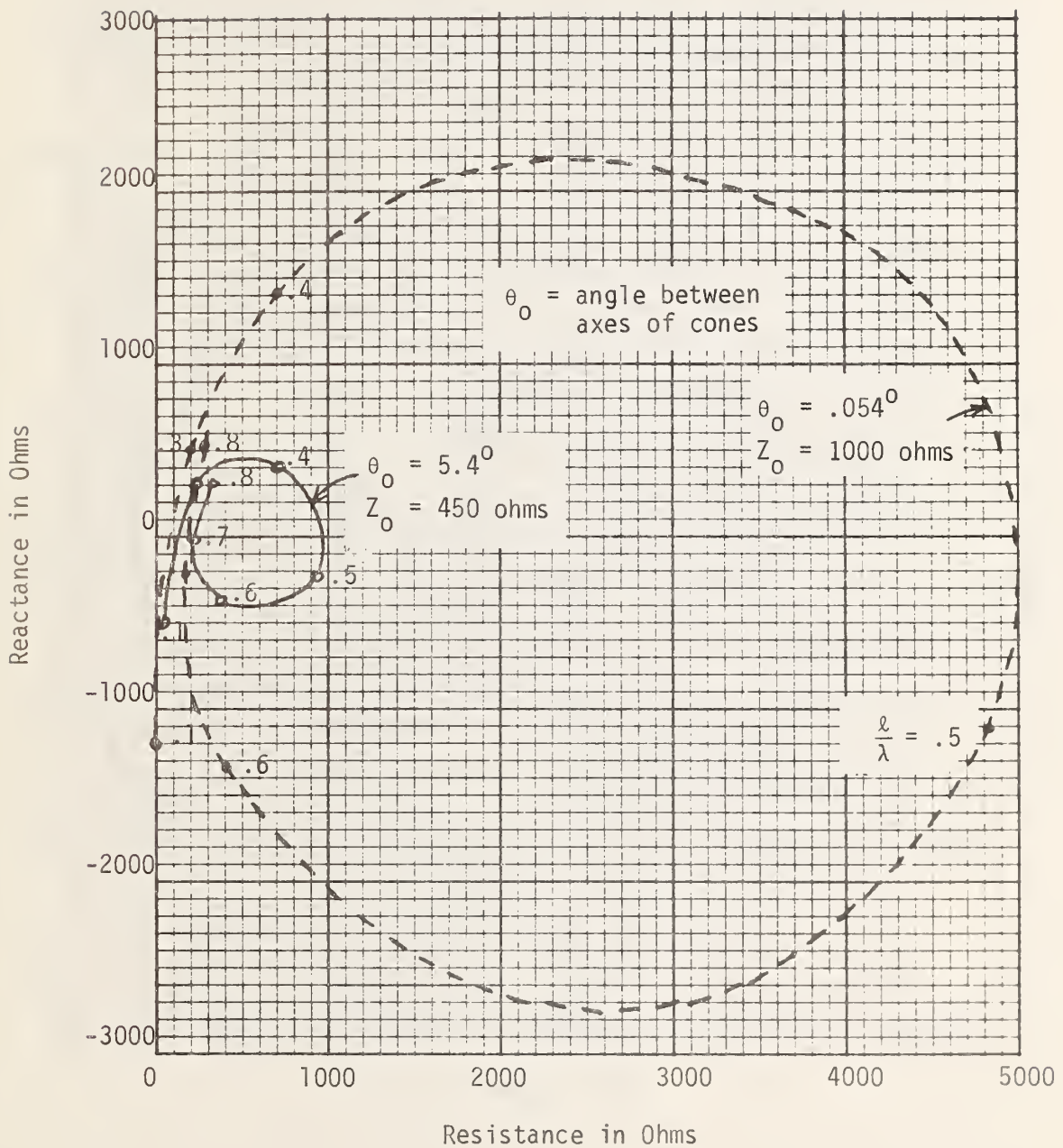


Figure 9. Input impedance of biconical antennas with  $5.4^\circ$  cone angle and  $.054^\circ$  cone angle as a function of the length,  $l$ , of the cone in wavelengths,  $\lambda$  (plotted from data presented by Kraus [12]).

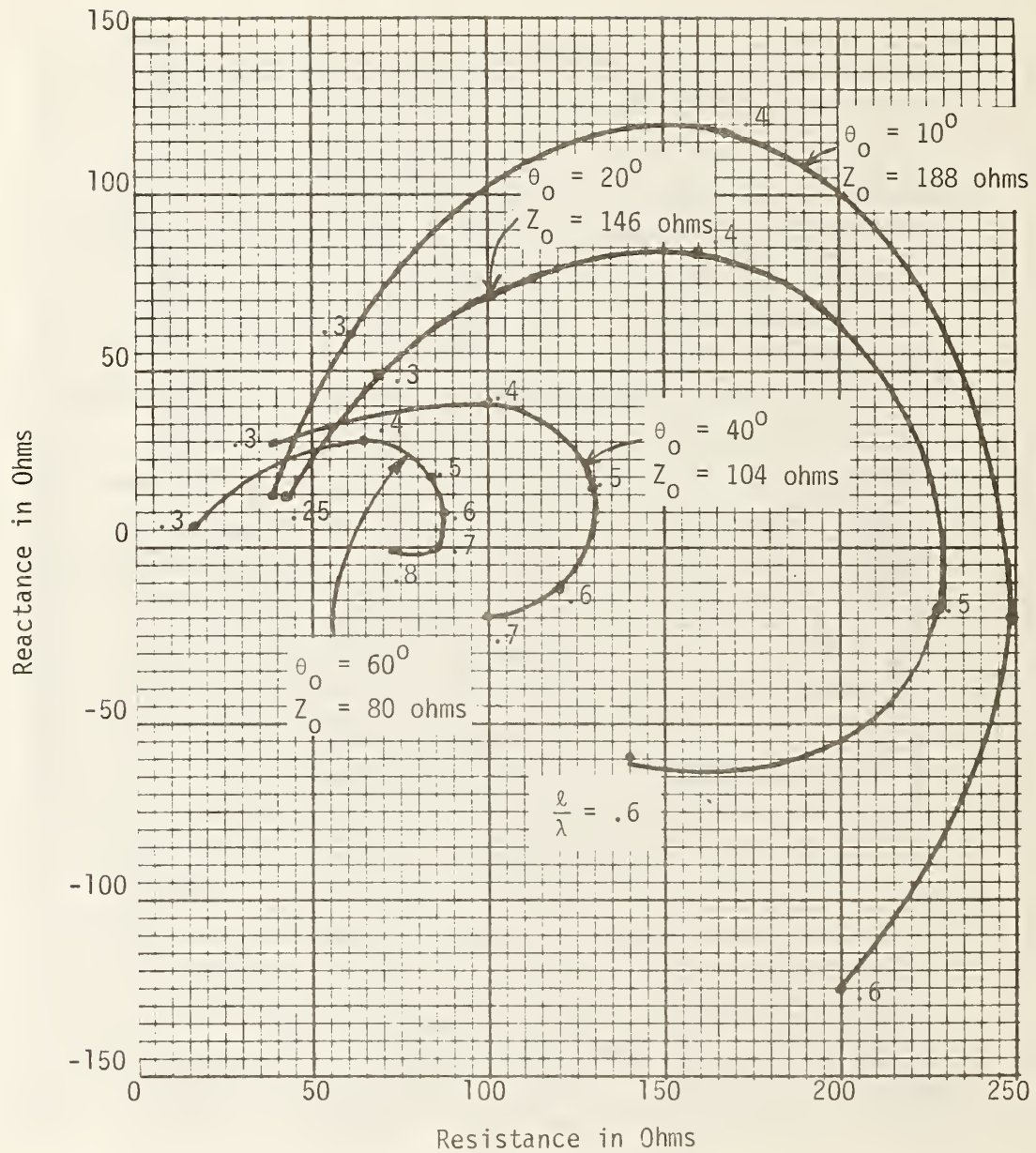


Figure 10. Input impedance of single cones with ground plane as a function of cone length,  $l$ , in wavelengths,  $\lambda$ . Cone angles are  $10^\circ$ ,  $20^\circ$ ,  $40^\circ$  and  $60^\circ$  (plotted from data presented by Kraus [12]).

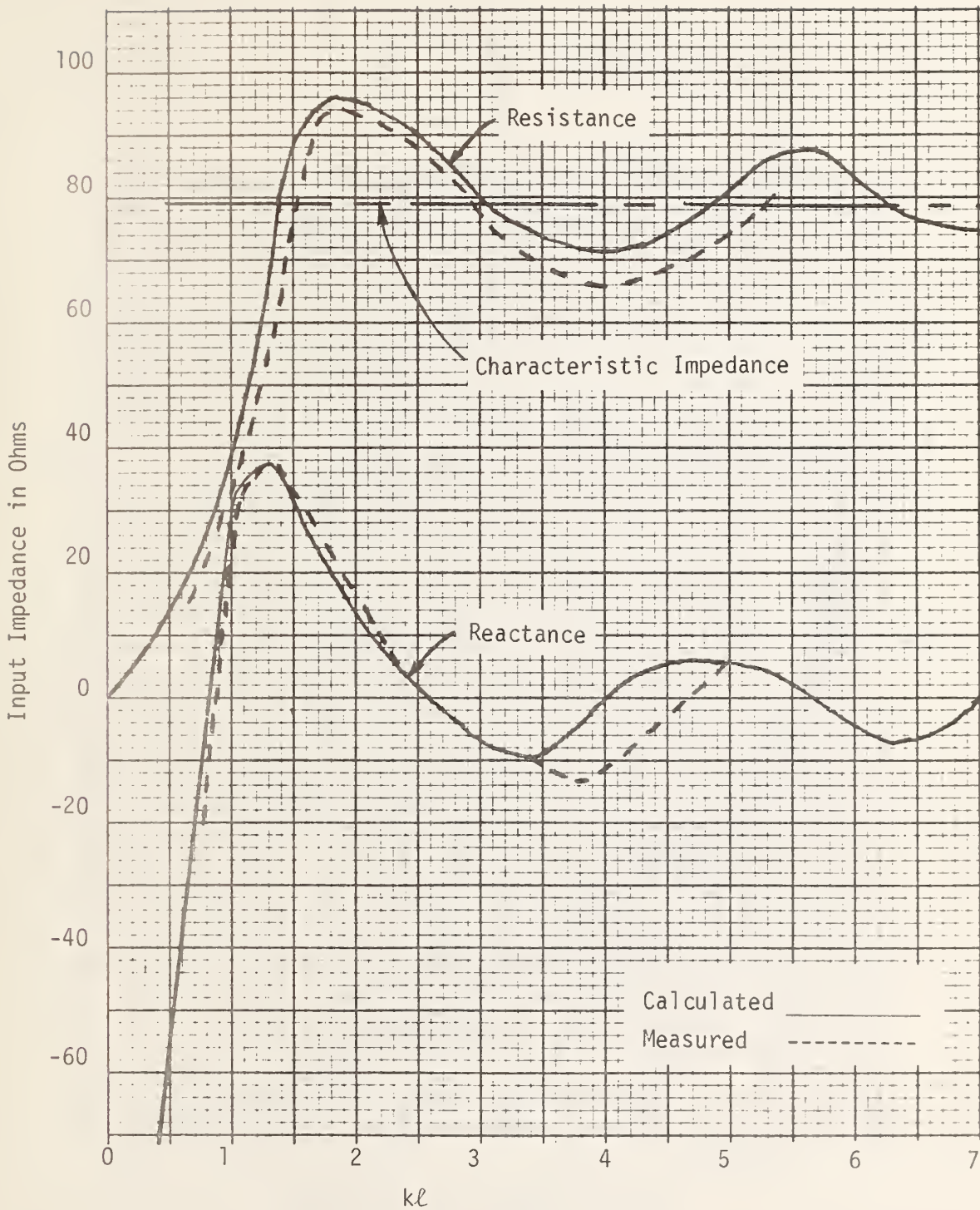


Figure 11. Input impedance of single cone with ground plane versus  $kl$ .  $K$  is the wave number,  $\ell$  is the cone length and the cone angle,  $\theta_0$ , is  $60^\circ$  (plotted from data presented by Papas and King [13]).

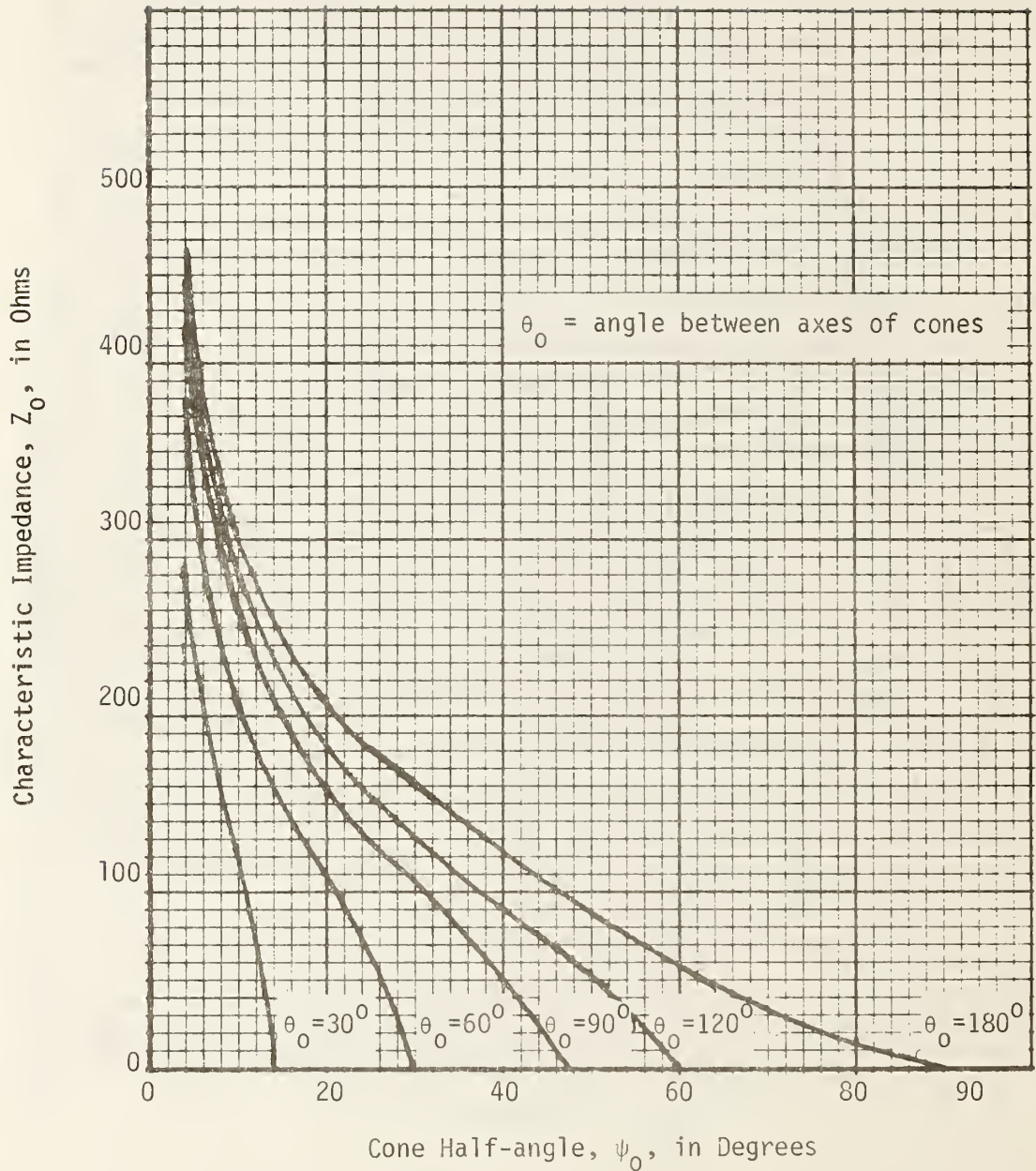


Figure 12. Characteristic impedance of a biconical antenna with equal cone angles,  $\psi_0$  (plotted from data presented by Carrel [9]).

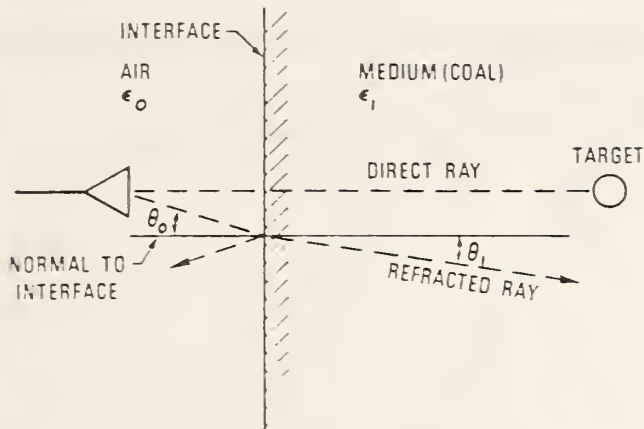


Figure 13a. Sketch of rays from source to field point (target). Rays are refracted into the second medium and partially reflected,  $n_0 < n_1$ .

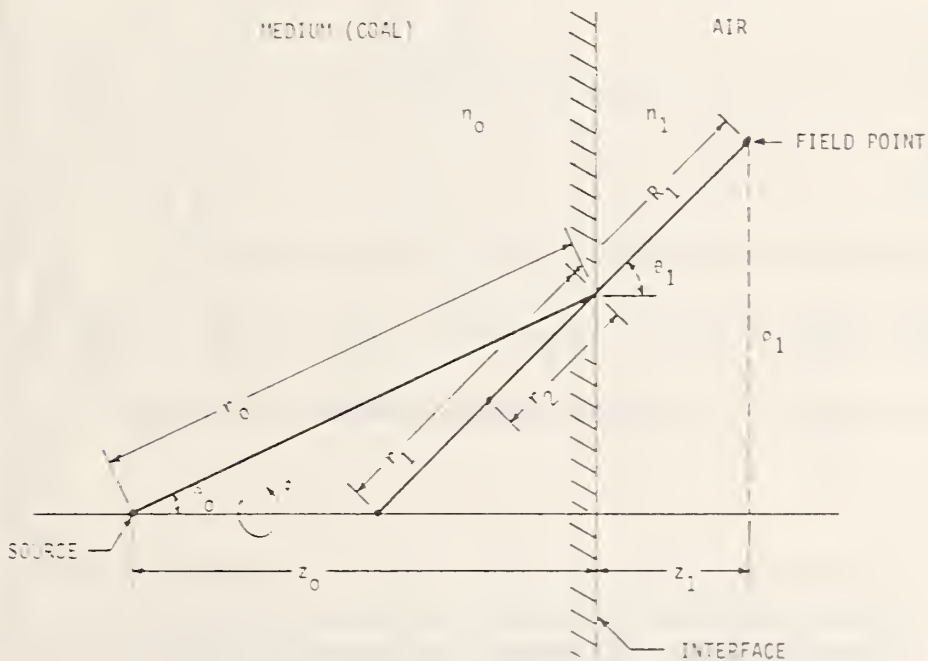


Figure 13b. Geometry for calculating Sommerfeld interface transmission. In this example, the source is in the denser medium with refractive index  $n_0 > n_1$ .

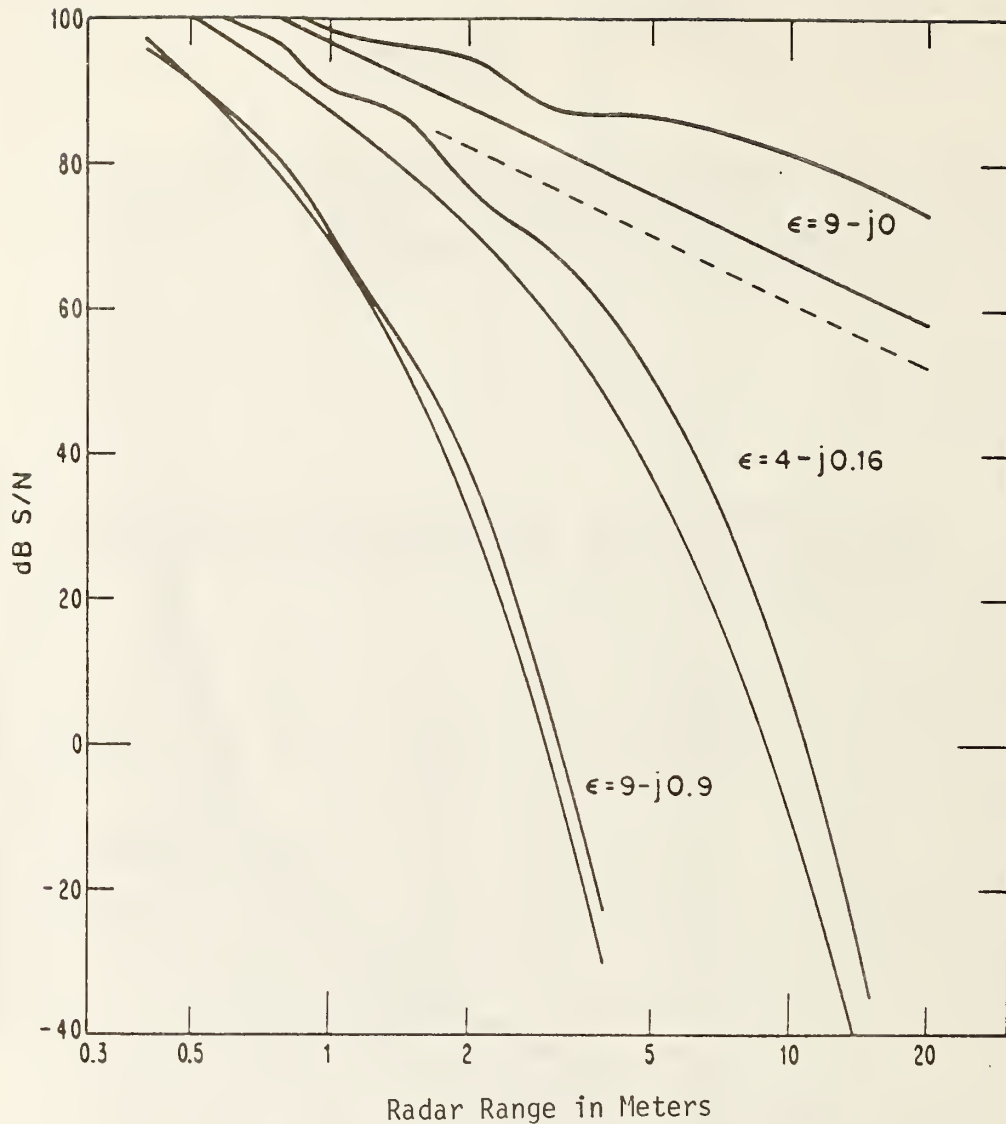


Figure 14. Signal-to-noise ratio for a CW radar system with the following parameters: 500 MHz source; horn antennas 50.8 cm by 76.2 cm; frequency = 0.5 GHz; complex permittivity =  $9 - j0$  for low loss curves,  $4 - j0.16$  for medium loss curves,  $9 - j0.9$  for high loss curves. The upper curve of each group is for a flat mine tunnel wall 1.5 meters high of infinite length with water in the tunnel. The lower solid curve of each group is for a 30 cm diameter cased borehole. The dashed curve is for a water filled borehole without casing having a 30 cm diameter. The system noise is assumed to be 8 dB greater than Johnson noise in a 1 MHz bandwidth and clutter is ignored.

SIMULATED TIME DOMAIN WAVEFORMS  
 5, 2, 1 AND 1/2 NS WIDE AT THE 50% POINT

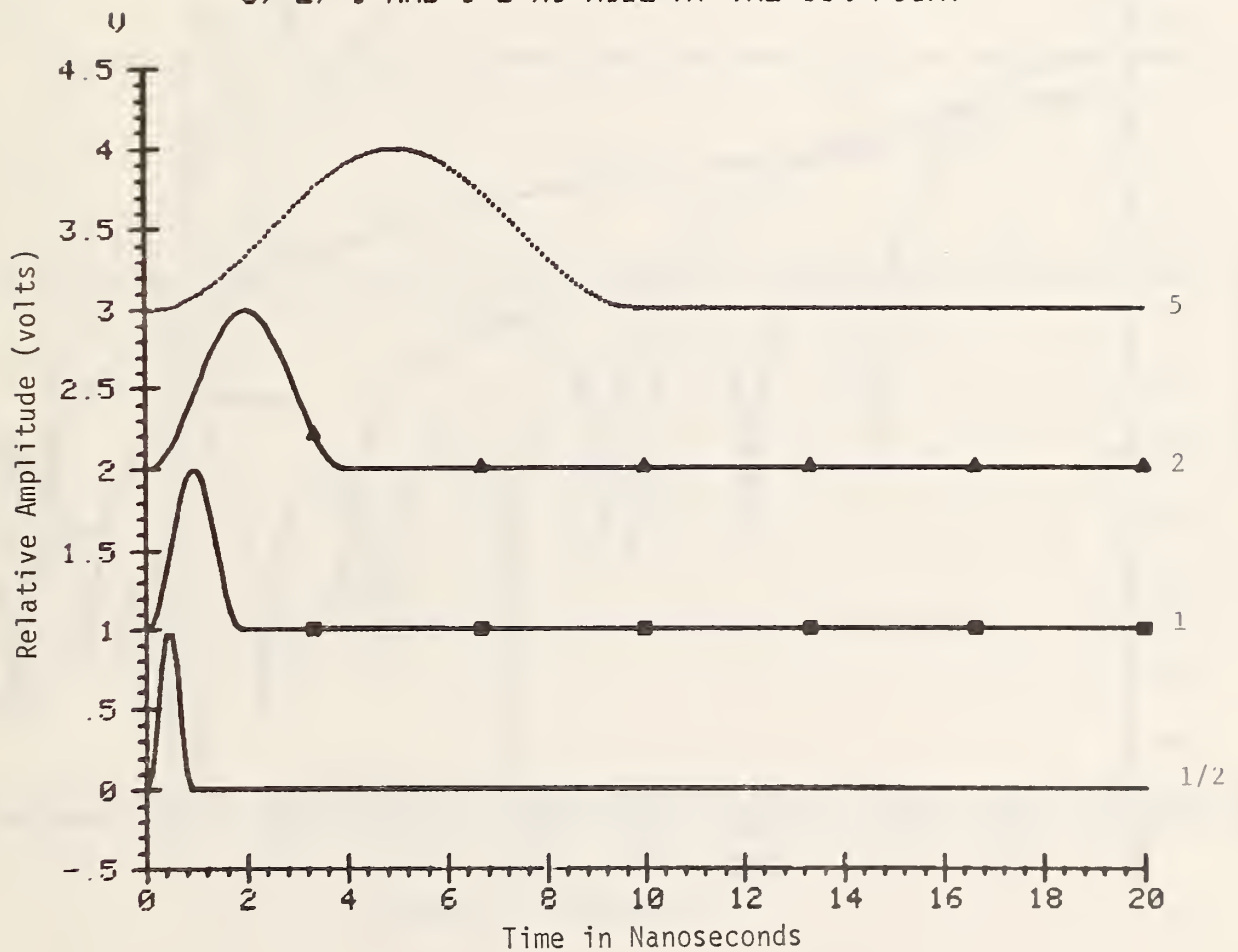


Figure 15. Simulated impulse waveforms having widths of 5, 2, 1, and 1/2 ns at the 50% point.

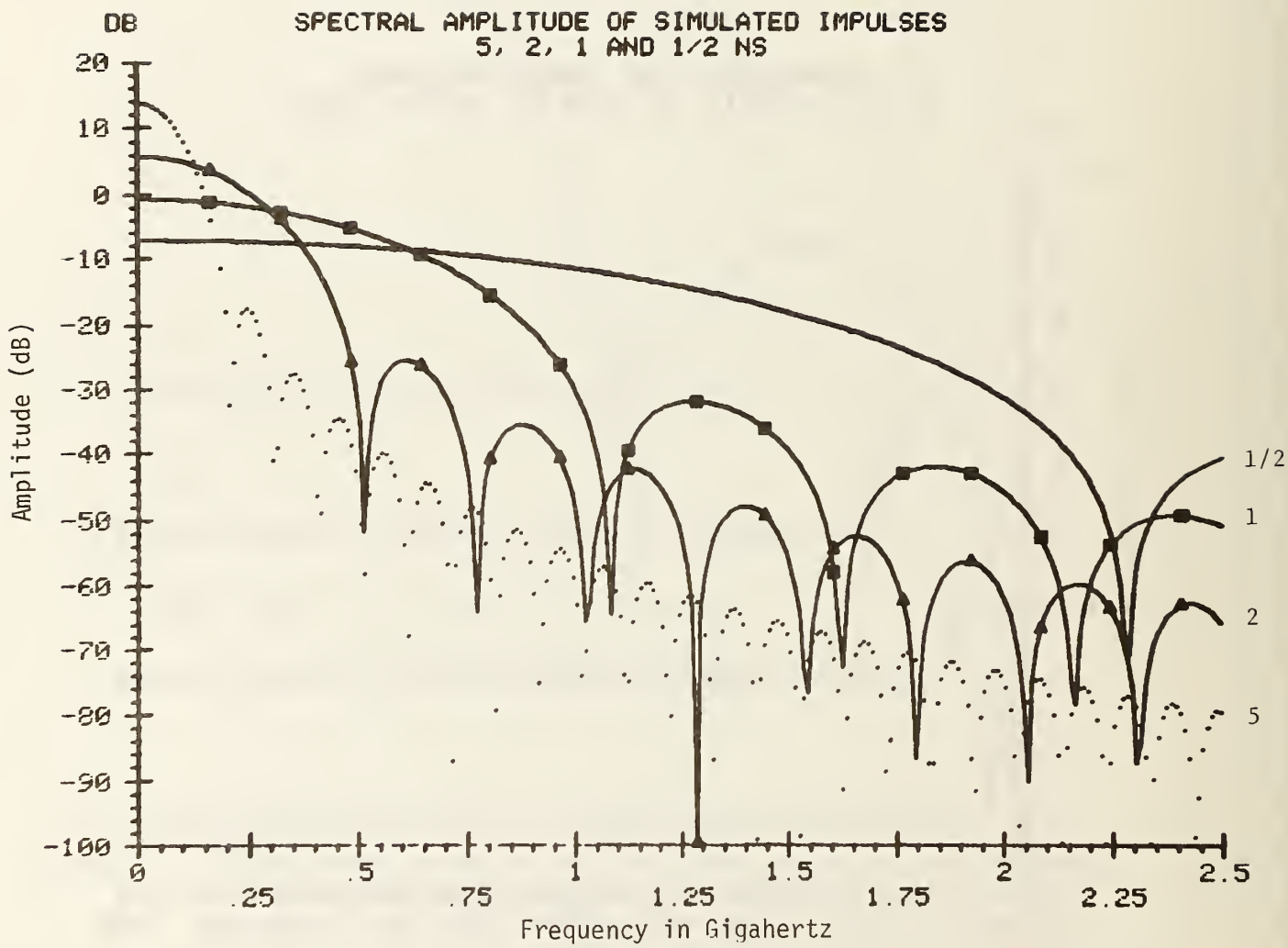


Figure 16. Resulting spectral energy distribution of the impulses shown in figure 15 in dB relative to  $10^{-9}$  volt-seconds.



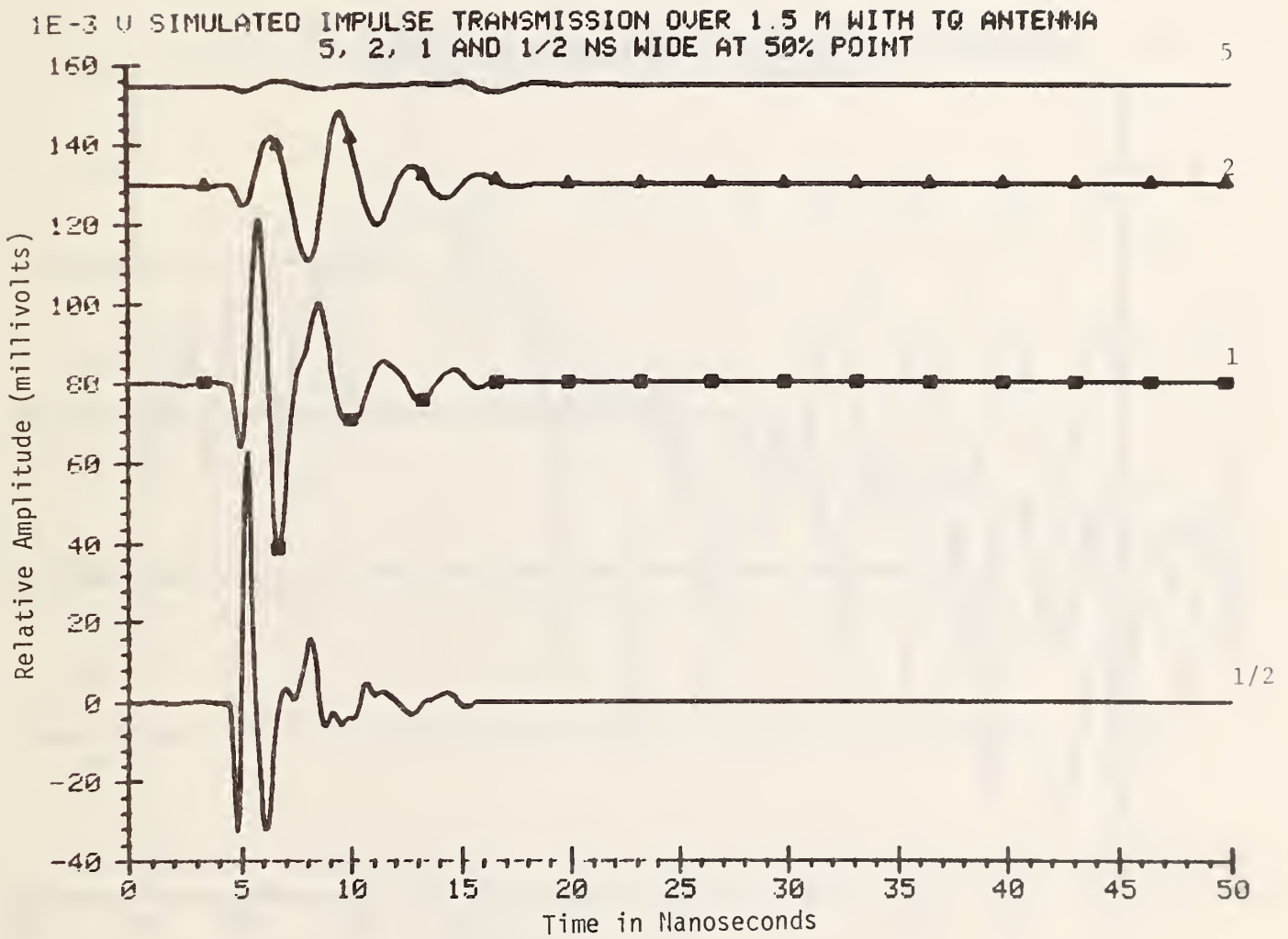


Figure 17. The signals resulting from transmission of the impulses shown in figure 15 over a 1.5 meter path with the TQ antennas.

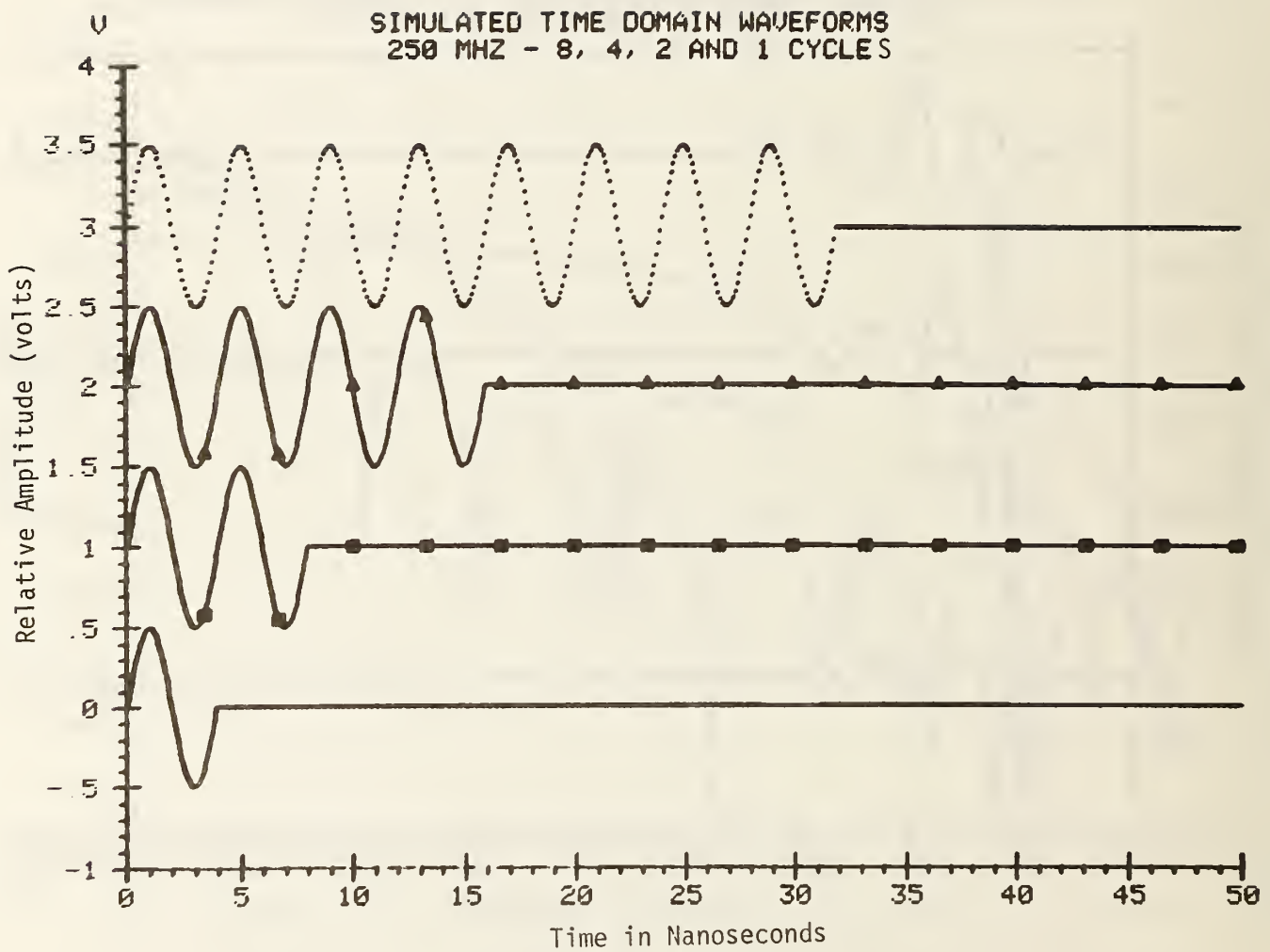


Figure 18. Simulated sinusoidal pulse waveforms having 8, 4, 2, and 1 cycles.

SPECTRAL AMPLITUDES OF SIMULATED 250 MHZ WAVEFORMS  
 8, 4, 2 AND 1 CYCLE WITH RESPECT TO  $1E-9$  VOLT-SECONDS

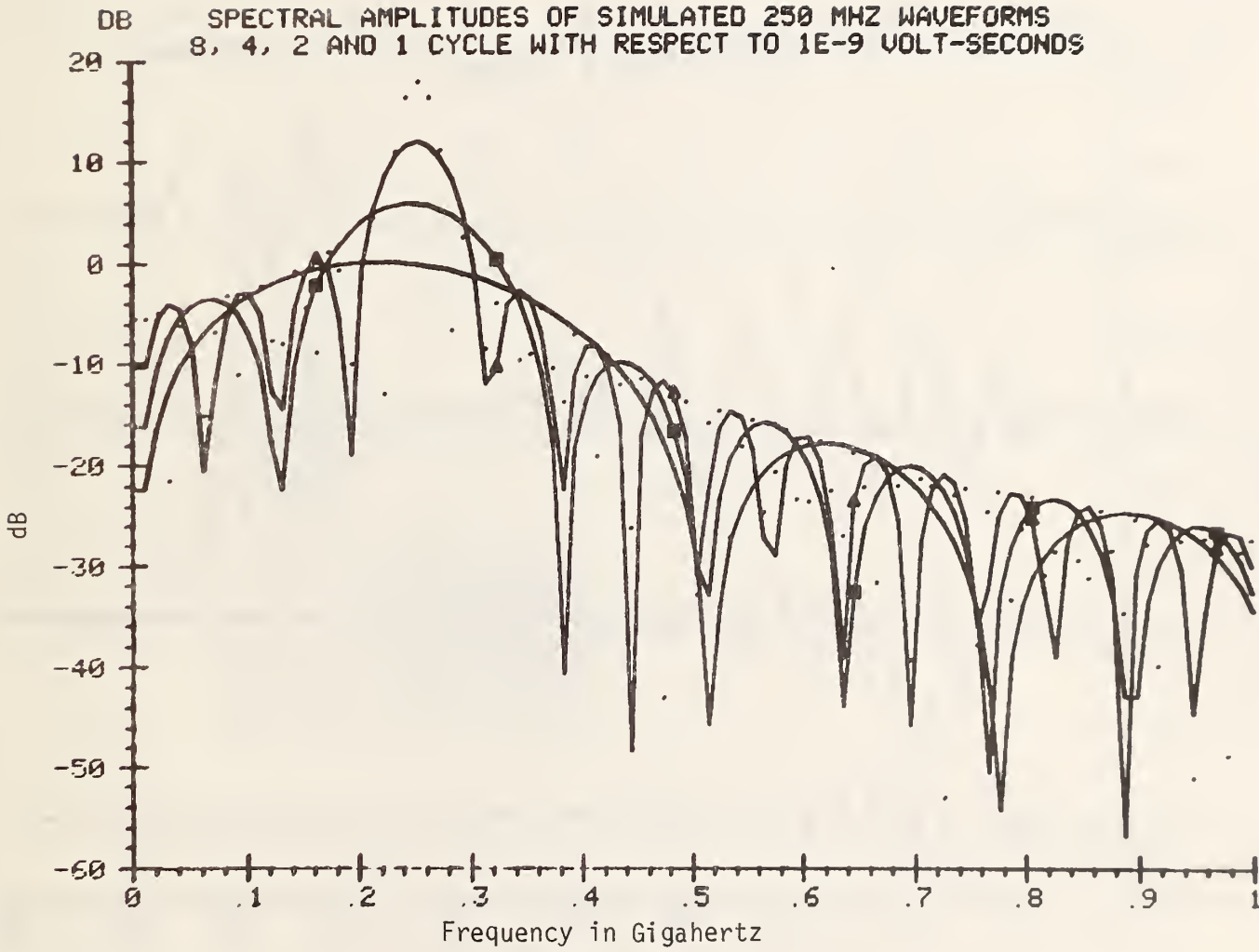


Figure 19. Resultant spectral amplitude of the sinusoidal pulses shown in figure 18. 8-cycle pulse, dotted curve; 4-cycle pulse, triangles; 2-cycle pulse, squares; 1-cycle pulse, solid line with no marker.

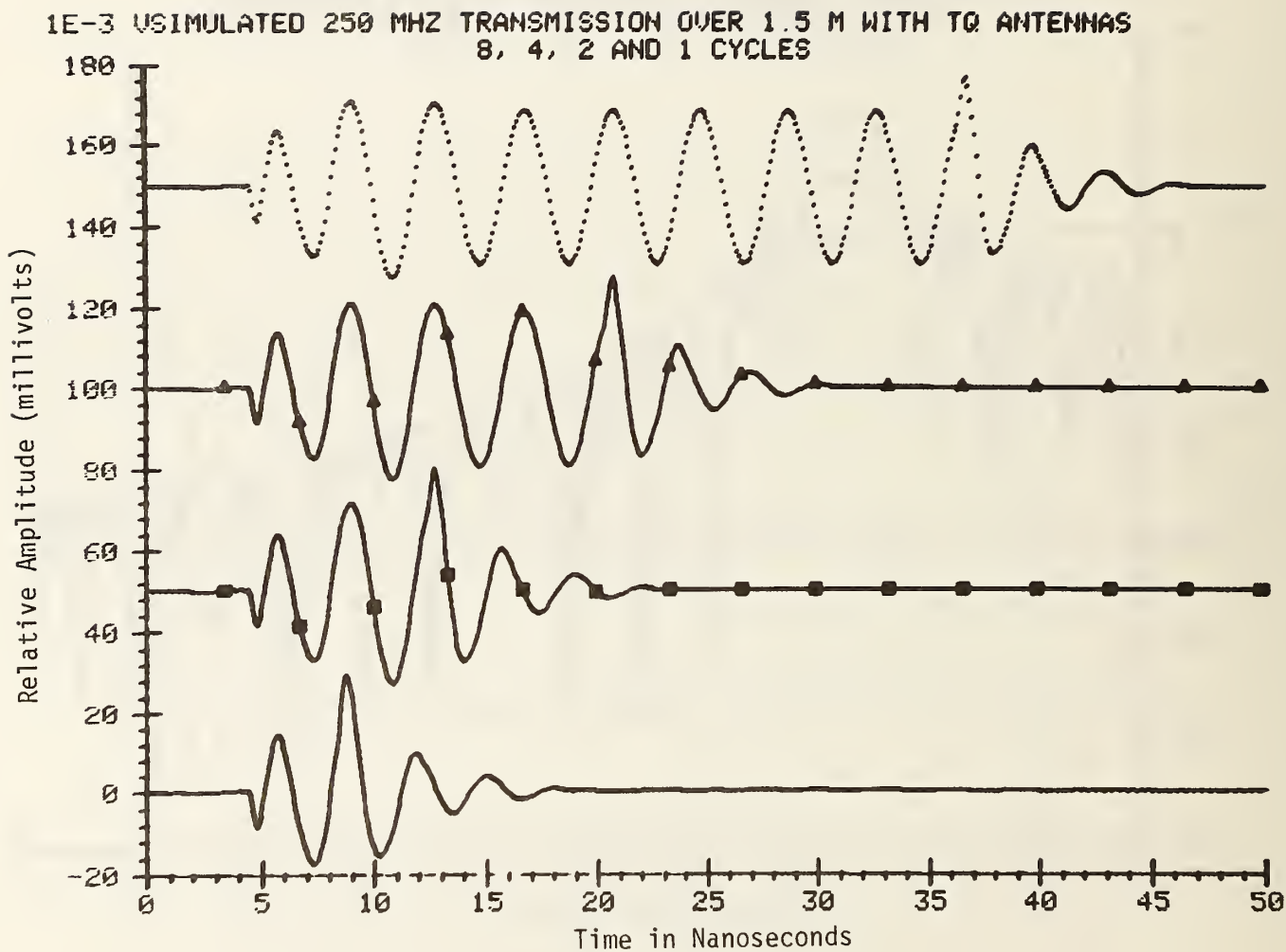


Figure 20. The signals resulting from the transmission of the sinusoidal pulse waveforms shown in figure 18 over a 1.5 meter path using TQ antennas.

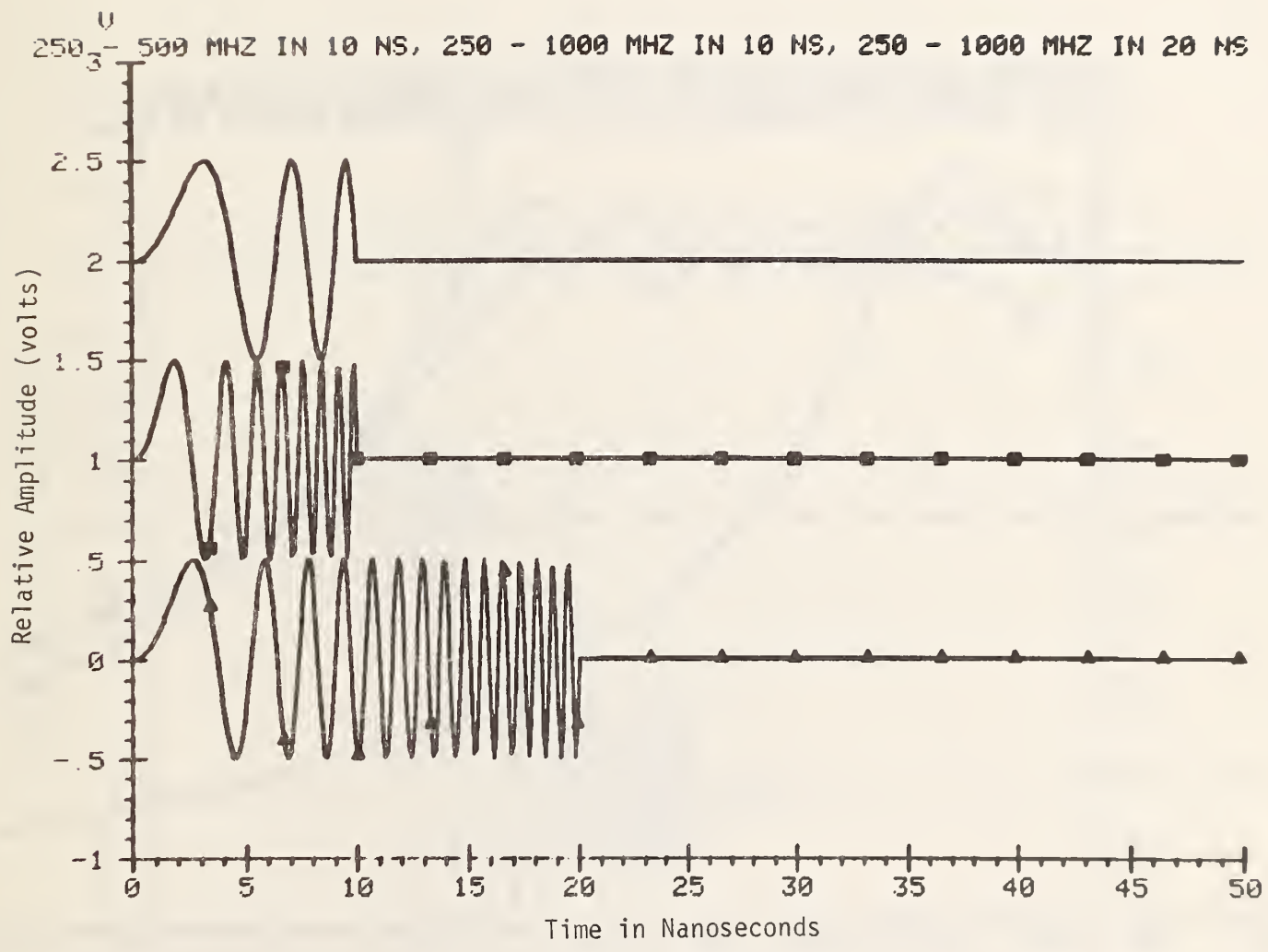


Figure 21. Simulated linear chirp pulse waveforms.  
 250-500 MHz in 10 nanoseconds, plain curve.  
 250-1000 MHz in 10 nanoseconds, square markers.  
 250-1000 MHz in 20 nanoseconds, triangle markers.

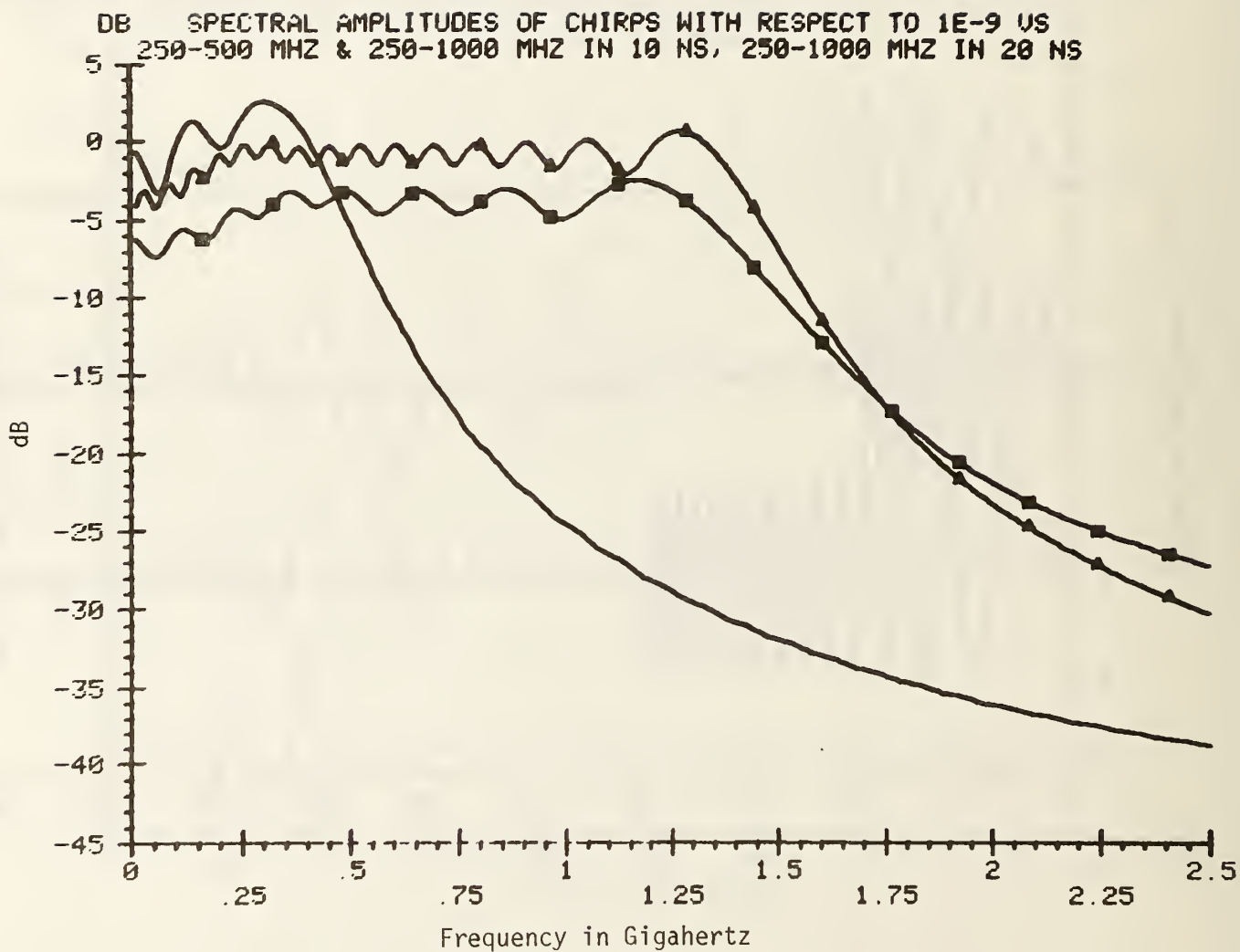


Figure 22. Resulting spectral amplitudes of the linear chirp pulse waveforms shown in figure 21. The curve markers correspond to figure 21.

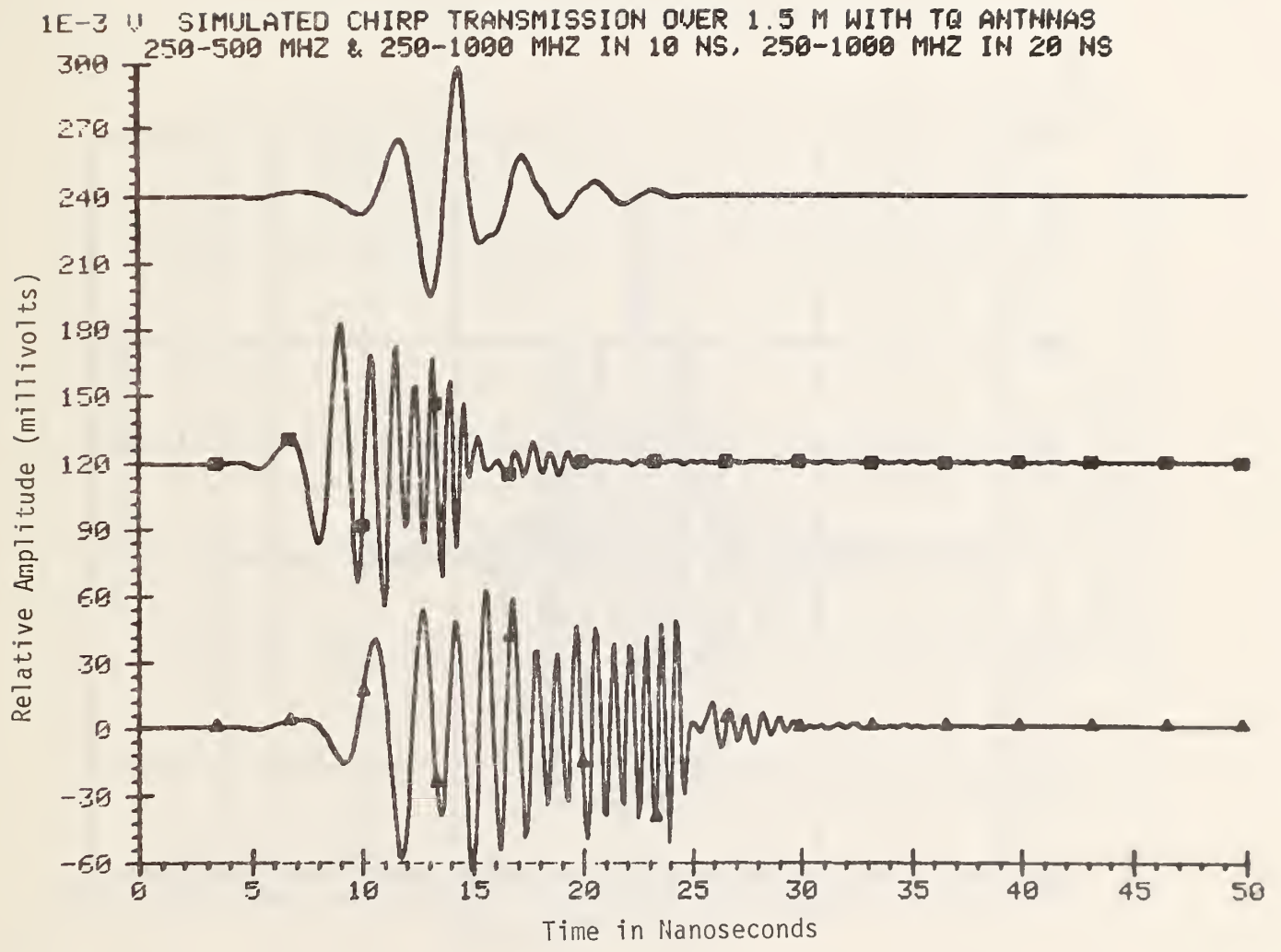


Figure 23. Resulting signals after transmission of the linear chirp pulses over a 1.5 meter path using TQ antennas. The curve markers correspond to figure 21.

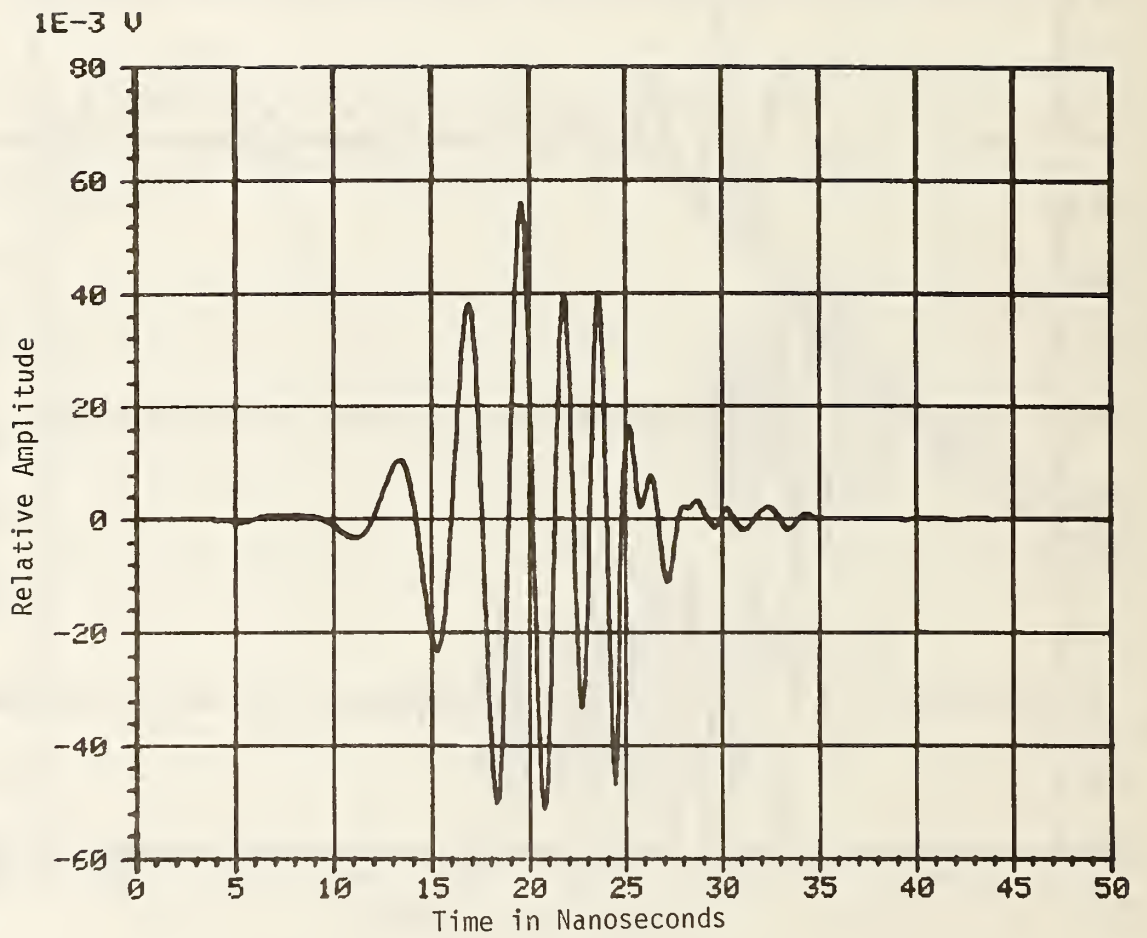


Figure 24. The result of transmitting a 300-600 MHz linear chirp pulse over a 1.5 meter path using the TQ antennas.



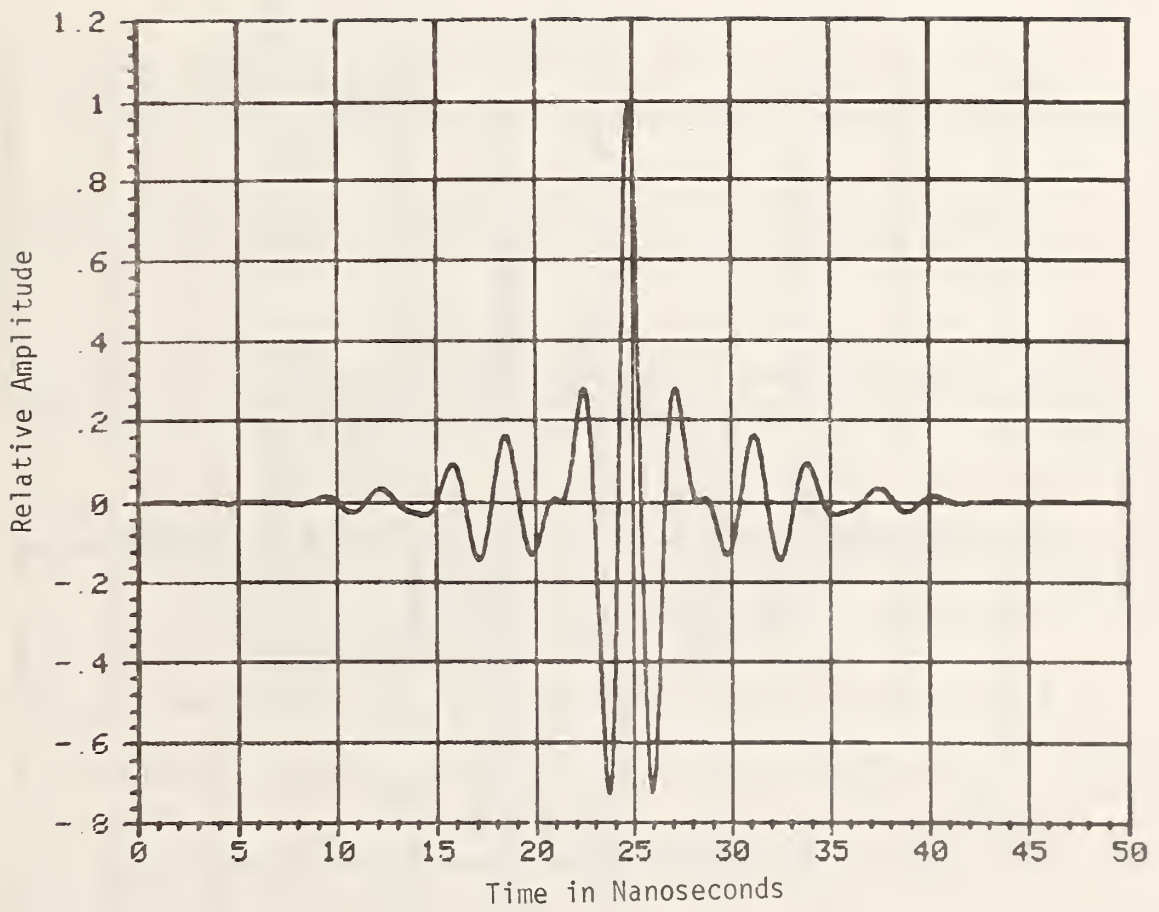


Figure 25. The result of autocorrelation of the waveform of figure 24.

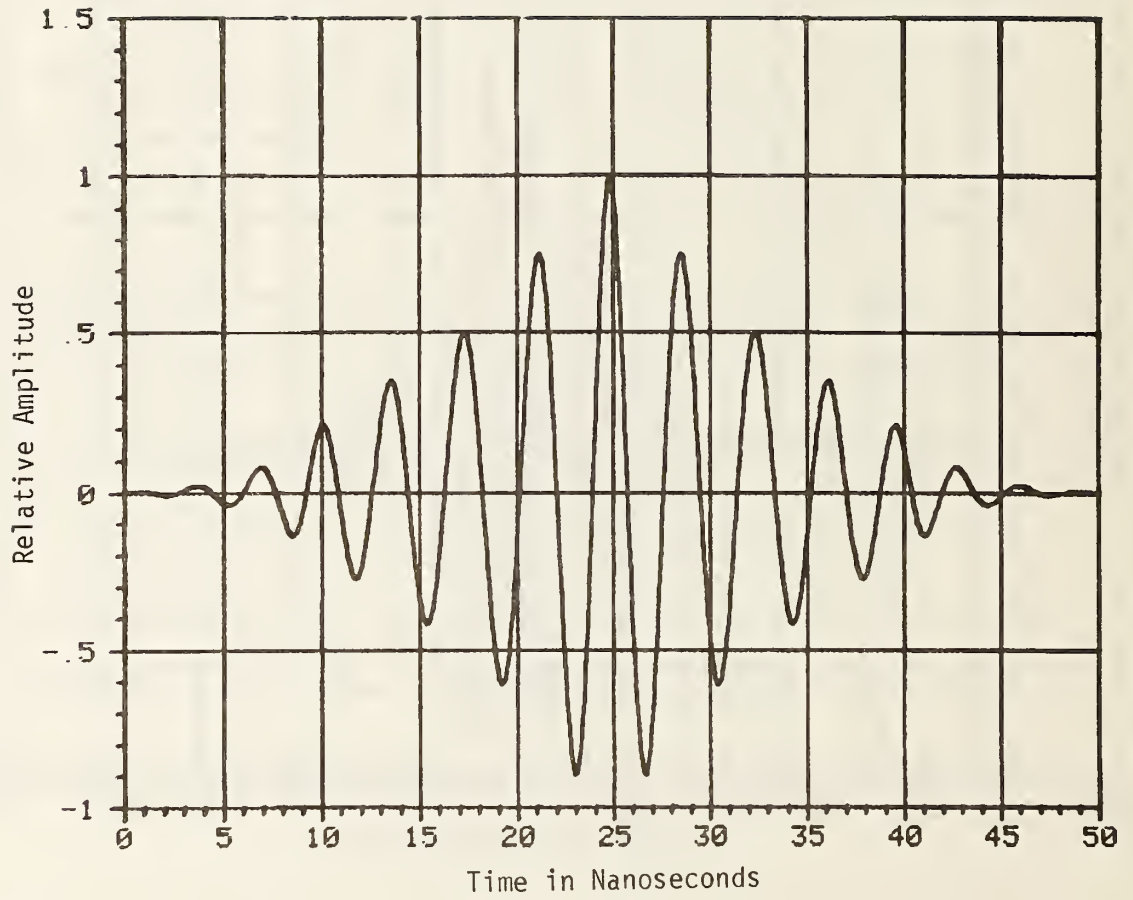


Figure 26. Autocorrelation of the transmitted waveform of the 4 cycle, 250 MHz sinusoidal pulse.

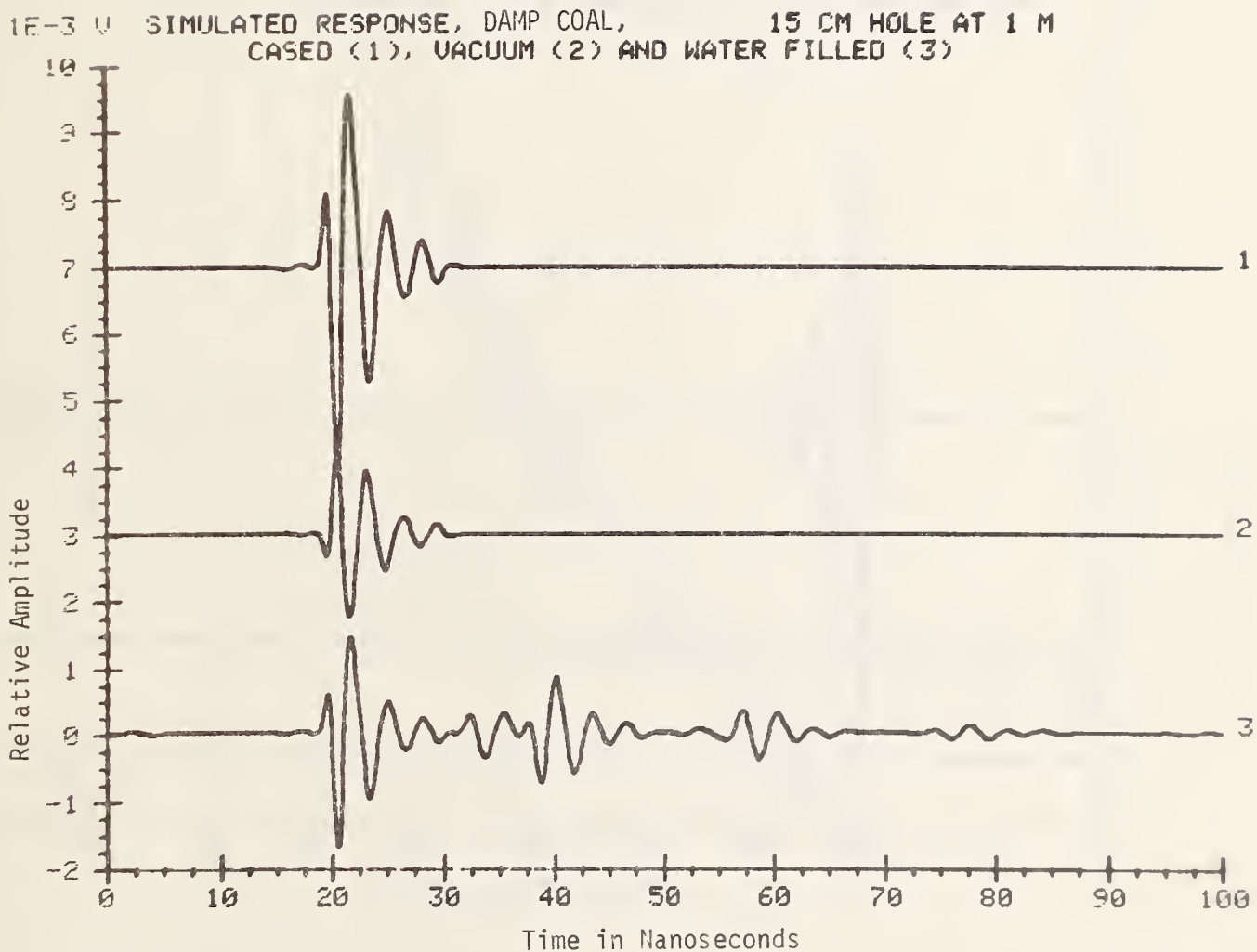


Figure 27. Simulated response in relatively damp coal for a 15 cm radius hole at 1 meter range. (1) cased hole, (2) air-filled hole, (3) water-filled hole.

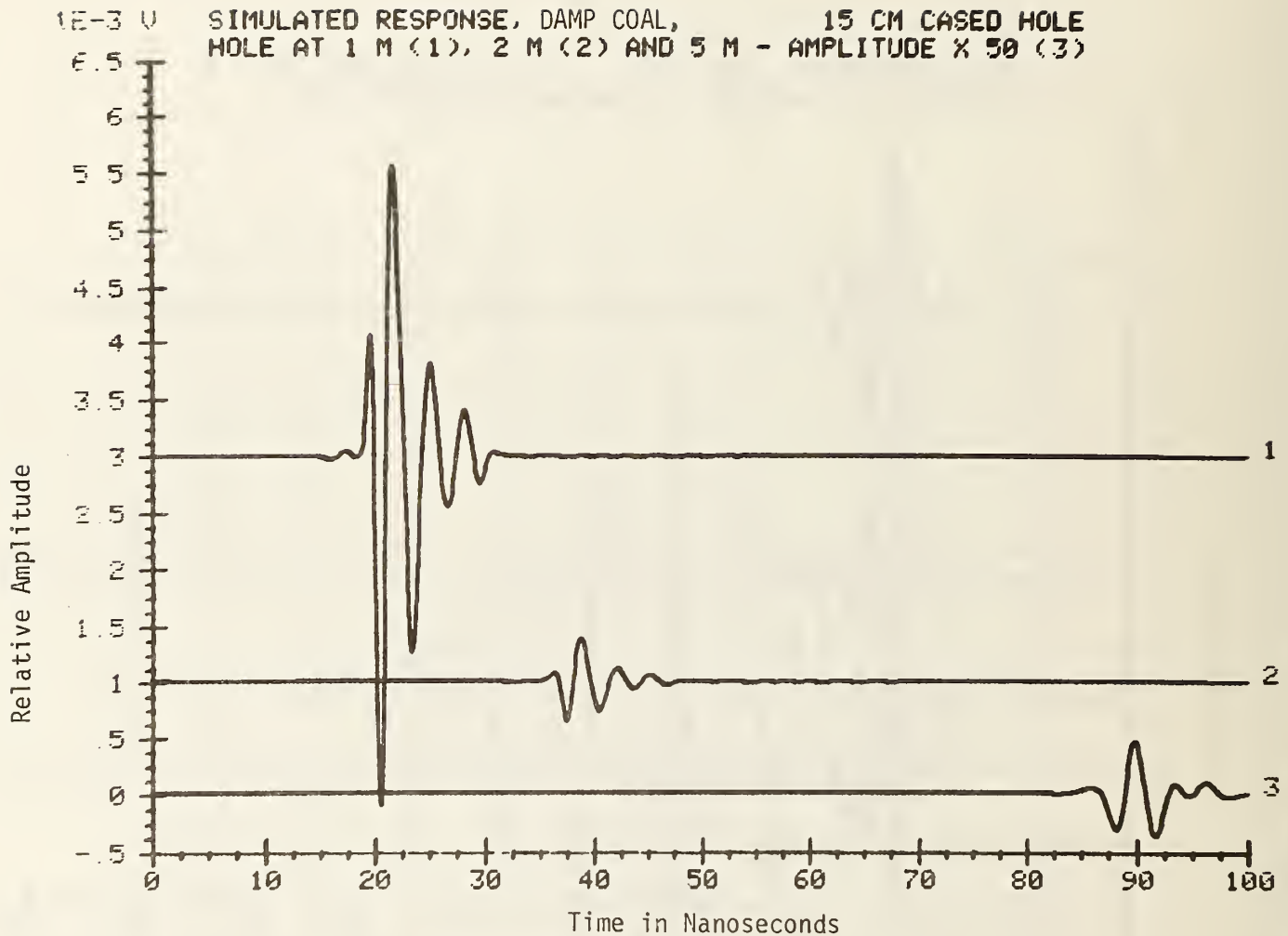


Figure 28. Simulated response in relatively damp coal for a 15 cm radius hole at a range of 1 meter (1), 2 meters (2), and 5 meters (3). The amplitude of the response at 5 meters has been amplified 50 times.

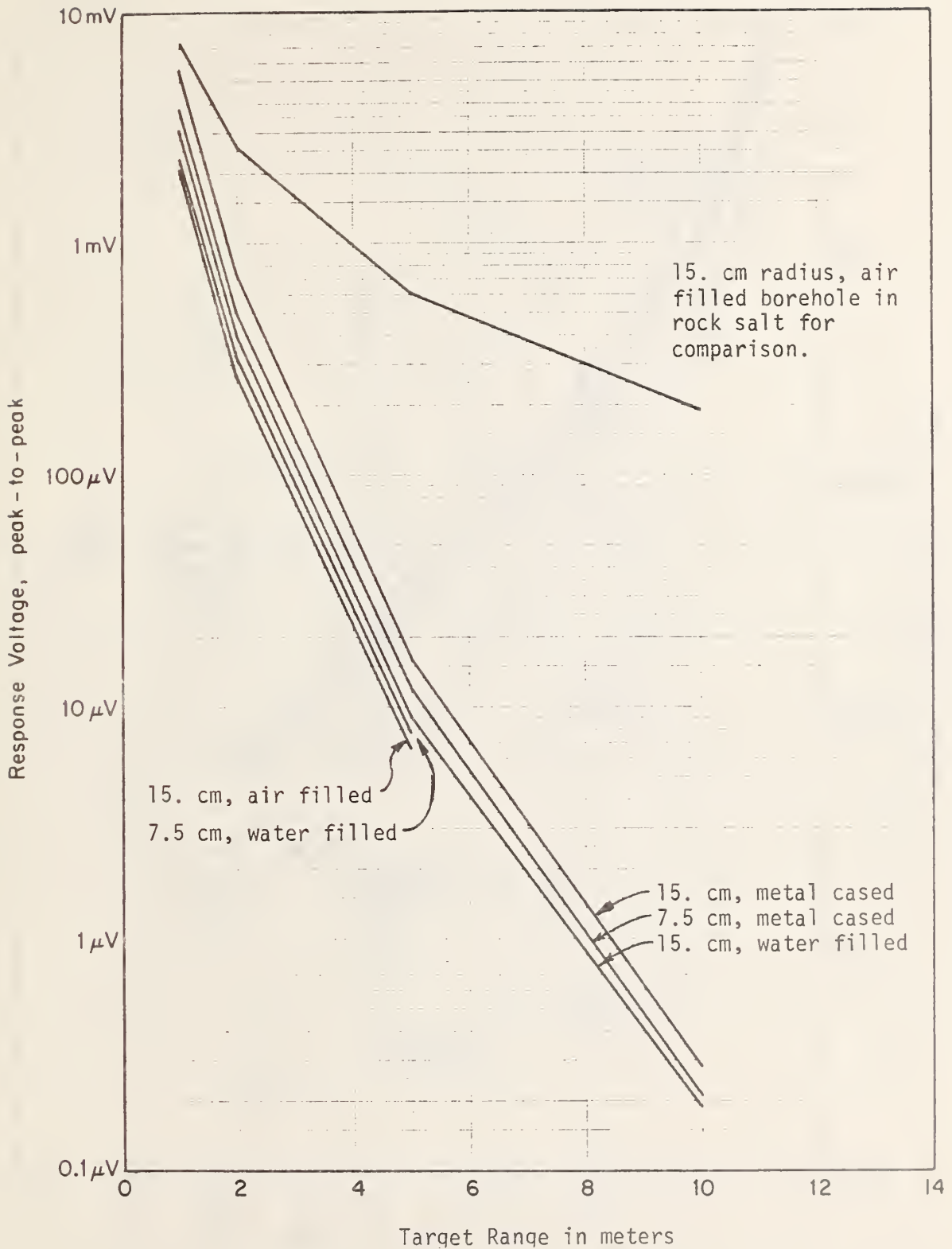


Figure 29. Simulated radar response in relatively damp coal for a 1.0 volt, 1 nanosecond input pulse reflected from a borehole. The given dimension is the borehole radius.

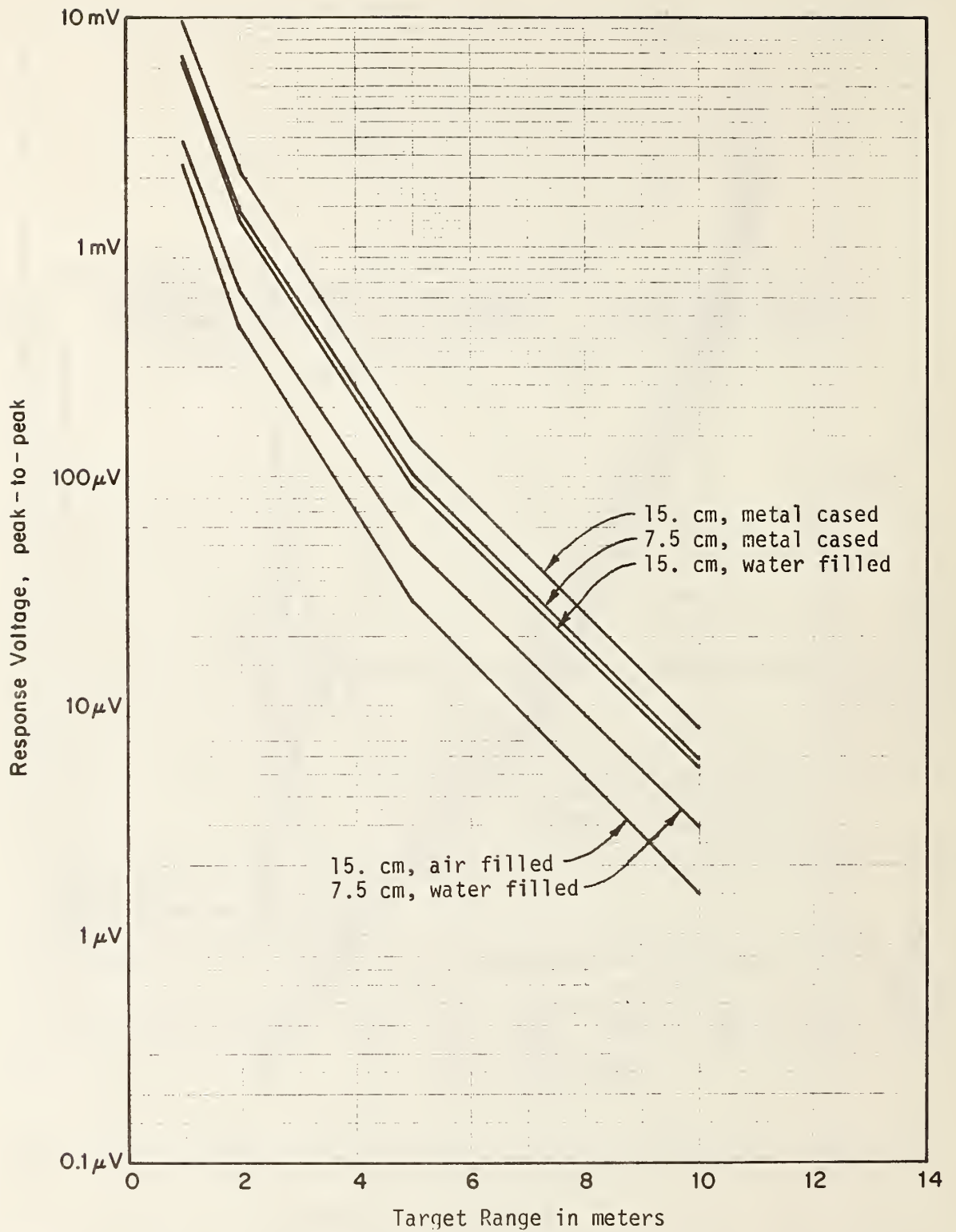


Figure 30. Simulated radar response in relatively dry coal for a 1.0 volt, 1 nanosecond input pulse reflected from a borehole. The given dimension is the borehole radius.

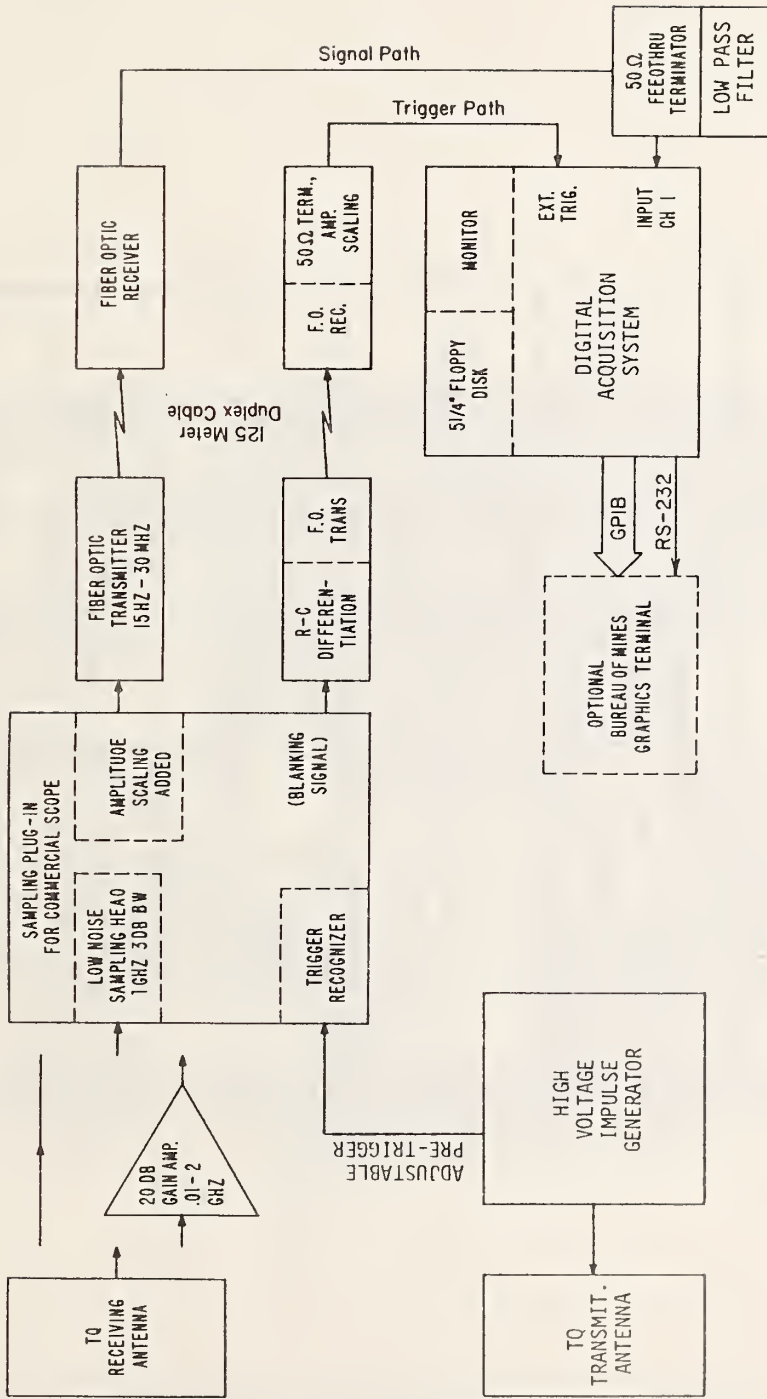


Figure 31. Preprototype pulse system block diagram.

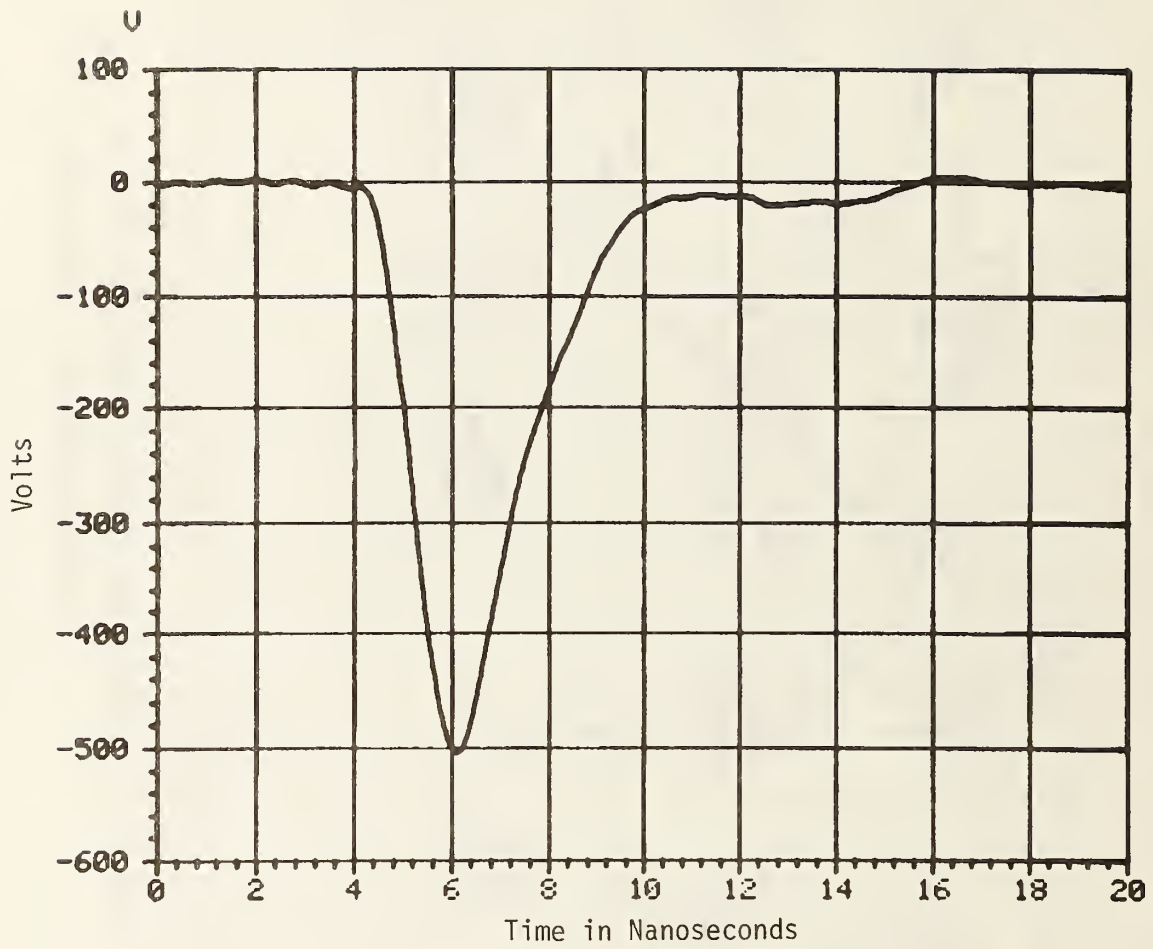


Figure 32. Output waveform of the high-voltage impulse generator.



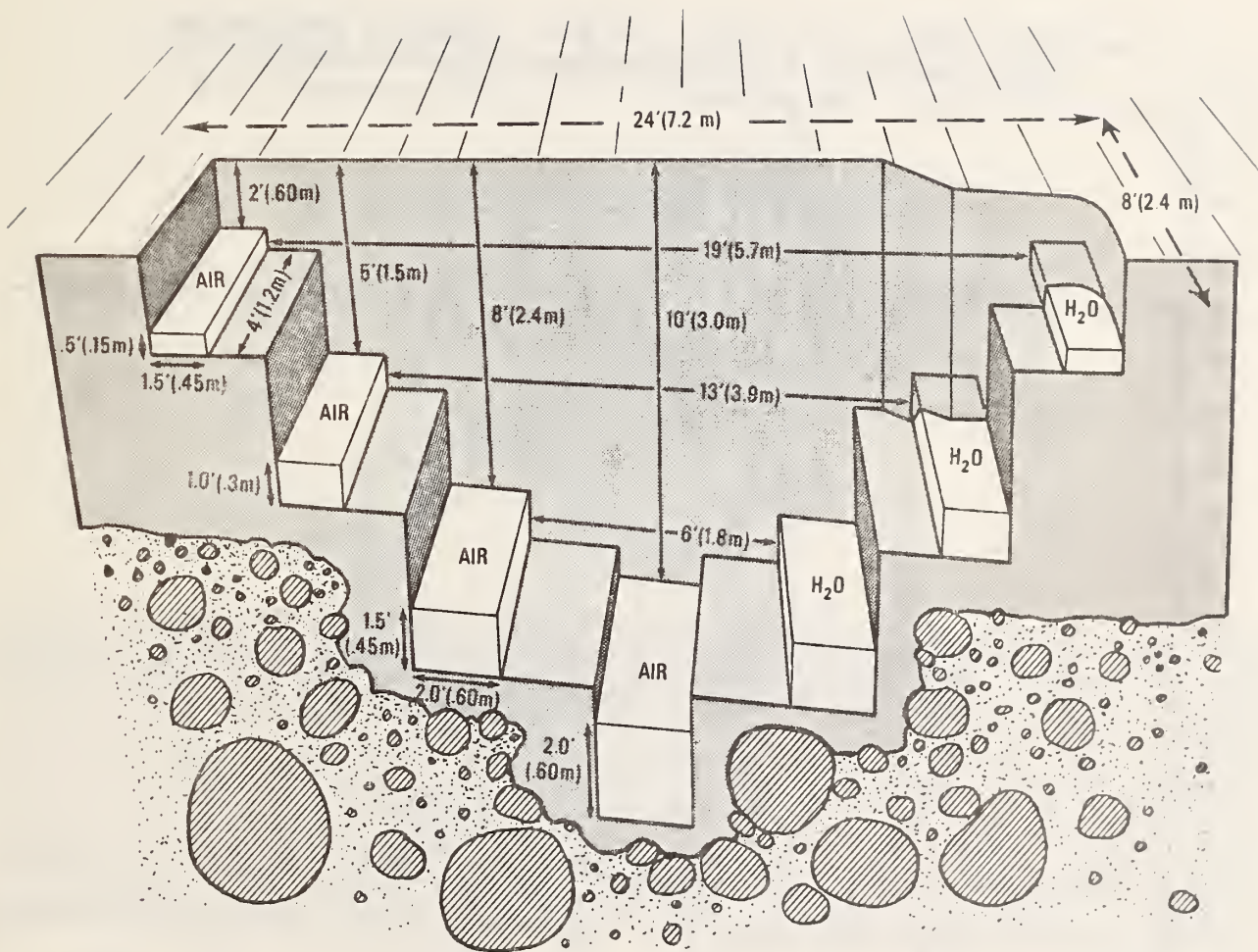


Figure 33. NBS range for subsurface anomaly measurements.

1E-3 UTQ ANTENNAS OVER 2 FOOT DEEP AIR BOX, AVERAGED BACKGROUND,  
OVER TARGET & OVER TARGET-AVERAGED BACKGROUND

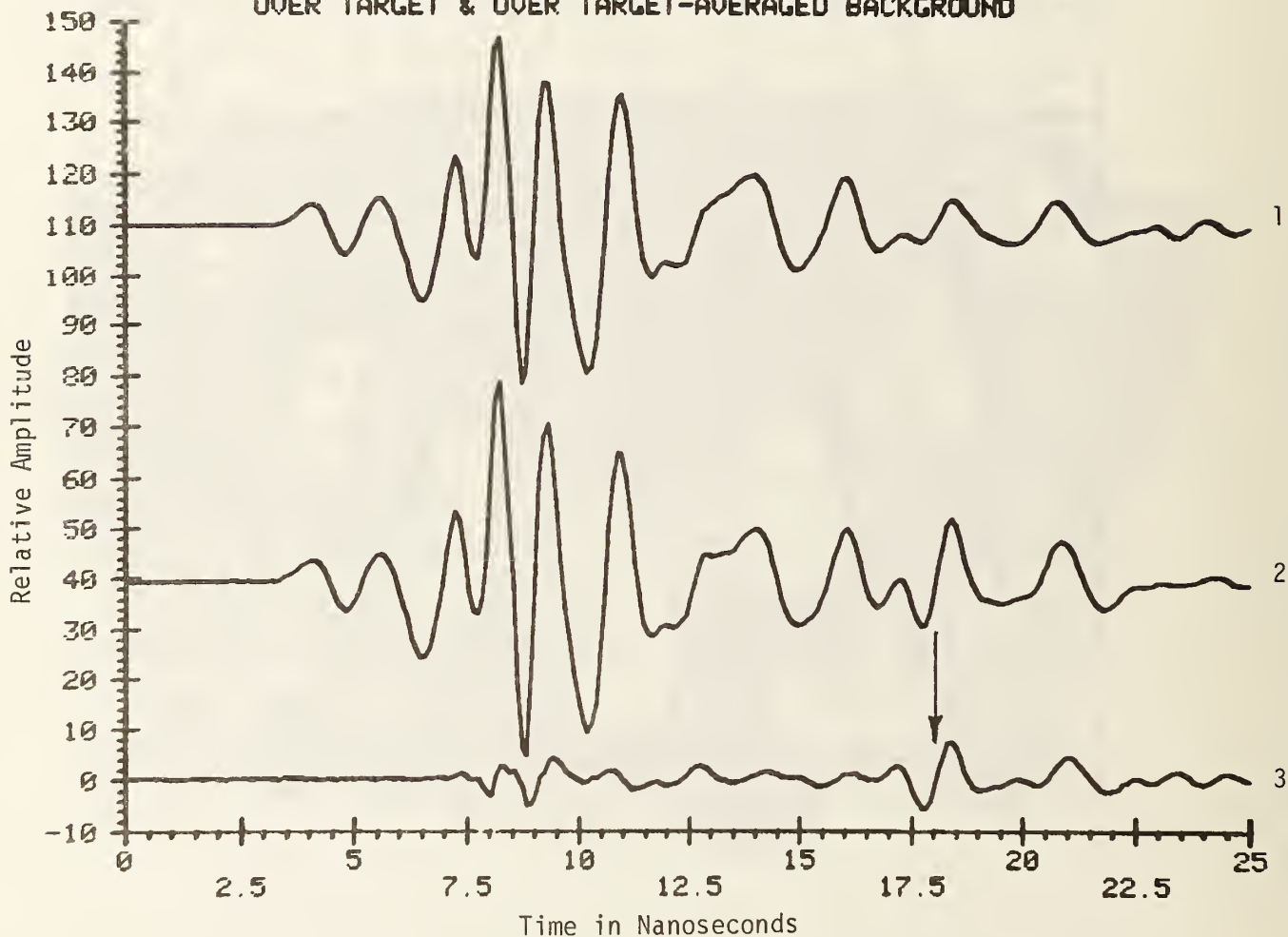


Figure 34. Pulse system response averaged over a sequence of 26 measurements (1). Single response from over the 0.6 meter deep air-filled target (2). The resulting response showing the target signal enhancement (arrow) obtained by subtracting the sequence average from the response at one position (3).

TQ ANTENNAS WITHOUT PRE-AMP SCANNING OVER 2' TARGET  
FILE TQ65MN.5 FROM 0 TO 2.49023E-08 MINUS TQ65MN.5AV

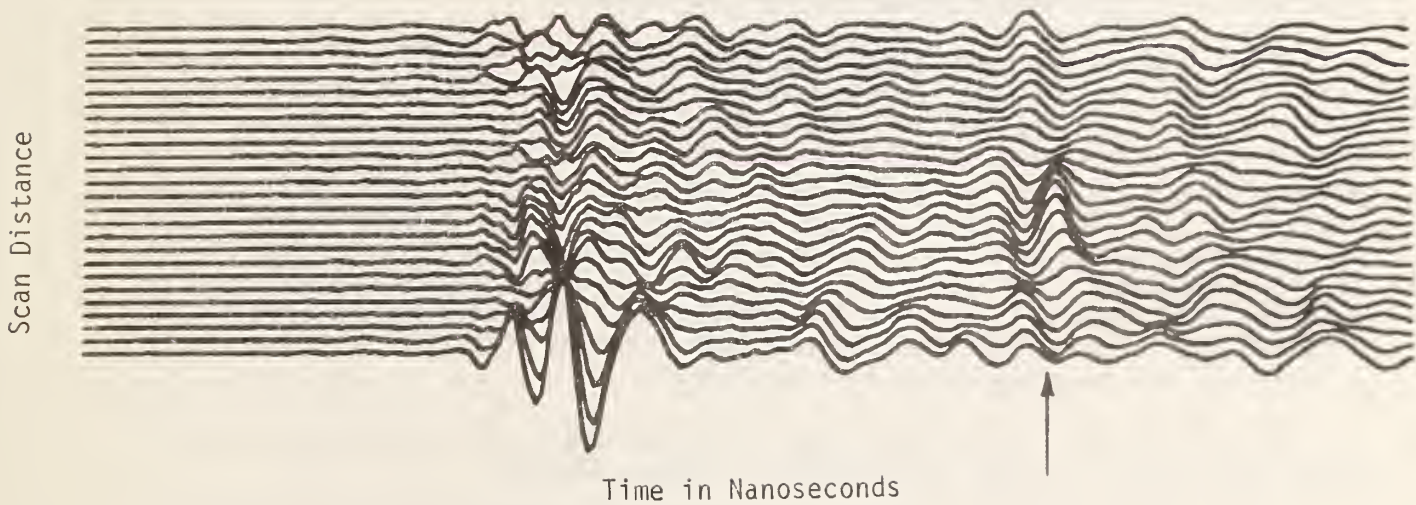


Figure 35. A stacked series of modified responses obtained by subtracting the average response of the series from each measured response. Target signal at arrow.

**APPENDIX A**

**COMPUTER PROGRAM FOR SIGNAL-TO-NOISE RATIO,  
AS A FUNCTION OF DISTANCE (RANGE) TO A SUBSURFACE TARGET**

The program listing, written in BASIC language, is included in this appendix. Some results from the program are shown in figure 14, which shows curves for the signal-to-noise ratio, S/N, as a function of distance for specific coal "atmospheres," specific targets, and a specific radar system model.

The radar system has some constant parameters and others as input variable. The constants are given in statement 20 (S20). The variable parameters required are frequency (S60), antenna dimensions (S90), dielectric permittivity and loss tangent of coal (S120), coal conductivity (if the dielectric tangent was entered as zero), and one of the five targets considered as described in S240 and S260, and the target dimension S550. The source power, 10 mW, and the frequency, 500 MHz, are assigned in S116 and S70, respectively.

The noise is that for a classical CW radar with Johnson noise in a 1 MHz bandwidth augmented by an 8 dB noise figure, i.e., multiplied by 6.31. The noise power is calculated as D6 in S490.

The received power is calculated as S4 in S670. The S/N is calculated in line S680.

S/N for other radar systems may require running the program. However, for simple cases, the graph may be reinterpreted. For example, if the source power is increased by 10 dB, the S/N at any range is increased by 10 dB. If the noise is 5 dB greater, then S/N is 5 dB smaller.

With different target dimensions and a different frequency, it is necessary to rerun the program. The statements from 750 to 1800 are used to calculate target cross section as a function of frequency and dimensions. The methods are approximate. The strip validity is discussed in the text. The method for the cylinder cross section branches to one of three methods depending on the  $ka$ . The small and large cases are well known approximations. The intermediate case, S840 to S1020, uses forward recursion to evaluate the cylinder functions (see S1350, S1360), which is ultimately an unstable procedure for S/N. However, for the present usage in the intermediate range,  $0.05 < ka < 5.99$ , the resulting truncated Bessel function series is accurate within  $\pm 1\%$  except for an anomaly for  $ka$  near unity.

It may be noted that the ratio of source power to noise power, with no propagation loss, is  $0.01 \text{ W}/0.0252 \text{ pW}$ , or about 116 dB.

The ultimate range of a radar is often taken to be  $S/N = 0 \text{ dB}$ . With signal processing, it may be at less than 0 dB. With clutter, it may be considerably above 0 dB.

Example of Results of the Radar Range Program

RADAR RANGE FOR DETECTION OF SUBSURFACE TARGETS:TUNNEL WALL OR BOREHOL  
 FREQ=MEGAHZ;DIMENS=CM. W= PIPE DIAM,OR HEIGHT OF TUNNEL. FILE13-27  
 INPUT F0

ANTENNA APERTURES,CM=

EARTH DIELECTRIC CONST &TANGNT=(TO USE CONDUCTIVITY ENTER 0)

9 0.1 3.003738342 0.149813315

TARGET CODE: 1=METAL WELL; 2=WATER WELL;3=AIR WELL

CODE= 1 4=WALL WITH WATER; 5= WALL W/AIR NOISE FIGURE DB 8

VELOC OF LIGHT= 29979.25 CM /MICROSEC

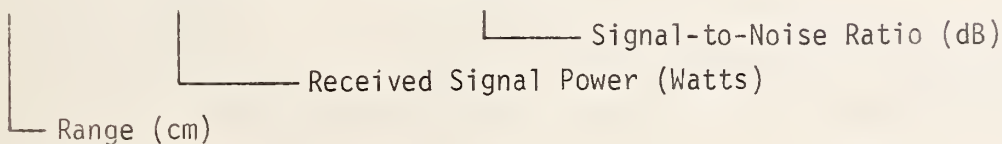
S/N OF 0.01 W RADAR IN HALFSpace; NOISE= 8 DB ABOVE KT IN 1MHZWIDTH

F0= 500 E1,T1= 9 0.1 L1,L2= 50.8 76.2

TARGET= 1 LAMDA= 59.9585 INTERFACE XMISSION= 0.749532926 NOISE=  
 2.52386E-14 X0= 1

W=

KA	EXACT:/S=REAL	/S=IMAG	S7	RATIO
4.721526878	1.314897197	1.43606495	3.833892003	1.0223712
20	4.35067E-03	112.364913		
40	1.54888E-04	97.87952724		
60	1.30706E-05	87.14230358		
80	1.57047E-06	77.93965560		
100	2.29009E-07	69.57786932		
150	2.93736E-09	50.65891682		
200	5.36438E-11	33.27454000		
250	1.18896E-12	16.73102488		
300	2.97853E-14	0.719372779		
350	8.11971E-16	-14.92524563		



```

5 REM RADAR RANGE
6 PRINT "RADAR RANGE FOR DETECTION OF SUBSURFACE TARGETS:TUNNEL WALL OR BOREHOL"
7 REM H.E.BUSSEH, DIV 723.02, NATIONAL BUREAU OF STANDARDS, BOULDER CO.
10 REM FILE 10-27 AS MODIFIED 12/12/80
20 REM "S/N OF .01WATT RADAR INHALF SPACE, W/NOISE=+8DB ABOVE KT IN 1MHZ WIDTH"
30 V1=29979.25
40 PRINT "FREQ=MEGAHZ; DIMENS=CM. W= PIPE DIAM, OR HALF HT OF TUNNEL. FILE 10-27"
50 REM TO CHANGE UNITS, SAY, METERS REPLACE V1 BY V1 IN METERS/MICROSEC
60 PRINT "INPUT F0";
70 INPUT F0
80 REM L1,L2=HORN DIMENSIONS. IF CIRCULAR DISH: USE L1=L2=0.886*DIAM.
90 PRINT "ANTENNA APERTURES, CM=";
100 INPUT L1,L2
110 REM P0=EFFECTIVE CW RADAR POWER IN WATT
116 P0=0.01
120 PRINT "EARTH DIELECTRIC CONST & TANGENT=(TO USE CONDUCTIVITY ENTER 0)";
130 INPUT E1,T1
140 IF T1>0 THEN 190
150 PRINT "INPUT CONDUCT. MHOS/METER"
160 INPUT S1
170 T1=S1/(E1*8.854E-06*F0*2*PI)
180 REM COMPLEX REFRACTIVITY N5&N6
190 N1=SQR(0.5*E1)
200 T=SQR(1+T1*T1)
210 N5=N1*SQR(1+T)
220 N6=N1*SQR(-1+T)
230 PRINT E1;T1;N5;N6
240 PRINT " TARGET CODE: 1=METAL WELL; 2=WATER WELL; 3=AIR WELL"
250 INPUT C7
260 PRINT "CODE="C7" 4=WALL WITH WATER; 5= WALL W/AIR ";
270 N8=0
280 PRINT "NOISE FIGURE DB"N8" VELOC OF LIGHT="V1" CM /MICROSEC"
290 REM G5= POWER REFLECTION OF TARGET=1 FOR METAL,=.25 FOR GAS&WATER
300 G5=1
310 IF C7<2 THEN 330
311 IF C7=2 OR C7=4 THEN 315
312 G5=((N5-1)/(N5+1))2
313 GOTO 330
315 G5=((N5-9)/(N5+9))2
330 PRINT "S/N OF 0.01 W RADAR IN HALFSpace, NOISE= 8 DB ABOVE KT IN 1MHZ WIDTH"
350 L=V1/F0
360 K0=2*PI/L
370 K=K0*N5
380 REM N7=KT NOISE IN 1MHZ WIDTH
390 N7=4E-15
400 REM 1-WAY POWR XMISS. OF INTERFACE =I
410 I=4*N5/((1+N5)*(1+N5))
420 REM DISPERSION MULTIPLIER=D
430 D=0.5
450 A0=0.55*L1*L2
460 G0=A0+4*PI/(L*L)
470 G1=G0*E1
480 REM D6=NF=NOISE FACTOR
490 D6=N7*EXP(2.3026*N8*0.1)
500 PRINT "F0="F0"E1,T1="E1;T1"L1,L2="L1;L2
510 PRINT "TARGT="C7;"LAMBDA="L;"INTERFACE XMISSION="I"NOISE="D6;"X0="1
520 REM S4= POWER*GAINS
530 S0=P0*G1*A0*0.0625*I*I/D/(PI*PI)
540 REM S3 IS RELATED (E SCATT/E INCID)2:GOT BY CYL SUBROUTINES, OR KIRCHHO

```

```

550 PRINT "W= ";
560 INPUT W
570 IF C7<4 THEN 770
580 REM STATEM600 THRU 630,720,730,GIVE VARIED RANGE STEPS.METHD 570REQS630-750
590 FOR R=20 TO 100 STEP 20
600 GOTO 630
610 R=R+50
620 IF R=1500 THEN 740
630 GOSUB C7 OF 750,750,750,1630,1630
640 REM S= CROSS SECTION=4*PI*R*R*((E SCATT/E INCID)SQUARED)
650 S=S3+4*PI*R*R
660 A6=EXP(-4*K0*N6*R)
670 S4=S*S0*A6/(R*R*R*R)
680 PRINT R;S4;10*LGT(S4/D6)
690 IF R=101 THEN 710
700 IF R>100 THEN 610
710 NEXT R
720 R=100
730 GOTO 610
740 END
750 S3=57/R
760 RETURN
770 REM METAL CYL SCATTERING
780 DIM J(16),Y(16)
800 PRINT " KA EXACT:/S=REAL /S=IMAG S7 RATIO"
810 A=W*0.5
820 X=K*A
830 IF X<0.05 THEN 920
840 IF X<5.99 THEN 1020
850 REM NEXT STEP=SCATTERING RATIO BY GEOM OPTICS=LARGE KA
860 S8=PI*A*1.008
870 F8=S8/(PI*A)
880 S7=G5*0.25*A*1.008
890 PRINT " "X" "S7;R8
900 GOTO 580
910 REM SMALL CYL SCATTER(RAYLEIGH)
920 D1=LOG(0.5*X)
930 D2=D1+0.5772157
940 D=D2+D2+0.25*PI*PI
950 S1=-0.25*PI*PI/D
960 S2=0.5*PI*D2/D
970 F8=S1*S1+S2*S2
980 S7=G5*F8/(PI*K)
990 F7=4*F8/(PI*X)
1000 PRINT X;S1;S2;S7;R7
1010 GOTO 580
1020 REM BESSEL (INTERMEDIATE CYL)
1030 X=X
1040 IF X>2.93 THEN 1150
1050 V=X*X/9
1060 V6=V*(1.2656208+V*(-0.3163866+V*(0.0444479+V*(-0.0039444+0.00021*V))))
1070 V6=1+V*(-2.2499997+V6)
1080 V7=V*(-0.74350384+V*(0.25300117+V*(-0.04261214+V*(0.00427916-V*0.00024846)))
1090 V7=2*LOG(0.5*X)*V6/PI+0.36746691+V*(0.60559366+V7)
1100 V8=0.21093573+V*(-0.03954289+V*(0.00443319+V*(-0.00031761+V*(1.109E-05))))
1110 V8=X*(0.5+V*(-0.56249985+V*V8))
1120 V9=V*(2.1682709+V*(-1.3164827+V*(0.3123951+V*(-0.0400976+V*0.0027873))))
1130 V9=2*LOG(0.5*X)*V8/PI+(-0.6366198+V*(0.2212091+V9))/X
1140 GOTO 1290
1150 V=3/X
1160 V6=V*(-0.0055274+V*(-0.00009512+V*(0.00137237+V*(-0.00072805+V*0.00014476)))

```

```

1170 V6=0.79788456+V*(-7.7E-07+V6)
1180 K8=V*(-0.00003954+V*(0.00262573+V*(-0.00054125+V*(-0.00029333+V*0.00013558)
1190 K8=X-0.78539816+V*(-0.04166397+K8)
1200 X2=SQRX
1210 V7=SINK8*V6/X2
1220 V6=COSK8*V6/X2
1230 V8=V*(0.01659667+V*(1.7105E-04+V*(-0.00249511+V*(0.00113653+V*-0.00020033))
1240 V8=0.79788456+V*(1.56E-06+V8)
1250 K8=V*(5.65E-05+V*(-0.00637879+V*(0.00074348+V*(0.00079824+V*(-0.00029166)))
1260 K8=X-2.35619449+V*(0.12499612+K8)
1270 V9=SIN(K8)*V8/X2
1280 V8=COS(K8)*V8/X2
1290 REM
1300 JC[1]=V6
1310 JC[2]=V8
1320 YC[1]=V7
1330 YC[2]=V9
1340 FOR P=2 TO 15
1350 JC[P+1]=(2*P-2)*JC[P]/X-JC[P-1]
1360 YC[P+1]=(2*P-2)*YC[P]/X-YC[P-1]
1380 IF YC[P]<-9E+05 THEN 1400
1390 NEXT P
1400 P1=P
1410 S1=0
1420 S2=0
1430 N=-1
1440 FOR P=1 TO P1
1450 N=N*-1
1460 Q2=JC[P]+JC[P]
1470 D1=Q2+YC[P]*YC[P]
1480 IF P>1 THEN 1510
1490 Q7=1
1500 GOTO 1520
1510 Q7=2
1520 F1=Q7/D1
1530 S1=S1-F1*Q2*N
1540 S2=S2+F1*JC[P]*YC[P]*N
1550 REM IF YC[P]>-1E+05 THEN 1570
1570 NEXT P
1580 F8=S1*S1+S2*S2
1590 S7=G5*F8/(PI*K)
1600 R6=4*F8/(PI*X)
1610 PRINT X;S1;S2;S7;R6
1620 GOTO 580
1630 REM KIRCHHOFF-FRESNEL FIELD OF A STRIP,TAPE #20,FILE 30
1640 REM W( CM )=HALF WIDTH;LENGTH=INFINIT;C&S FOR Z=SQR2*W/R1
1650 REM WIDTH&RANGE IN CM. FRSNL C & S DEFINED IN AMS55 EQ7.3.1&2
1660 R1=SQR(0.5*R*L/N5)
1670 Z=SQR2*W/R1
1680 U=0.5*PI*Z*Z
1690 F=(1+0.926*Z)/(2+1.792*Z+3.104*Z*Z)
1700 G=1/(2+4.142*Z+Z*Z*(3.492+6.67*Z))
1710 S1=SIN(U)
1720 C1=COS(U)
1730 C=0.5+F*S1-G*C1
1740 S9=0.5-F+C1-G*S1
1750 E2=0.5*(C*C+S9*S9)
1770 S3=G5*E2
1780 PRINT "Z C S9 S3=E2+G5"Z;C;S9;S3
1790 RETURN
1800 END

```



U.S. DEPT. OF COMMERCE  
BIBLIOGRAPHIC DATA SHEET (See instructions)

1. PUBLICATION OR REPORT NO.  
NBSIR 84-3017

2. Performing Organ. Report No.

3. Publication Date

4. TITLE AND SUBTITLE  
Microwave Detection of Lost Wells and Unknown Water-Filled Voids in Coal Mines

5. AUTHOR(S)  
D.R. Belsher; R.H. McLaughlin; A.G. Repjar; and H.E. Bussey

6. PERFORMING ORGANIZATION (If joint or other than NBS, see instructions)  
NATIONAL BUREAU OF STANDARDS  
DEPARTMENT OF COMMERCE  
WASHINGTON, D.C. 20234

7. Contract/Grant No.  
8. Type of Report & Period Covered

9. SPONSORING ORGANIZATION NAME AND COMPLETE ADDRESS (Street, City, State, ZIP)

10. SUPPLEMENTARY NOTES

Document describes a computer program; SF-185, FIPS Software Summary, is attached.

11. ABSTRACT (A 200-word or less factual summary of most significant information. If document includes a significant bibliography or literature survey, mention it here)

Work on contract H0272007 is summarized for the period of January 1979 through March 1984. The development of improved antennas useable with both a pulse system or an FM-CW system is described. The development of a field prototype pulse sampling system is described. Initial theoretical work on the problem of dielectric loading of antennas as well as a study of potential system range is included.

12. KEY WORDS (Six to twelve entries; alphabetical order; capitalize only proper names; and separate key words by semicolons)  
antennas; dielectric load; pulsed system; radar range

13. AVAILABILITY  
 Unlimited  
 For Official Distribution. Do Not Release to NTIS  
 Order From Superintendent of Documents, U.S. Government Printing Office, Washington, D.C. 20402.  
 Order From National Technical Information Service (NTIS), Springfield VA. 22161

14. NO. OF PRINTED PAGES  
86  
15. Price

11

11